KfK 5283
Januar 1994

Lifetime Prediction for the First Wall of a Fusion Machine

IAEA Co-Ordinated Research Programme Second Interim Report: Behaviour of First Wall Components under Thermal Fatigue-Stress Analysis and Life Assessment

E. Diegele, D. Munz, G. Schweinfurther
Institut für Materialforschung
Projekt Kernfusion

Kernforschungszentrum Karlsruhe

KERNFORSCHUNGSZENTRUM KARLSRUHE

Institut für Materialforschung
Projekt Kernfusion

KfK 5283

LIFETIME PREDICTION FOR THE FIRST WALL OF A FUSION MACHINE

IAEA CO-ORDINATED RESEARCH PROGRAMME SECOND INTERIM REPORT: BEHAVIOUR OF FIRST WALL COMPONENTS UNDER THERMAL FATIGUE- STRESS ANALYSIS AND LIFE ASSESSMENT

E. Diegele, D.Munz, G.Schweinfurther

Kernforschungszentrum Karlsruhe GmbH, Karlsruhe

Als Manuskript gedruckt

Kernforschungszentrum Karlsruhe GmbH
Postfach 3640, 76021 Karlsruhe

ISSN 0303-4003

LIFETIME PREDICTION FOR THE FIRST WALL OF A FUSION MACHINE

Abstract:

A Co-ordinated Research Program (CRP) on 'Lifetime Behaviour of the First Wall of Fusion Machines' was initiated by the International Atomic Energy Agency (IAEA). In this report the results of the benchmark calculations for a First Wall component tested in the JRC-Ispra high heat flux test facility are presented. Results of thermal, elastic, elasto-plastic analysis and lifetime assessment based on code rules and inelastic analysis are included.

LEBENSDAUERVORHERSAGE FÜR DIE ERSTE WAND EINER FUSIONSANLAGE

Zusammenfassung:

Die International Atomic Energy Agency (IAEA) organisierte eine vergleichende Analyse (Co-ordinated Research Program) über die Lebensdauerberechnung der ersten Wand von Fusionsanlagen. In diesem Bericht sind die Berechnungen für eine Komponente zusammengefaßt, die bei JRC-Ispra in einer Versuchsanlage mit großem Wärmefluß untersucht wurde. Die Ergebnisse umfassen thermische, elastische und elasto-plastische Analysen sowie Lebensdauerberechnungen nach Codes und basierend auf inelastischen Rechnungen.

Table of Contents

Fusion machines of the next generation as ITER or NET will be operated in a cyclic mode. Under normal operation conditions the loading of plasma facing components like the First Wall (FW) are characterized by periodically high heat fluxes. Several First Wall concepts have been proposed and investigated by thermo-mechanical analyses and by fatigue testing on mock-ups during the last years.

At the International Atomic Energy Agency (IAEA) Technical Committee Meeting on Lifetime Predictions for the First Wall and Blanket Structure of Fusions Reactors held in Karlsruhe 1985, the need was identified to compare component lifetime analyses with experimental results from data obtained from high heat flux tests. Therefore, a Co-ordinated Research Program (CRP) on 'Lifetime Behaviour of the First Wall of Fusion Machines' was initiated. The main concern of the CRP is to compare the applied structure mechanical tools and computer codes and to check and to validate lifetime predicting codes and rules.

The IAEA First Wall benchmark components B1, B2 and B3 have been tested for more than 20.000 cycles in the JRC-Ispra high heat flux test facility, up to now without lifetime limiting failure.

Information on the geometry of the specimens tested, on the material and on the thermal load cycles has been provided to participants of the benchmark Ref. [1] . Analyses of the thermo-mechanical behaviour of the test specimen have been performed and presented at a Co-ordinated Research Meeting in Ispra and in a first intermediate report. However, some input data assumptions for the calculations differed signifanctly between the participants of the benchmark. Therefore, the need for further calculations on a common input data base was agreed upon. Additionally, results have been specified, that should be compared among the participating parties.

Investigations performed during the last period include

- thermal analyses,
- elastic analyses,
- elasto-plastic analyses,
- lifetime assessment based on the elastic analyses using the RCC-code rules,
- lifetime prediction based on the inelastic analyses.

Thermo-mechanical calculations have been carried out using the FE-code ABAQUS [2] . According to the benchmark requirements, results of the FE calculations carried out by utilizing the updated data base will be reported.

1. Basis of the analyses

1.1 Geometry and loading conditions

The test specimen considered is made of AISI 316 LSPH. It consists of a steel plate with 5 cooling tubes with inner diameter of 8 mm. A cross section of the geometry is shown in Fig. 1. The dimensions can be taken from this figure.

A typical load cycle in a fusion reactor, e.g. ITER in its technology phase, could be characterized by several phases:
Start up, burn with constant fusion power, shut down and dwell.
During this report period thermal cycles have been considered with 52.5 s start-up, 45.5 s hold time at the maximum surface heat flux of 50 W/ cm^2, a shut down time of 21.4 s and a dwell time of 63 s with a heat flux of 4 W/ cm^2. A load histogram is given in Fig. 2.

The cooling media is water of 10 °C. The heat transfer coefficient of h = 9 kW/(m^2 K) as well as the coolant temperature are assumed to be constant during the cycles.

1.2 Meshes used in FE analyses

The surface heat and the cooling temperature are assumed to be uniform. Therefore, the FE model is restricted to (a symmetry) half of a cross-section. A nodalization of the FE mesh used in 2D analysis is shown in Fig. 3. This mesh is built of 650 isoparametric 2D elements and 2097 nodes in total. A coarse FE-mesh as shown in Fig. 4 is used to assess the influence of the FE discretization on the results. This mesh consists of 300 two-dimensional 8-node elements with 1013 nodes. If it is not specially indicated, the results will always refer to the fine mesh, which, if any comparison is drawn, for short will be denoted by "mesh f", whereas the other model is called "mesh c".

1.3 Structural boundary conditions

In mechanical analysis the conditions of support are given by prescribed diplacements $u = 0$ at the midplane ($x = 39$mm), i.e. symmetry conditions, and $v = 0$ at the edgepoint ($x = 0$, $y = 0$) as shown in Fig. 3. Generalized plane strain (with 'free' expansion in z-direction, i.e. normal to the figure plane, free rotation about the x-axis and bending suppressed around the y axis) has been shown to be most suitable in the previous report.

1.4 Material model in heat transfer analysis

The material data of AISI 316 LSPH steel for the temperature field calculations are given in Ref. [1]. Table 1 shows a summarization of the thermo-physical data.

T [°C]	λ [W / mm K]	c_p[J / kg K]
20	14.5 10^{-3}	480
300	18.0 10^{-3}	550
500	20.0 10^{-3}	580

Table 1: Material data used for temperature analysis

1.5 Material model in mechanical analysis

Stress and strain analyses are performed using elastic and inelastic material models.

1.5.1 Linear elastic analysis

The data used for linear elastic calculations are given in Ref. [1] and Ref. [3] and summarized in table 2.

T [°C]	E [N / mm²]
20.	192000
100	186000
200	178000
300	170000
400	161000
500	153000

Table 2: Material data - Young's modulus

1.5.2 Inelastic analysis

The inelastic model, that was used in the first intermediate report was a plasticity model with linear cyclic and kinematic hardening, where the yield surface is defined by the von Mises criteria.

Two different material data sets have been investigated in this first report. Their characteristics will be shortly repeated here.

- (i) elastic-plastic analysis using the monotonic loading data.
- (ii) elastic-plastic analysis using the cyclic hardening curve.

For short, the models will be referred as (M) and (C), respectively.

Linearized monotonic curves, model M

Denoting C as the point ($\varepsilon = 1\%$, $\sigma(1\%)$) and B as the point ($\varepsilon = 0.2\%$, $\sigma(0.2\%)$) the stress-strain curve at each temperature is linearized in the following manner:

- design A as intersection of the straight, line BC and the equation in straight form $\sigma = E\,\varepsilon$,
- take B and C as fixed points on the bi-linear curve,
- the material model is then described by the curve O A B C .

Linearized cyclic hardening curves, model C

Denoting B_2 as the point ($\Delta\varepsilon = 0.6\%$, $\Delta\sigma(0.6\%)$), the stress- strain curve at each temperature is linearized in the following manner:

- find the point B_0 where the plastic strain is 0.005% with total strain ε_0 ,
- B_1 is the point that has a total strain of (ε_0 + 0.2 %).
- keep B_1 and B_2 as points fixed on the bi-linear curve,
- design A as intersection of the straight, line B_1B_2 and the equation in straight form $\sigma = E\,\varepsilon$.
- the material model is then described by the curve O A B_1 B_2.

The construction rules for the linearizations (M) and (C) at the 20°C curves are given in the first interim report. (therein Fig. 5 and Fig. 6, respectively)

The input data of models (M) and (C) are summarized in table 3 and table 4.

T [°C]	A [*MPa*]	C [*MPa*]
20.	249.0	315
100	207.4	264
200	172.6	220
250	160.8	204
300	150.2	191
350	143.3	182
400	138.4	175
450	134.6	170
500	131.7	166

Table 3: Material data - Linearized monotonic curves

T [°C]	A [*MPa*]	B_2 [*MPa*]	ε [%] (plastic strain at B_2)
20	271.0	533	0.3224
450	207.6	440	0.3198
550	258.6	485	0.2745

Table 4: Material data - Linearized cyclic hardening curves

Both models will be used for comparison. Within this report, a material model is used following strictly the ORNL requirements. For short, this model is noted as (O66) and evaluated in detail in the next section.

1.5.3 ORNL material model

The ORNL model is a plasticity model, which includes, both, a kinematic hardening rule and an isotropic hardening rule. A consistent procedure is provided in the ORNL-TM-3602 recommendations. This procedure is proposed for the use in constructing bilinear representations from actual nonlinear monotonic and cyclic stress-strain curves.

For a given material and a given temperature, the bilinear representations to be used depend on the expected range of elastic-plastic strain ε_{max}. In the bilinear representations, the material is characterized by the elastic-modulus E and a material constant C, which are related to the slope E_p of the elastic-plastic segment by

$$C = \frac{2}{3}\frac{(E\ E_p)}{E - E_p}$$

and by a material constant κ, which is related to the yield point σ_0 by

$$\kappa = \frac{\sigma_0^2}{3} .$$

For a given analysis, C should be kept constant at a given temperature. However, the value of κ may split into κ_0 characterizing the first inelastic loading and a value κ_1 for subsequent loading cycles. Often the latter is taken from the tenth cycle.

Bilinear representation of the initial monotonic stress-strain curve:

- The elastic segment of the bilinear curve is determined by the initial response of the virgin material, i.e. by a straight line with slope E.
- For a given maximum mechanical strain ε_{max}, the elastic-plastic segment of the bilinear curve is determined by a straight line connecting the actual stress points in the material curve at the maximum strain ε_{max} to the stress point at $\varepsilon_{max}/2$.
- The yield point σ_0 is defined as the intersection of these two straight lines.
- In case of multiaxial loading, the maximum strain should be assessed on the basis of the work-equivalent effective strain $\bar{\varepsilon}$ defined by

$$\bar{\varepsilon} = \frac{2}{3}\sqrt{(\varepsilon_{ij}\varepsilon_{ij})}$$

Bilinear representation of cyclic stress-strain curves:

As it is recognized, that the AISI 316 LSPH material is hardened by prior loading, the use of stress-strain data from virgin material can actually lead to prediction of large plastic strains. Therefore, calculations for subsequent loading cycles have to be based on the cyclic stress-strain curve. It is recommended to use the curves for the tenth-cycle obtained from constant strain-range cylic test. Thus, for each temperature, κ_1 should be determined by the following procedure:

- The slope of the bilinear portion of the bilinear representation is equal to that of the bilinear representation of the monotonic curve.
- The intersection of the elastic and elastic-plastic part have to be calculated so that the areas below the actual cyclic stress-strain curve and the fitted one are equal, i.e. to ensure equal dissipated work during one complete cycle.
- The areas of the tensile and compressive portion are equal.

- The value of κ_1 is related to the total stress range by $\kappa_1 = \frac{1}{12} \Delta\sigma^2$.

The problem arising is characterized by mechanical strain, that is mostly determined by the thermal strain, i.e. by $\varepsilon \simeq - \alpha (T - \bar{T})$. During the complete cycle, therefore, the strains are either "positive" or "negative" dependent on their location in the cold or in the hot part of the component. From elastic analysis it comes out, that the elastic energy density $W = E \varepsilon$ is about 1.85 (in units of $\frac{N}{mm^2}$) at point F. Therefore, 0.6% is a good approach for the ε_{max} expected during elastic-plastic analysis.

The parameter adjustment for the ORNL material model is performed according to the recommendations given above, with $\varepsilon_{max} = 0.6\%$ in case of monotonic loading and $\Delta \varepsilon_{max} = 0.6\%$ in case of cyclic loading. Within the data base common to all participants, a cyclic stress-strain curve is not included. Therefore, Masing's rule is applied to construct cyclic (hysteresis-) stress-strain curves from the reduced cyclic stress-strain(-range) curves as they are given in the RCC-code Annex A3-1S. An example of the construction rule is illustrated in Figs. 7 and 8, for 20 °C and 450 °C, respectively. The results of the construction of the bilinear representation of the virgin material at 20 °C is depicted in Fig. 5. The curve labeled $\Delta \varepsilon = 0.6$ % in Fig. 7 is used to determine the bilinear representation of a cycle of saturation at 20 °C. The construction of the bilinear representation of strain versus stress for 450 °C is shown in Fig. 10 as an example.

The application of the ORNL model causes some difficulties:

1. There is no hysteresis-stress-strain data included in the RCC-code.

2. The given reduced cyclic stress-strain curve is fitted over a large strain range. There are parts of the cyclic hardening curve, which lie under the values of the monotonic loading curve. Together with the requirement of cyclic hardening, this leads to some inconsistency within the framework of the ORNL model.

1.6 *Finite Element Code*

The calculations are performed using the ABAQUS FE Code. Therein, a Newton method is used as a numerical technique for solving the equilibrium iterations at any time. The integration can be performed "directly", i.e. the user has to determine the time steps, or in an "automatic mode", where the time steps are controlled automatically by the program. The calculations presented within this report are carried out using the latter possibility. In that case, the user has to specify some tolerances for the equilibrium iterations. Within this study, a force tolerance PTOL $<$ 0.1 MPa is applied. Within the temperature analysis, the integration is limited by two parameters: first, by TEMTOL $<$ 0.1 °C, which within heat transfer problems is the same as the PTOL parameter of stress analysis, and, second, by the parameter DELTMX $<$ 20 °C, which restricts the temperature change at any nodal point within a time increment of less than 20 °C.

Within all ABAQUS procedures, material properties are interpolated linearly.

1.7 *Finite Element calculations*

The ABAQUS code is run on a IBM 3090-600 computer. The heat transfer analysis of a complete cycle needs a total CPU time of 6:02 min including compilation, presteps, input- and output routines. The analysis is carried out within 60 time increments and all togehter 87 iterations (i.e. passes through the equation solver).

The elasto-plastic analysis of a complete cycle requires a total CPU time of 11:20 min. The time integration of a stable cycle is solved within 24 time increments and all togehter 71 iterations.

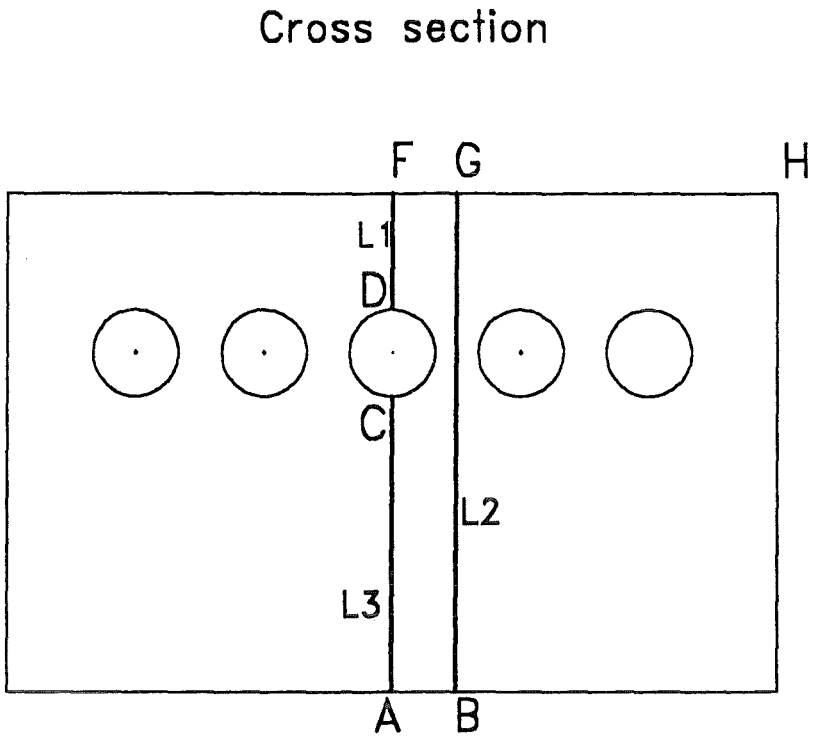

Figure 1. Cross-section of specimen:

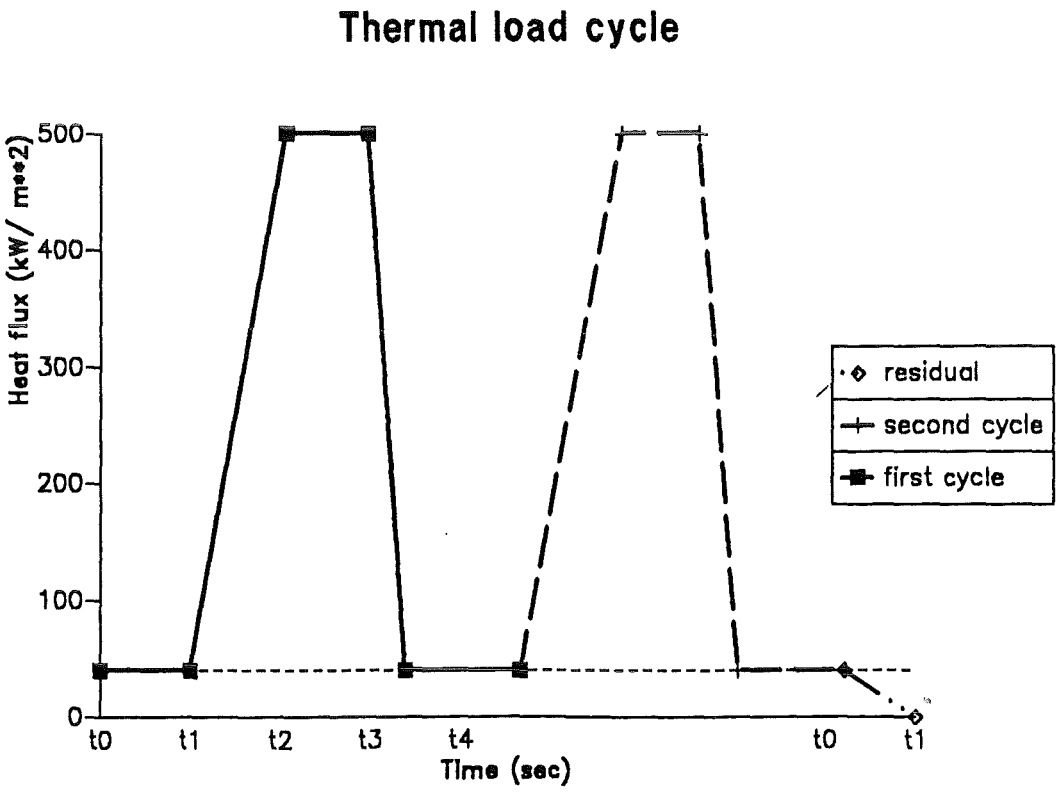

Figure 2. Loading history:

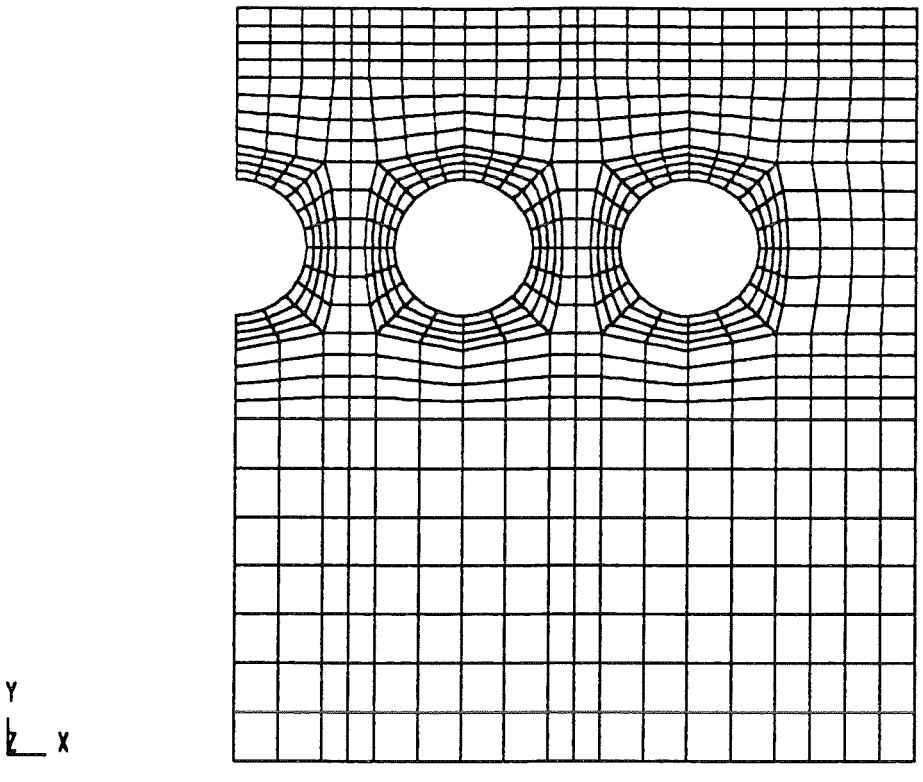

Figure 3. Finite Element nodalization: fine mesh

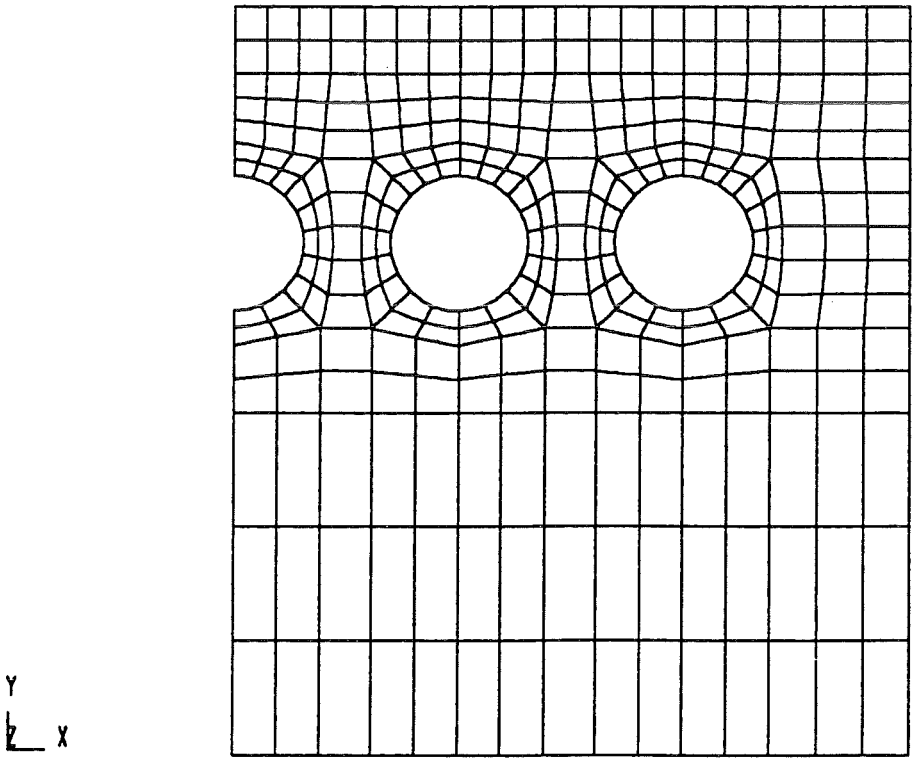

Figure 4. Finite Element nodalization: coarse mesh

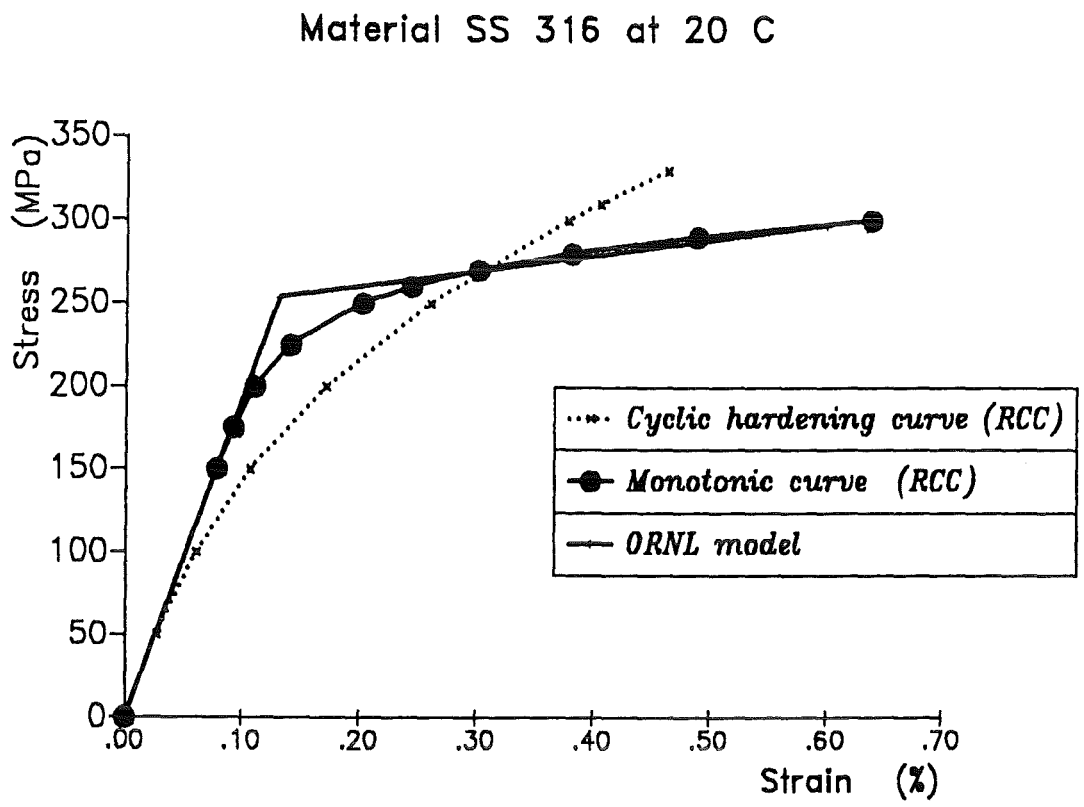

Figure 5. Monotonic loading curve at 20 °C: Parameter adjustment of ORNL model

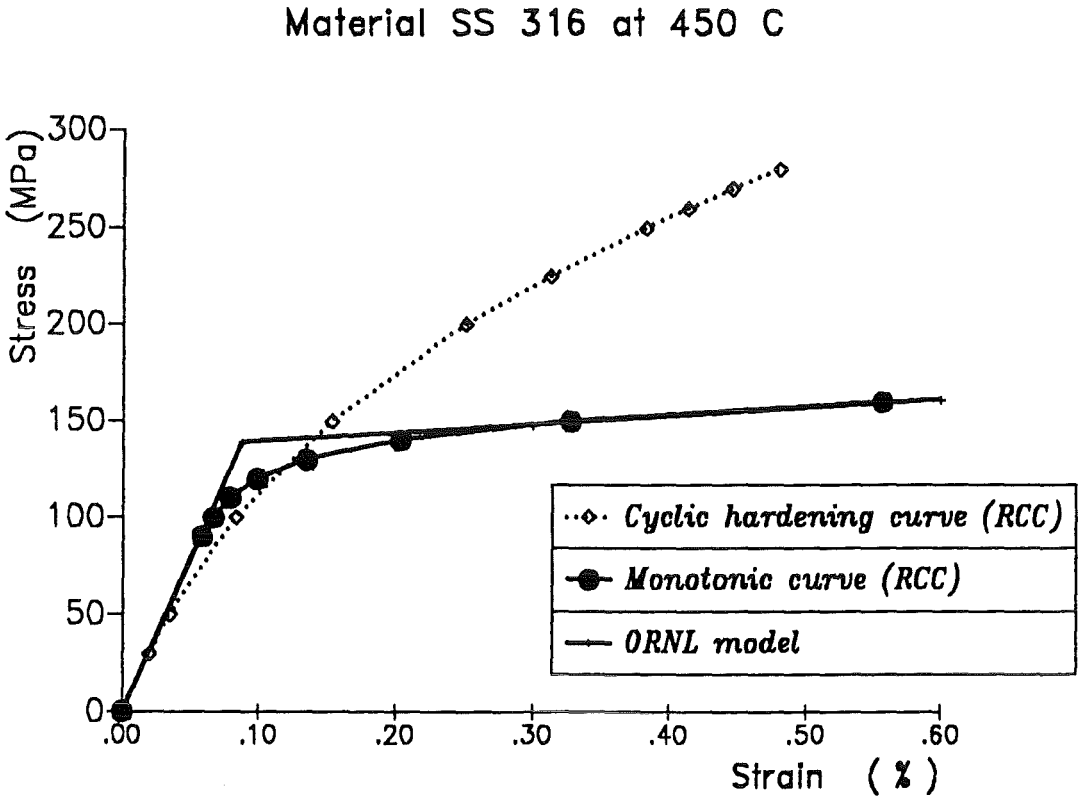

Figure 6. Monotonic loading curve at 450 °C: Parameter adjustment of ORNL model

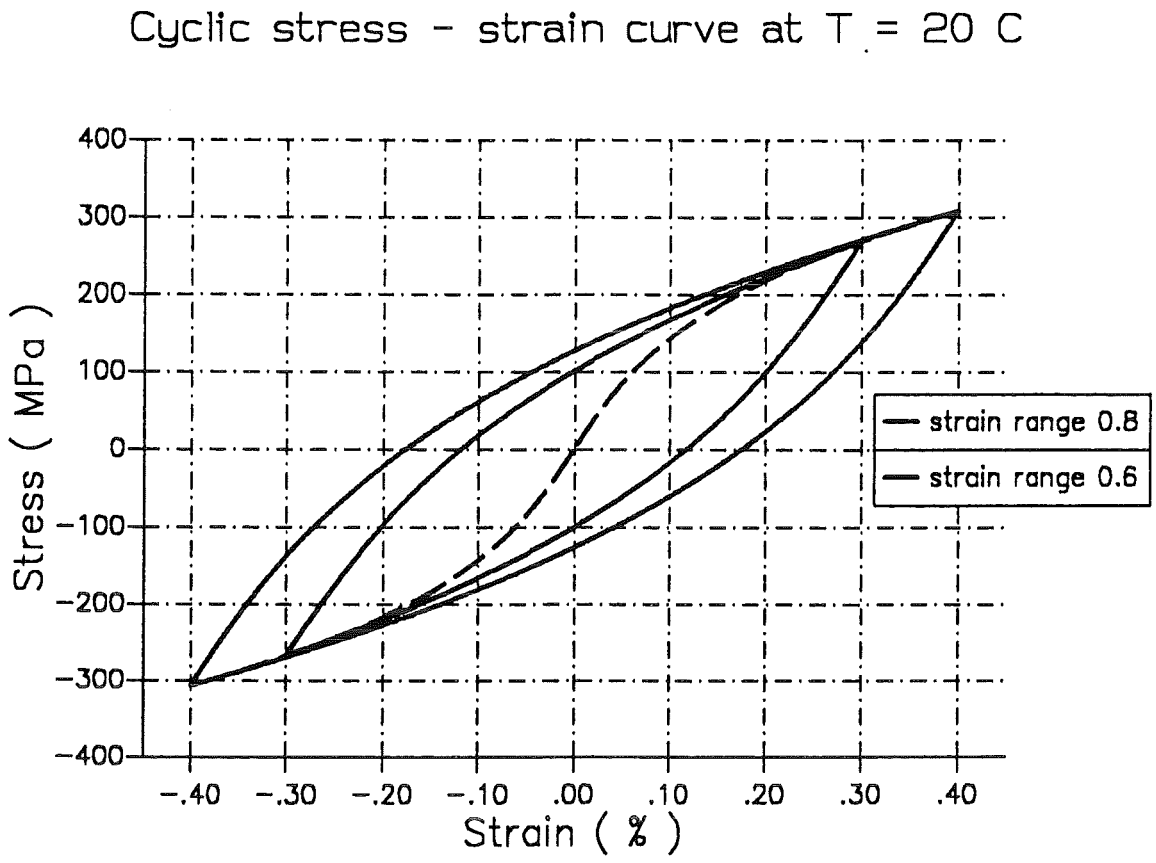

Figure 7. **Cyclic hardening curve at 20 °C:** Construction of stress-strain relation (hysteresis-loop) by means of Masing's rule.

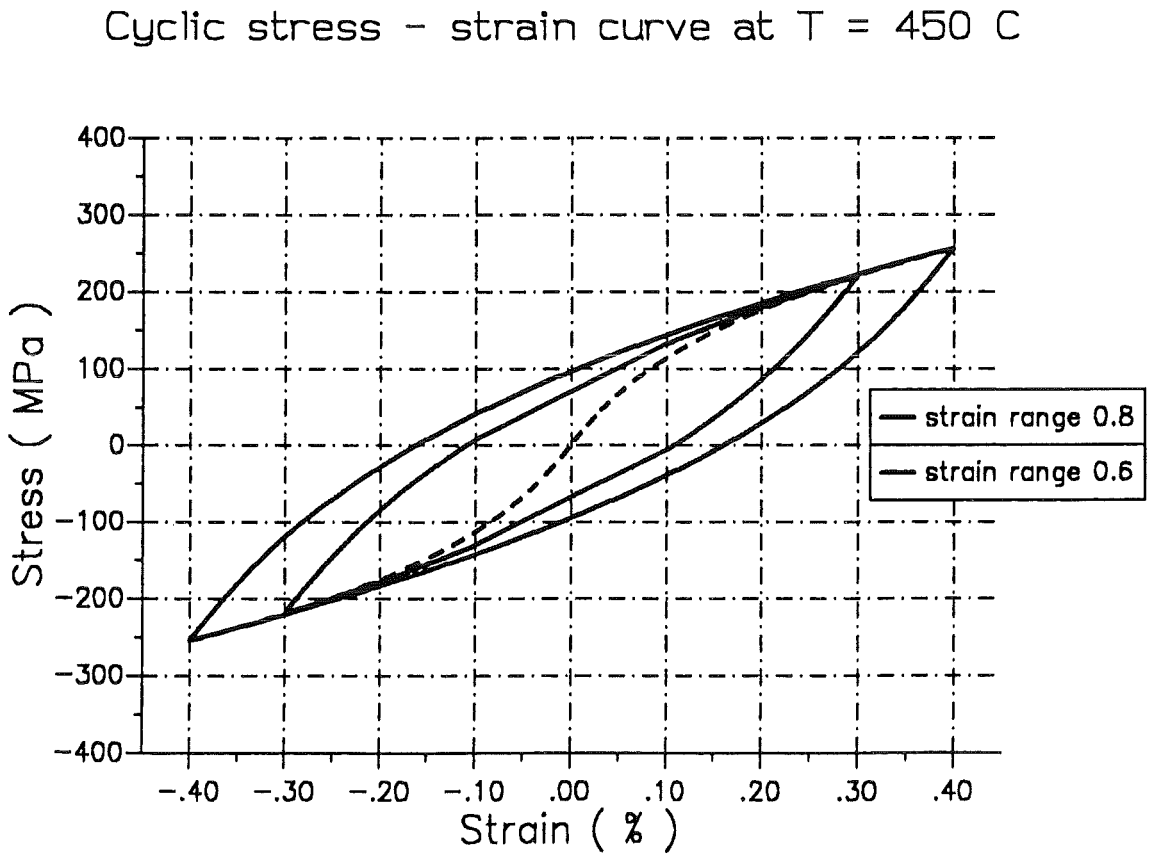

Figure 8. **Cyclic hardening curve at 450 °C:** Construction of stress-strain relation (hysteresis-loop) by means of Masing's rule.

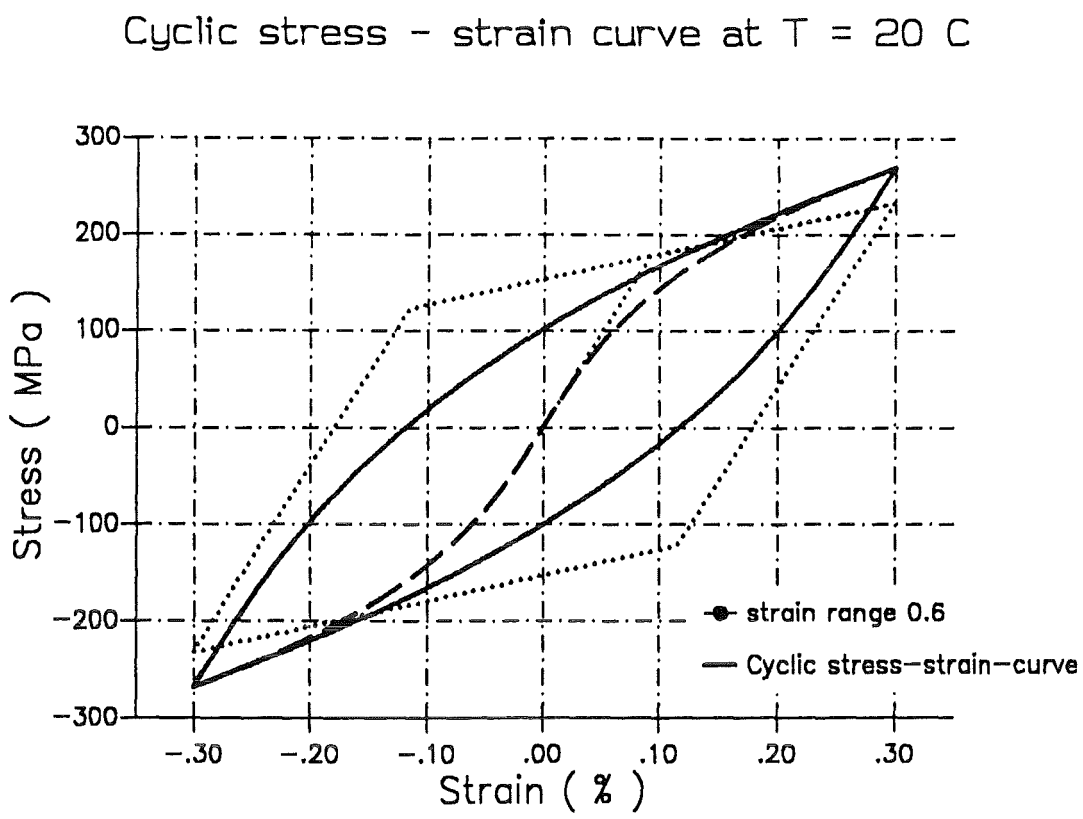

Figure 9. **Cyclic hardening curve at 20 °C:** Adjustment of ORNL model

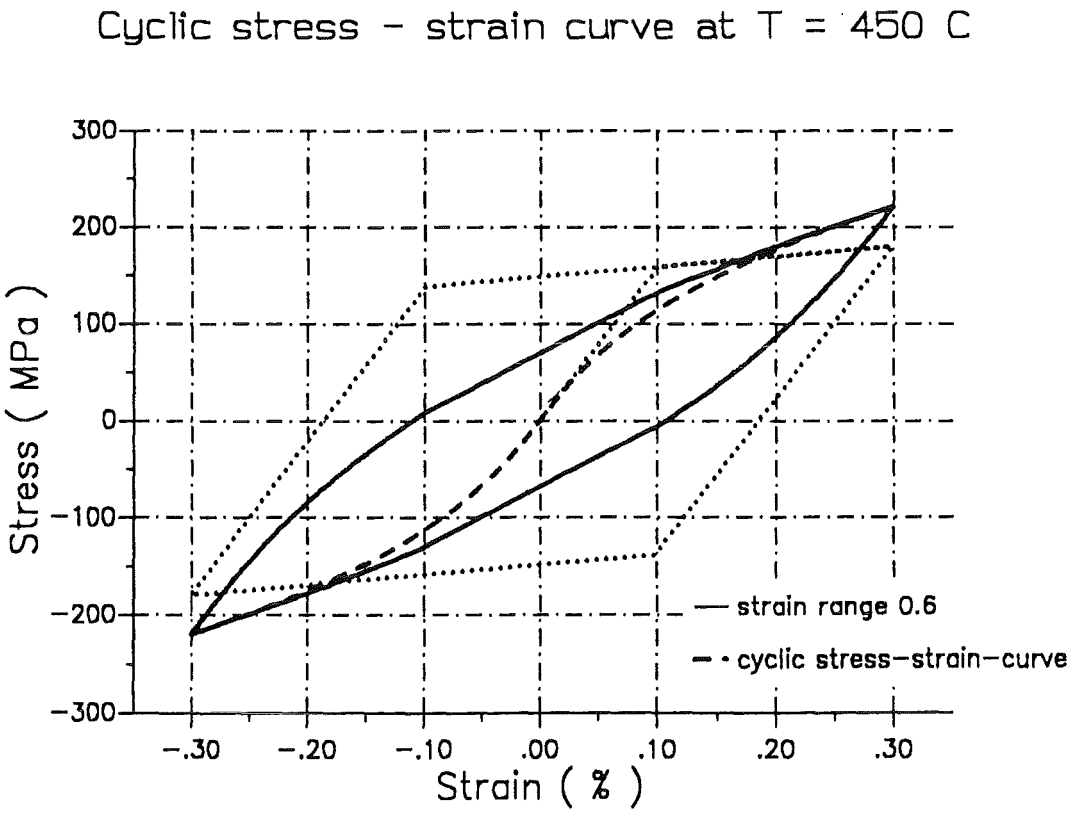

Figure 10. **Cyclic hardening curve at 450 °C:** Adjustment of ORNL model

2. Temperature analysis

Transient analyses of 3 thermal cycles are performed using the two dimensional models.

Main results

are given as temperature histories at highly exposed points H and F and as plots along some lines.

List of results and figures

Fig.11: Plot along line L1 at end and begin of heating
Fig.12: Plot along line L2 at end and begin of heating
Fig.13: Plot along line L3 at end and begin of heating
Fig.14: History plot at point H
Fig.15: History plot at point F

Values of temperatures at points (A-H) are given in Appendix 3.

Discussion of results

The maximum values of the temperature field are reached at location H and amount to 431.6°C at the end of burn and 70.2°C at the end of the thermal cycle, if the fine mesh is used, and 431.0°C at the end of burn and 70.9°C at the end of cycle, if the coarse mesh is considered. Thus, the difference in results are negligible. There are some locations, i.e. point F, where the difference is somewhat more pronounced. Due to the very steep temperature gradient along line DF, a signifanctly fine discretization is required. Near point F, the mesh f has exactly twice the number of nodal points per unit lenght compared to mesh c. The length of an element was chosen to be 1 mm, i.e. 1/10 of the total lenght of the line DF.

The evaluation of the maximum temperature (at the hot spot H) at the end of the first three cycles results in values of 430.4, 431.6 and 431.6 °C. From that, it can be concluded, that the thermal cycles are stable.

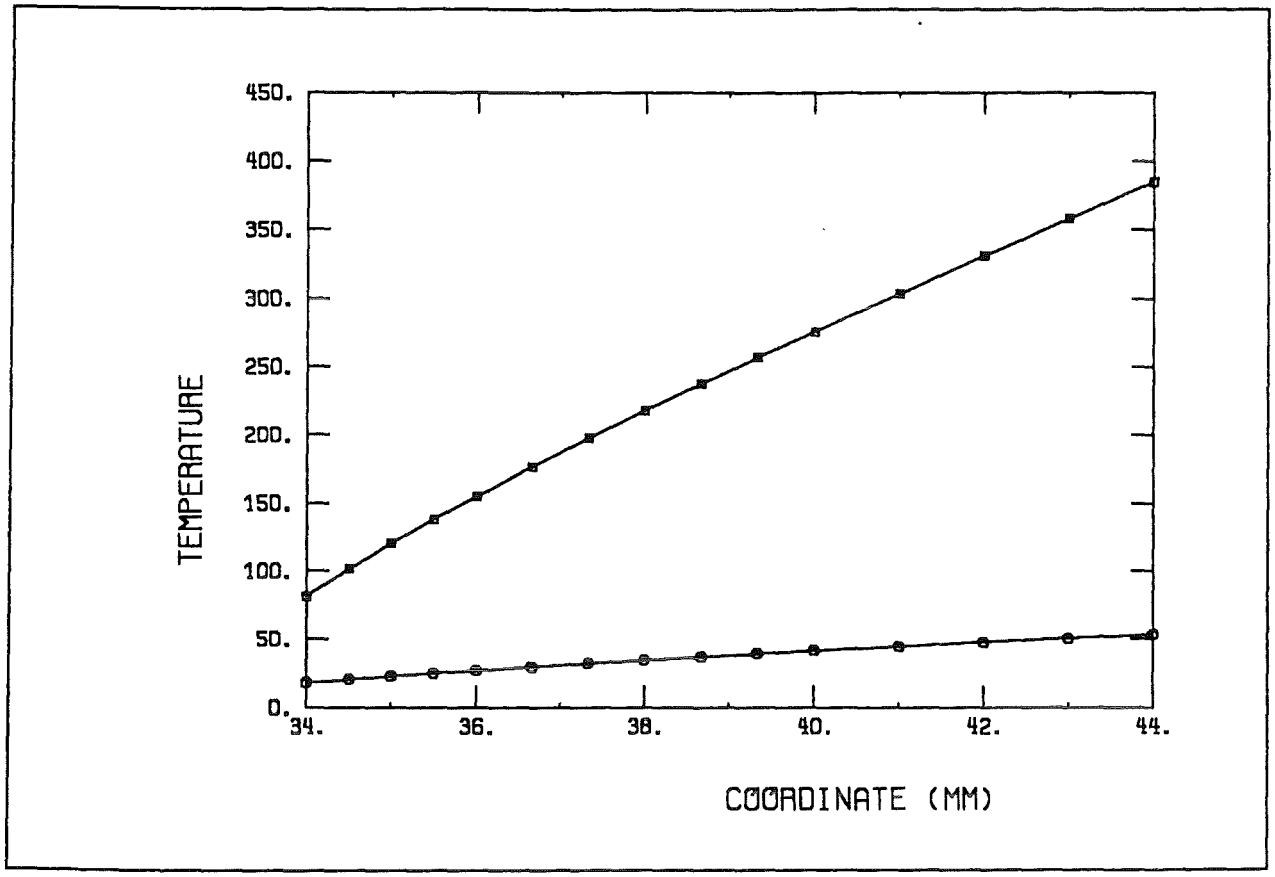

Figure 11. Temperature along line L1: (□ end of heating, O end of cycle)

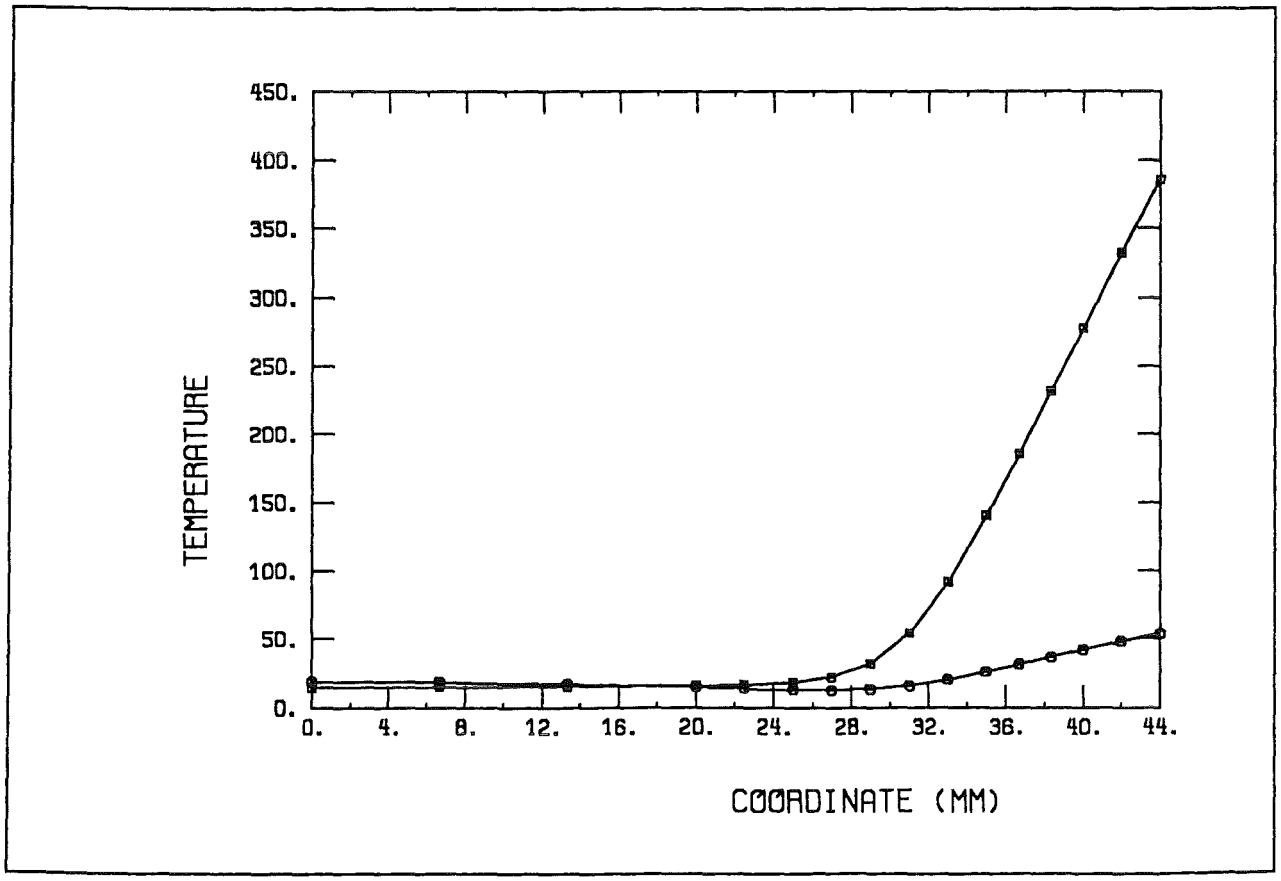

Figure 12. Temperature along line L2: (□ end of heating, O end of cycle)

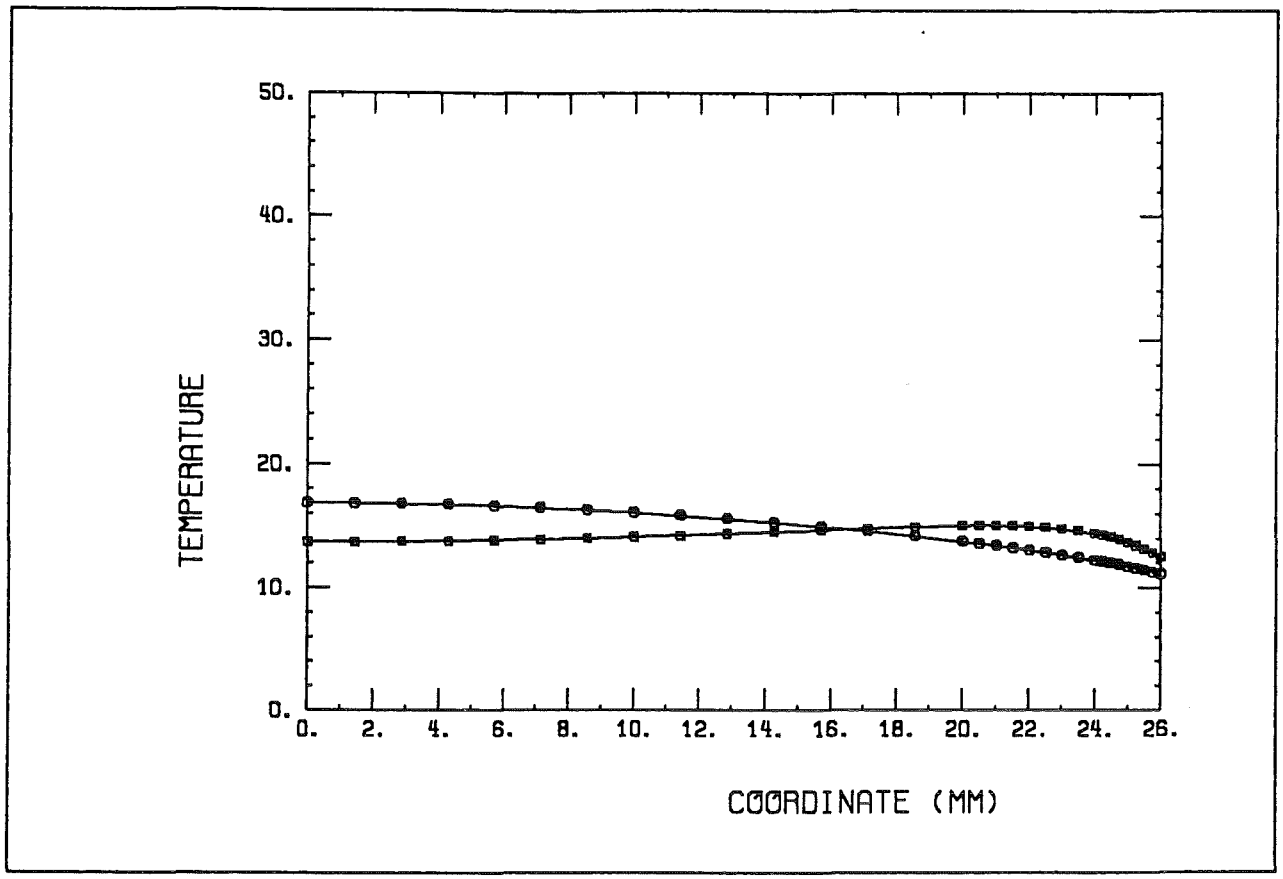

Figure 13. Temperature along line L3: (□ end of heating, O end of cycle)

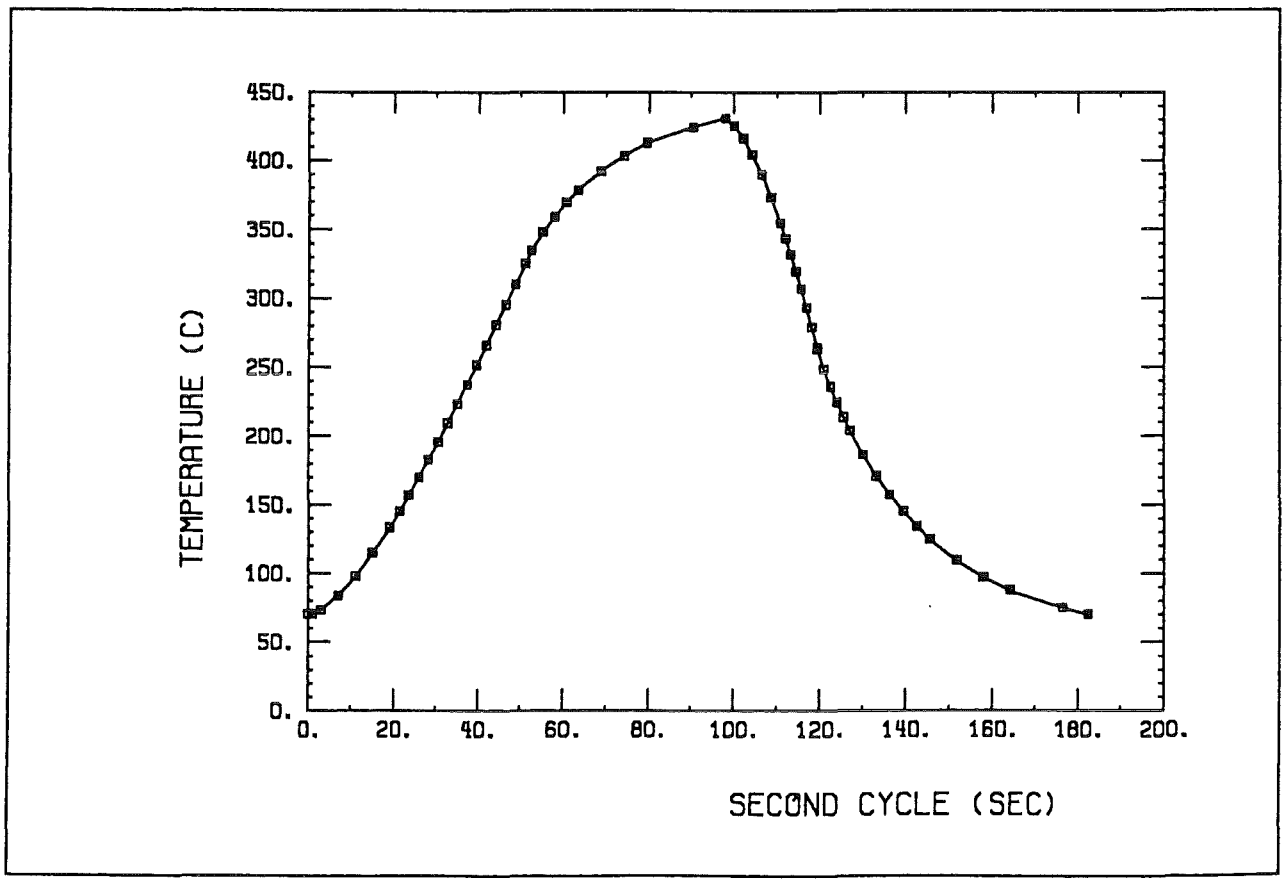

Figure 14. Temperature history at point H

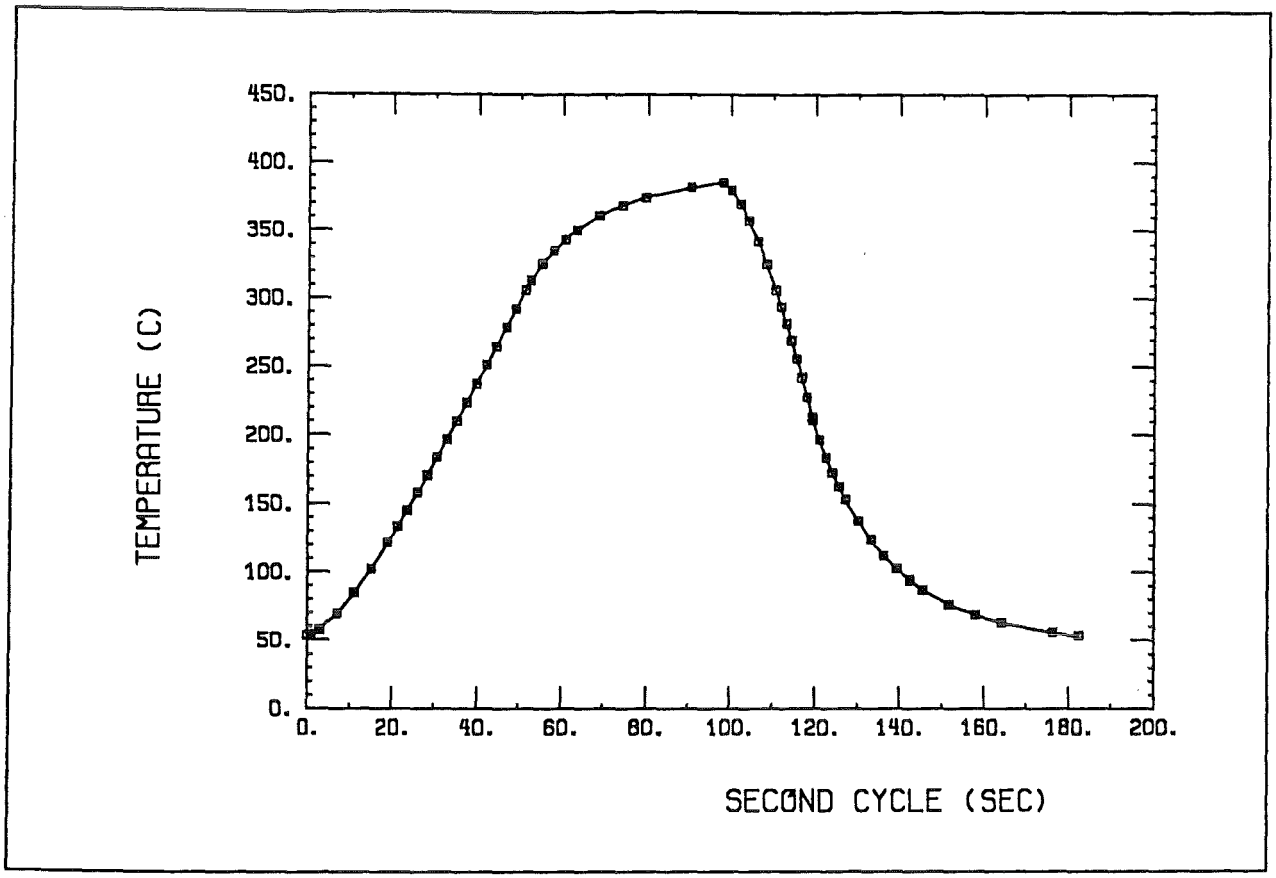

Figure 15. **Temperature history at point F**

3. Elastic analysis

The temperature fields referred in the last section are used to compute stress and strain fields by elastic analyses. The calculations are performed on the second thermal load cycle.

The aims of these analyses are

- to specify the most heavily loaded parts of the component in terms of stress and strain,
- to give a comparison of the calculated stress and strain fields at heavily stressed locations between FE-meshes of different discretization,
- to find the elastic energy density in order to get a good guess for the representation of the ORNL plasticity model,
- and finally, to assess lifetime according to the RCC codes by means of the calculated stress invariants.

Results

Main results of the elastic analysis are:

1. Identification of highly loaded locations

   The stresses are tensile near the coolant tubes, i.e. in the cold part of the component, and compressive at the heated front part of the specimen.
   The highest tensile loading as well as the maximum von Mises and Tresca equivalent stresses occur at point C, whereas, both, the highest compressive stress and the highest strain range are found for point F.

   The evaluation of equivalent strain is performed for all nodal points. According to the requirements of, both, the ASME code and the RCC code, the strains are normalized, in this special loading case with respect to the end of the cooling period, i.e.

$$\Delta\varepsilon_{eq}(t) = \frac{\sqrt{2}}{3}\left[(\Delta\varepsilon_{xx} - \Delta\varepsilon_{yy})^2 + (\Delta\varepsilon_{yy} - \Delta\varepsilon_{zz})^2 + (\Delta\varepsilon_{zz} - \Delta\varepsilon_{xx})^2 + \Delta\varepsilon_{xy}{}^2\right]^{\frac{1}{2}}$$

   where $\Delta\varepsilon_{ij} = \varepsilon_{ij}(t) - \varepsilon_{ij}(t_e)$, t_e = end of cooling period

   The maximum range of mechanical strain is found to be

   $\Delta\varepsilon_{eq}$ = .3147 % at point F.

2. Test of FE discretization in 2D linear elastic computations

The results of calculations using the coarse mesh c and the fine mesh f are in fair agreement. A priori, there isn't any indication, which values should be higher. This is confirmed by the analysis: On one hand side, the values calculated at point C are up to 5% higher in case of a fine mesh compared to the results basing on a coarse mesh. On the other hand side, the values calculated at point F are up to 3% lower comparing the results of a fine mesh with those of a coarse mesh. The results of the comparison are summarized in table 5 .

stresses [*MPa*]	fine mesh	coarse mesh
Results at point C		
σ_{xx}	923	866
σ_{zz}	621	606
von Mises	823	765
Tresca	932	862
Results at point F		
σ_{xx}	-672	-696
σ_{zz}	-665	-652
von Mises	668	674
Tresca	672	695

Table 5: Results of linear elastic calculations - Comparison of stresses at point C and F.

List of results and figures

The results are listed in the tables of Appendix 4.

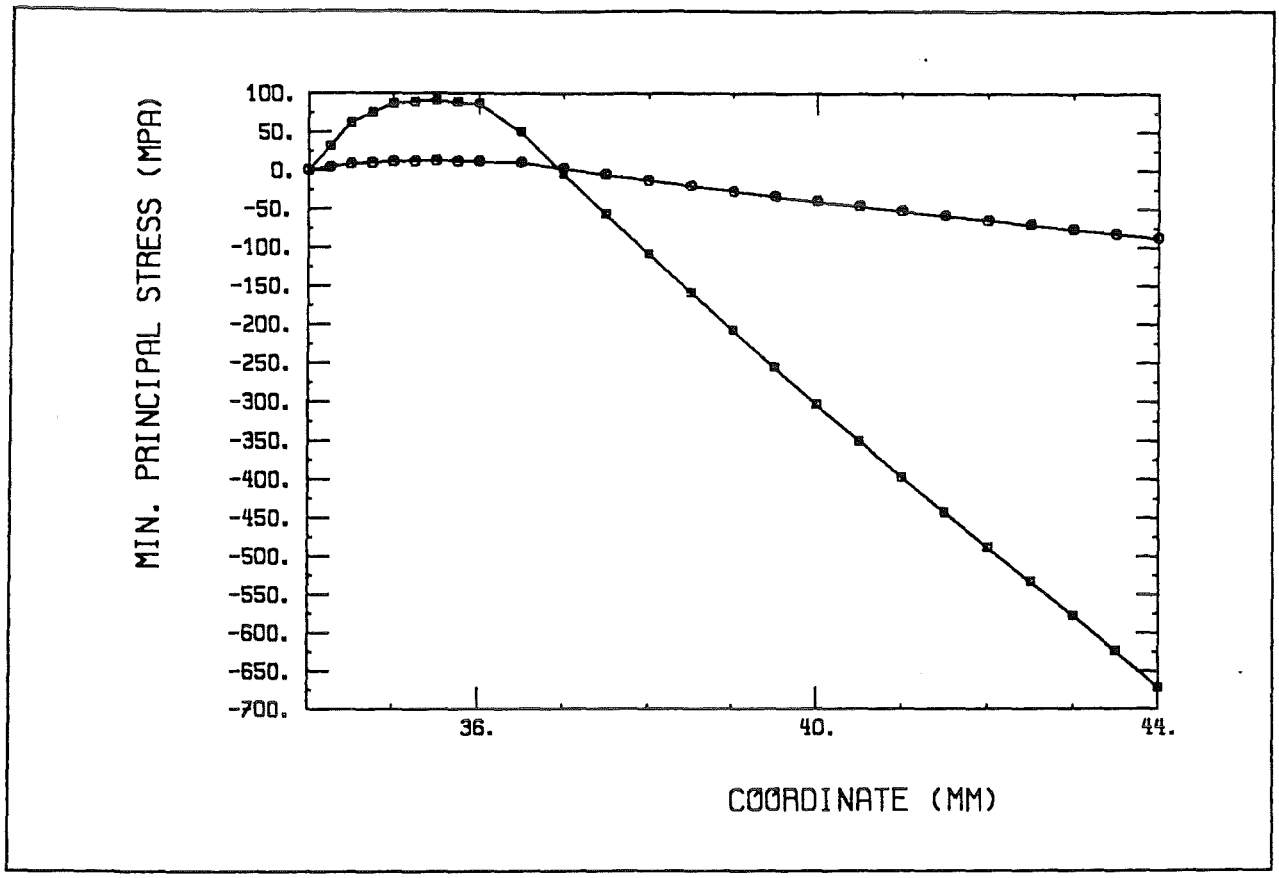

Figure 16. **Results of elastic analysis:** Minimum principal stress along line L1
(□ end of heating, O end of cycle)

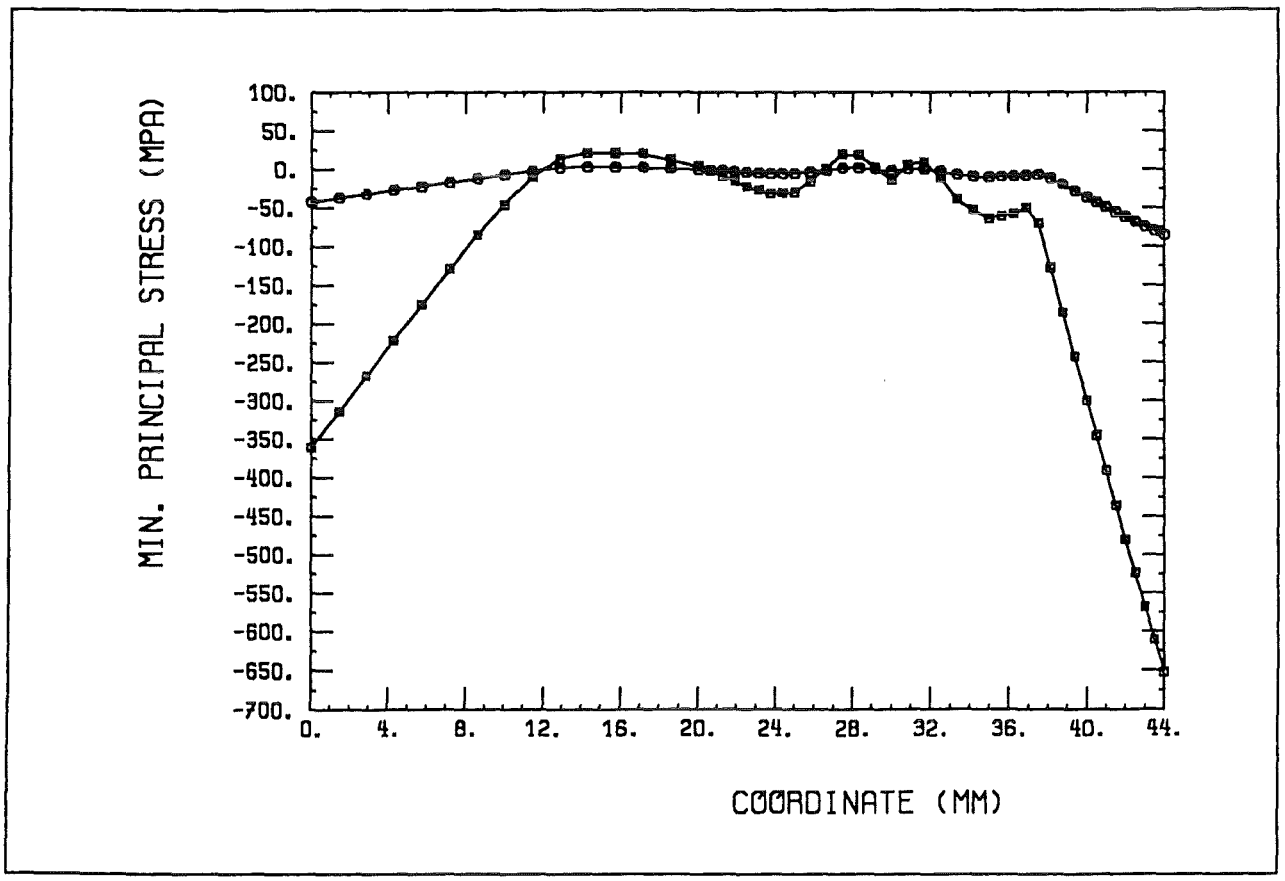

Figure 17. **Results of elastic analysis:** Minimum principal stress along line L2
(□ end of heating, O end of cycle)

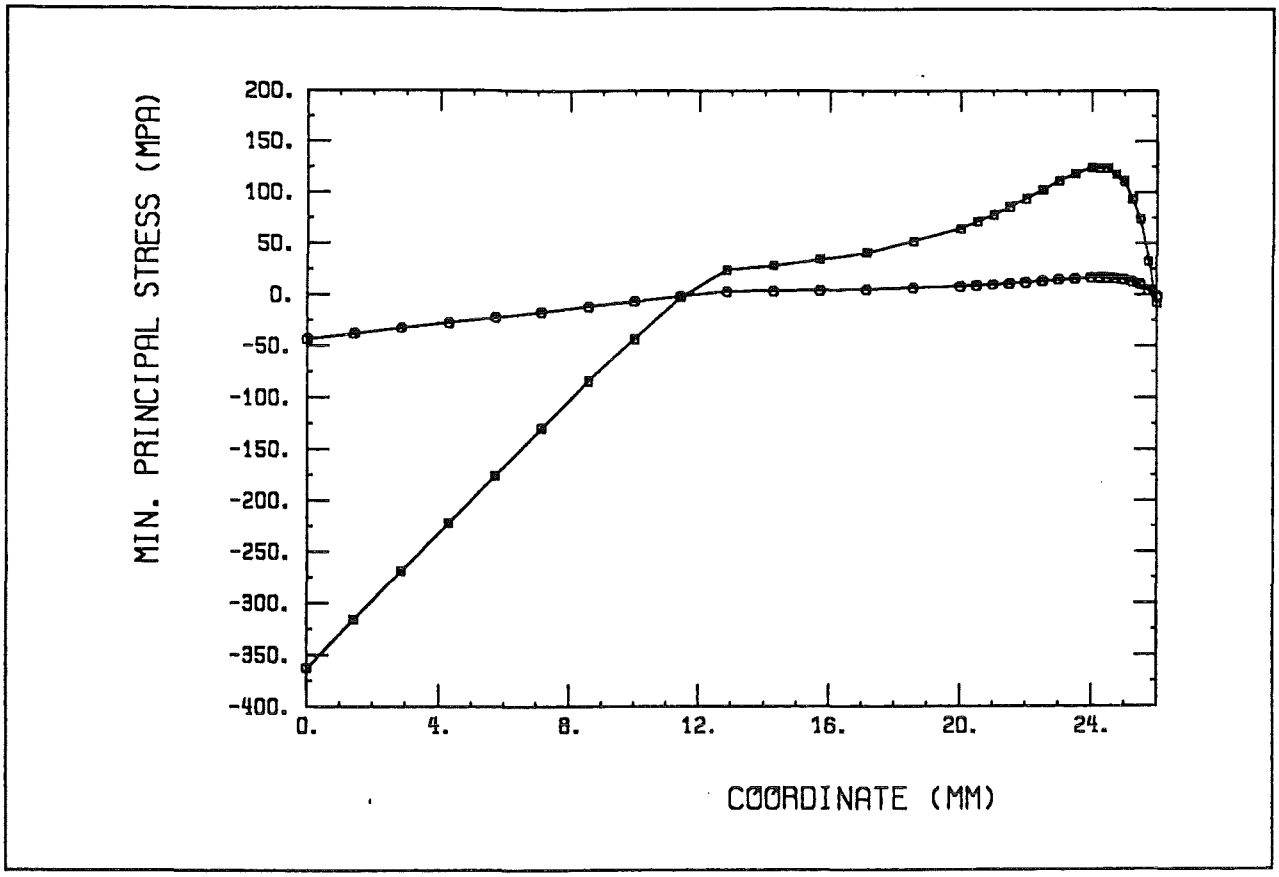

Figure 18. **Results of elastic analysis:** Minimum principal stress along line L3
(□ end of heating, O end of cycle)

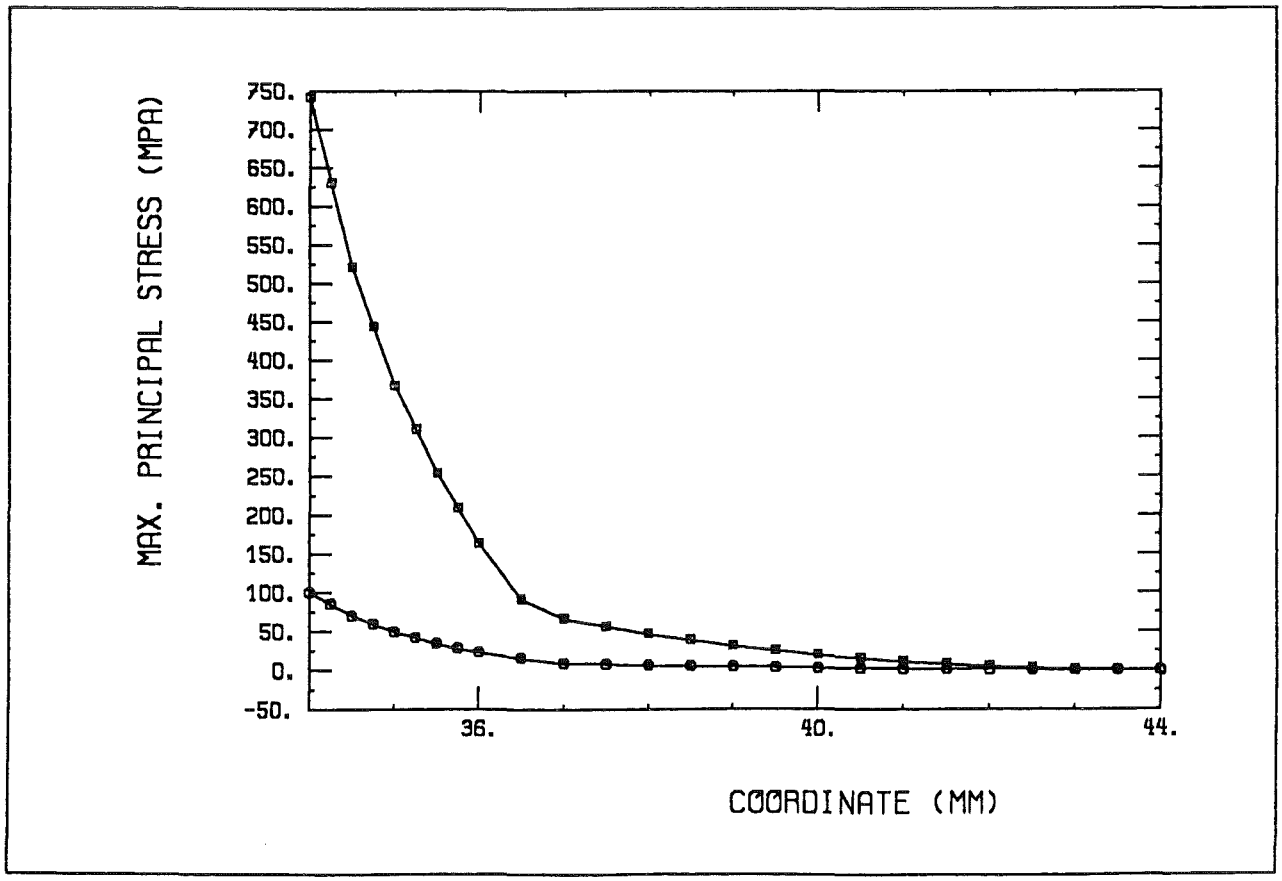

Figure 19. **Results of elastic analysis:** Maximum principal stress along line L1
(□ end of heating, O end of cycle)

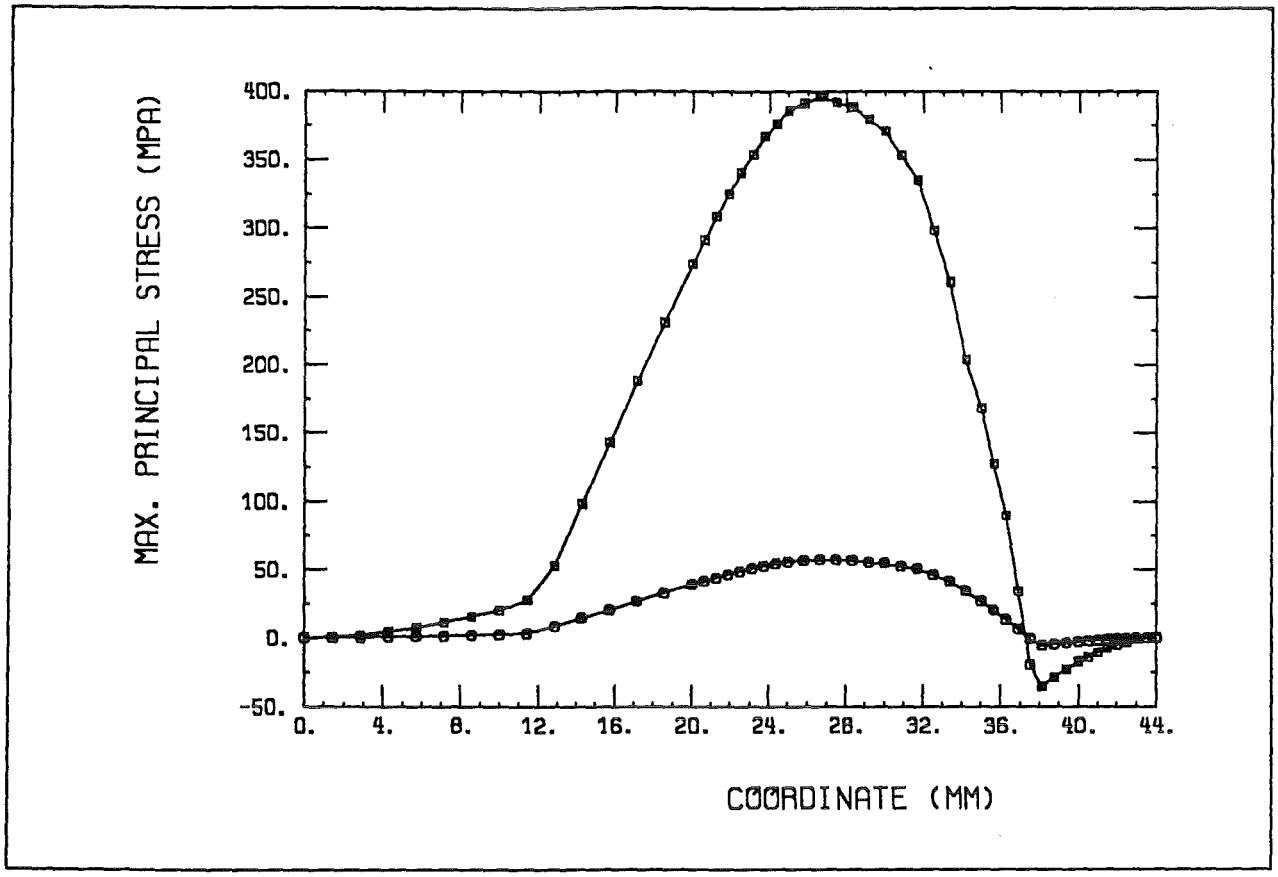

Figure 20. **Results of elastic analysis:** Maximum principal stress along line L2
(□ end of heating, O end of cycle)

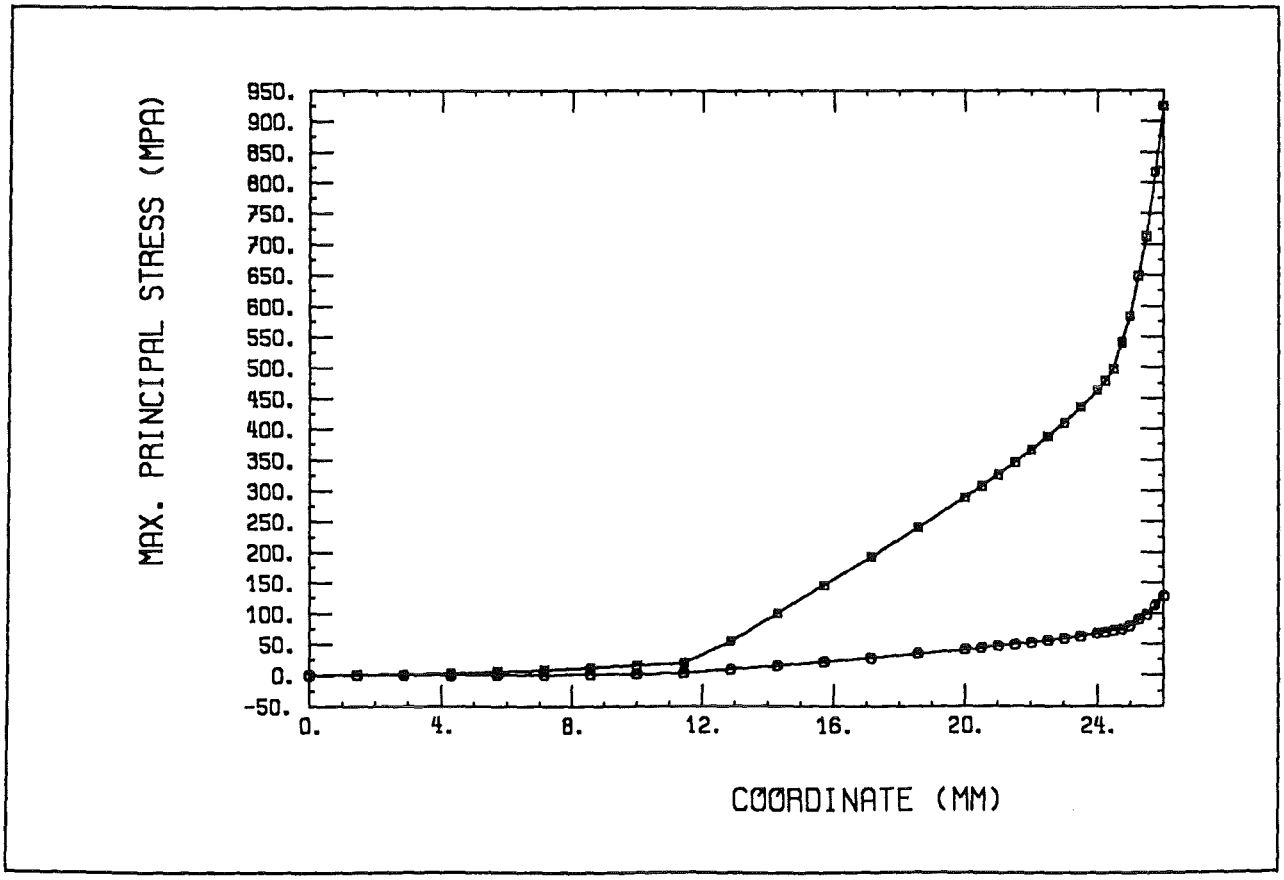

Figure 21. **Results of elastic analysis:** Maximum principal stress along line L3
(□ end of heating, O end of cycle)

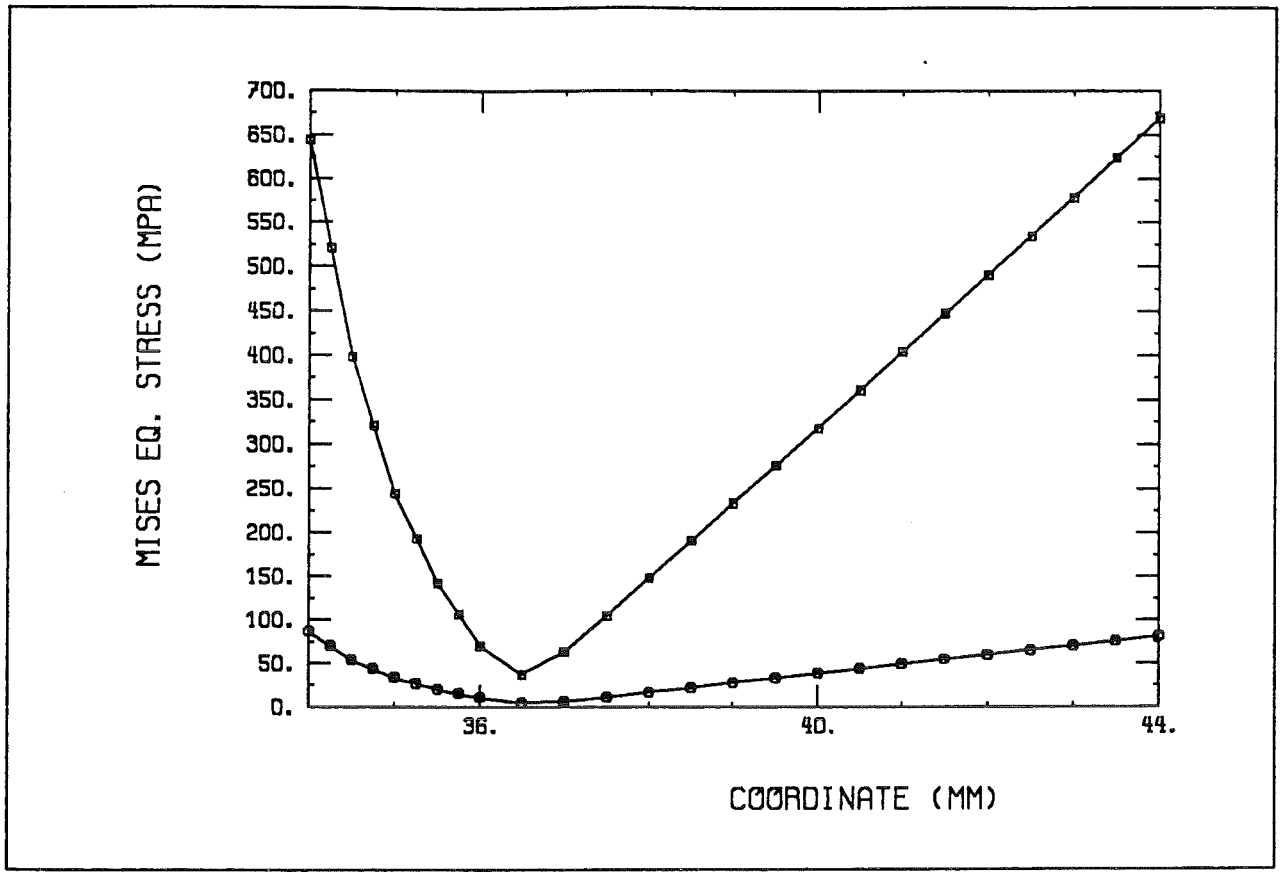

Figure 22. **Results of elastic analysis:** Von Mises equivalent stress along line L1
(□ end of heating, O end of cycle)

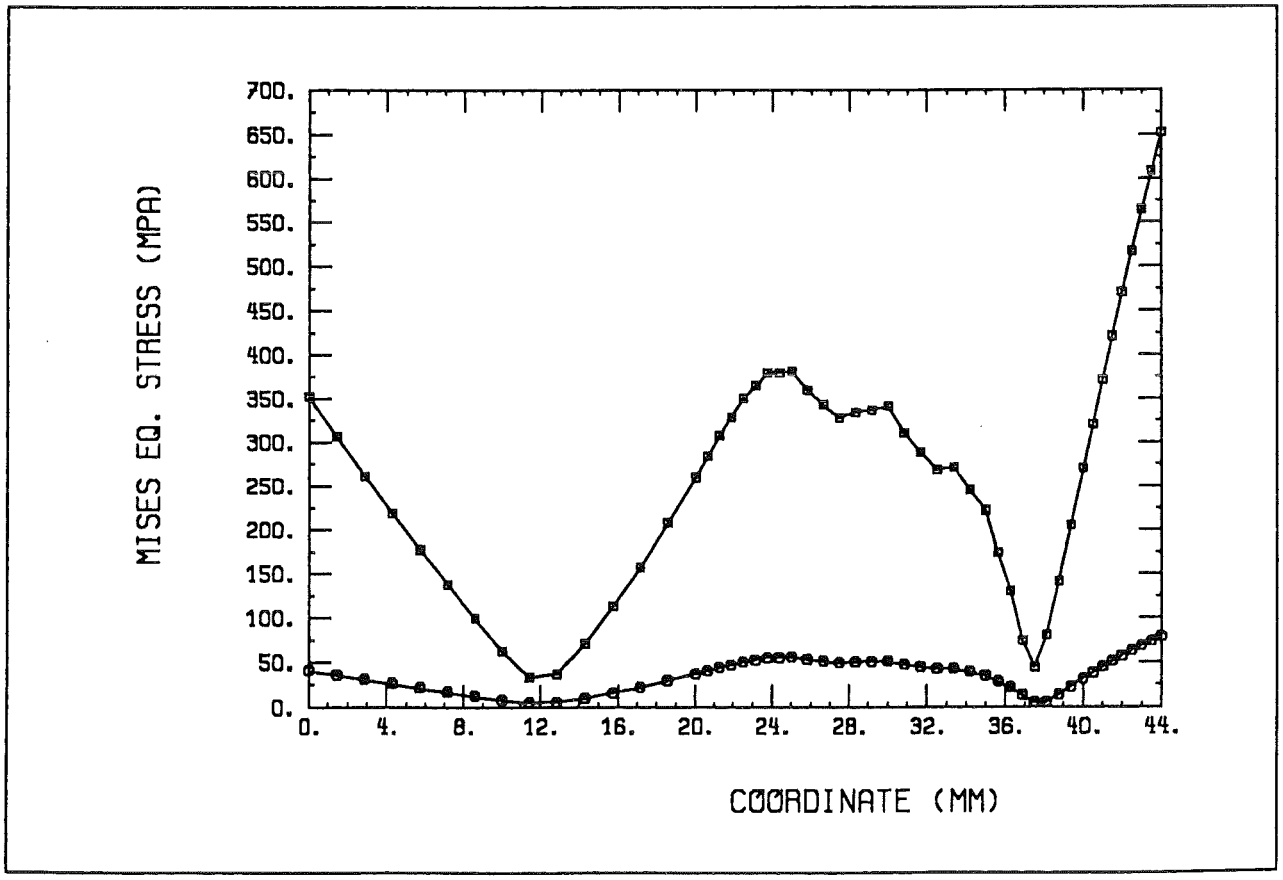

Figure 23. **Results of elastic analysis:** Von Mises equivalent stress along line L2
(□ end of heating, O end of cycle)

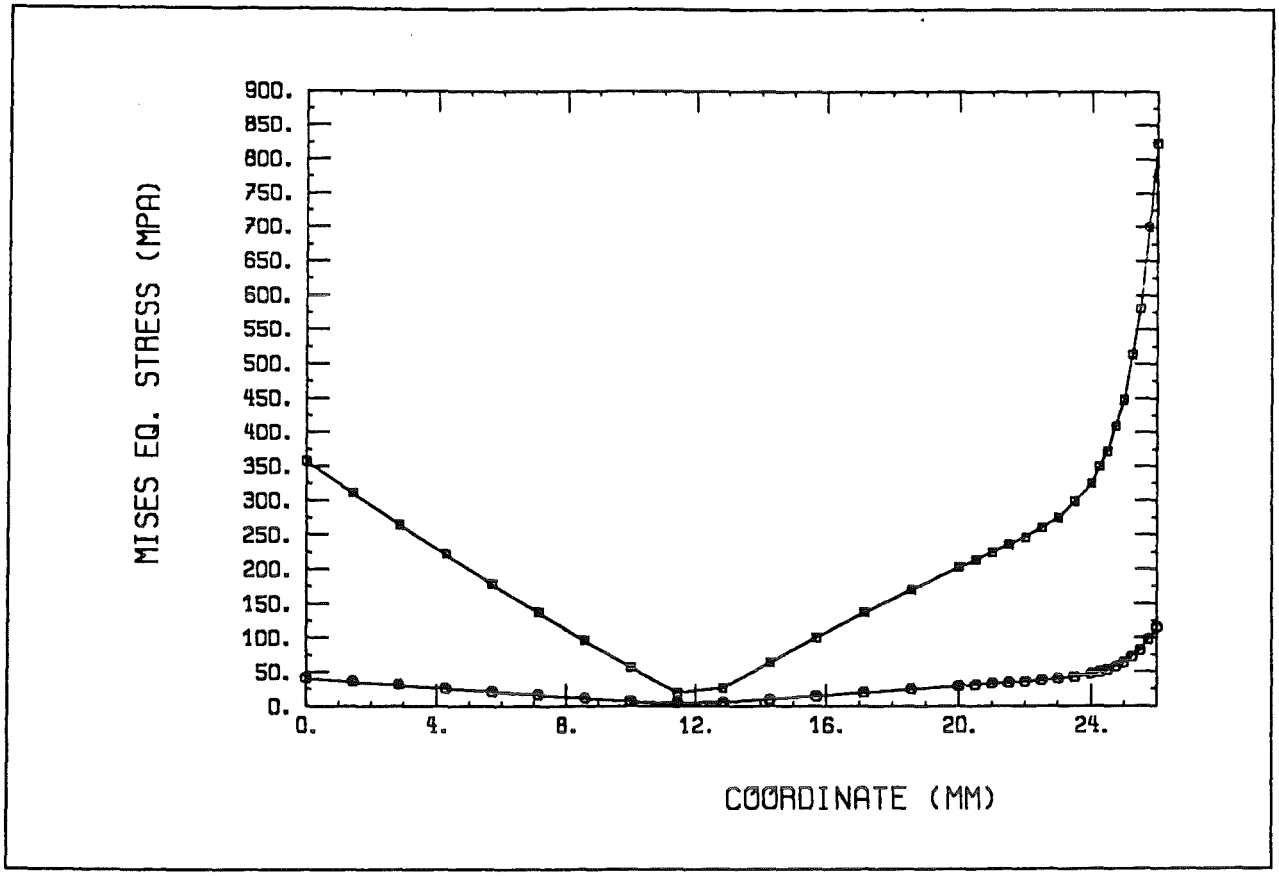

Figure 24. **Results of elastic analysis:** Von Mises equivalent stress along line L3
(□ end of heating, O end of cycle)

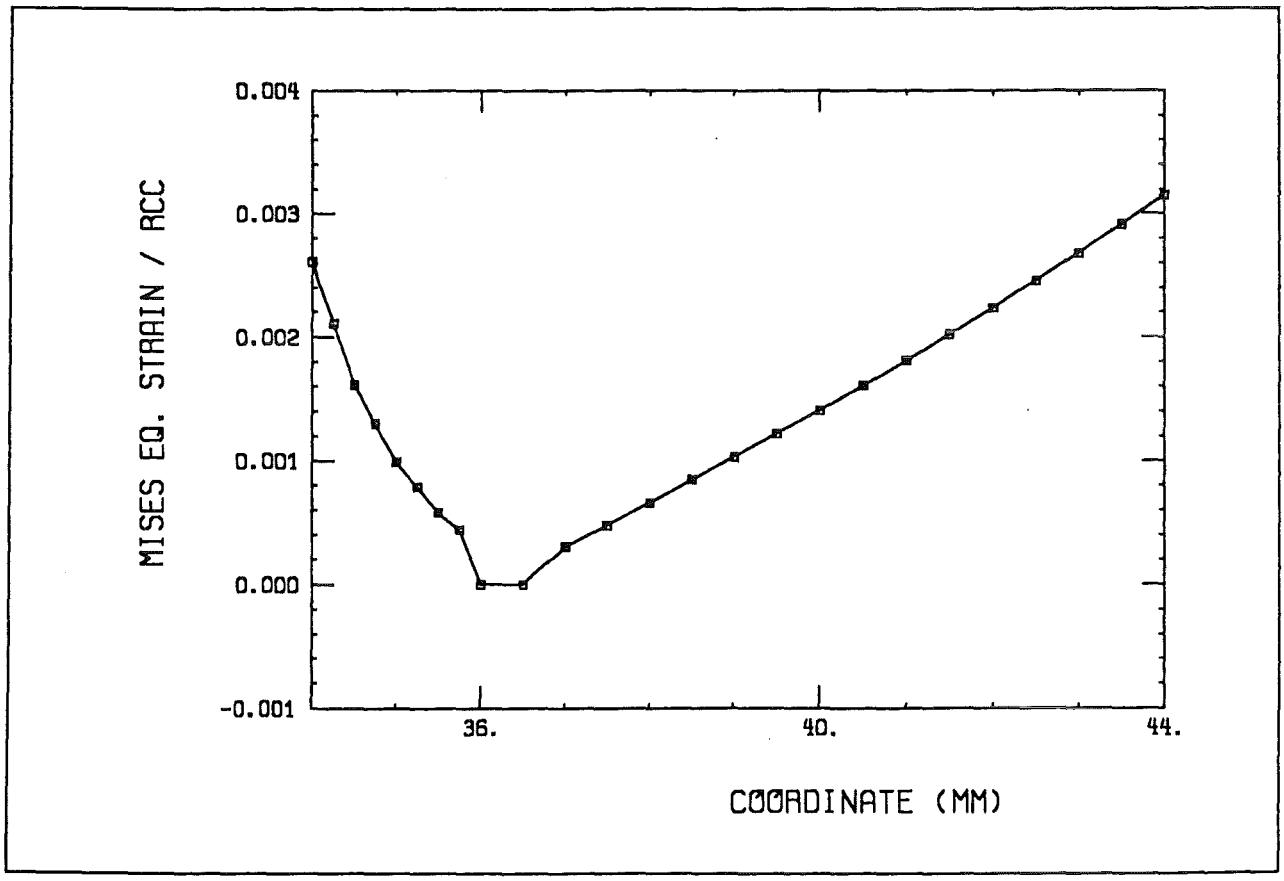

Figure 25. **Results of elastic analysis:** Von Mises equivalent mechanical strain along line L1

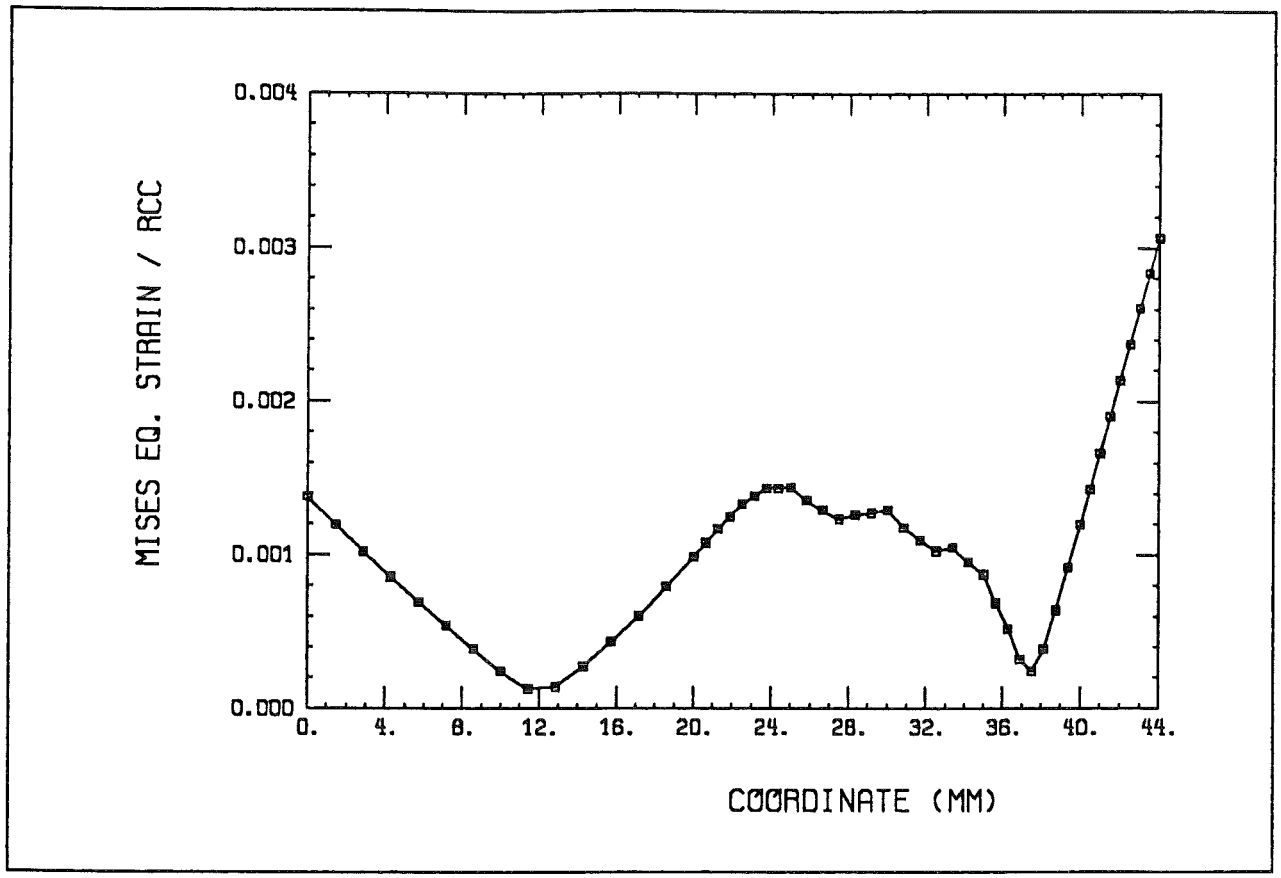

Figure 26. Results of elastic analysis: Von Mises equivalent mechanical strain along line L2

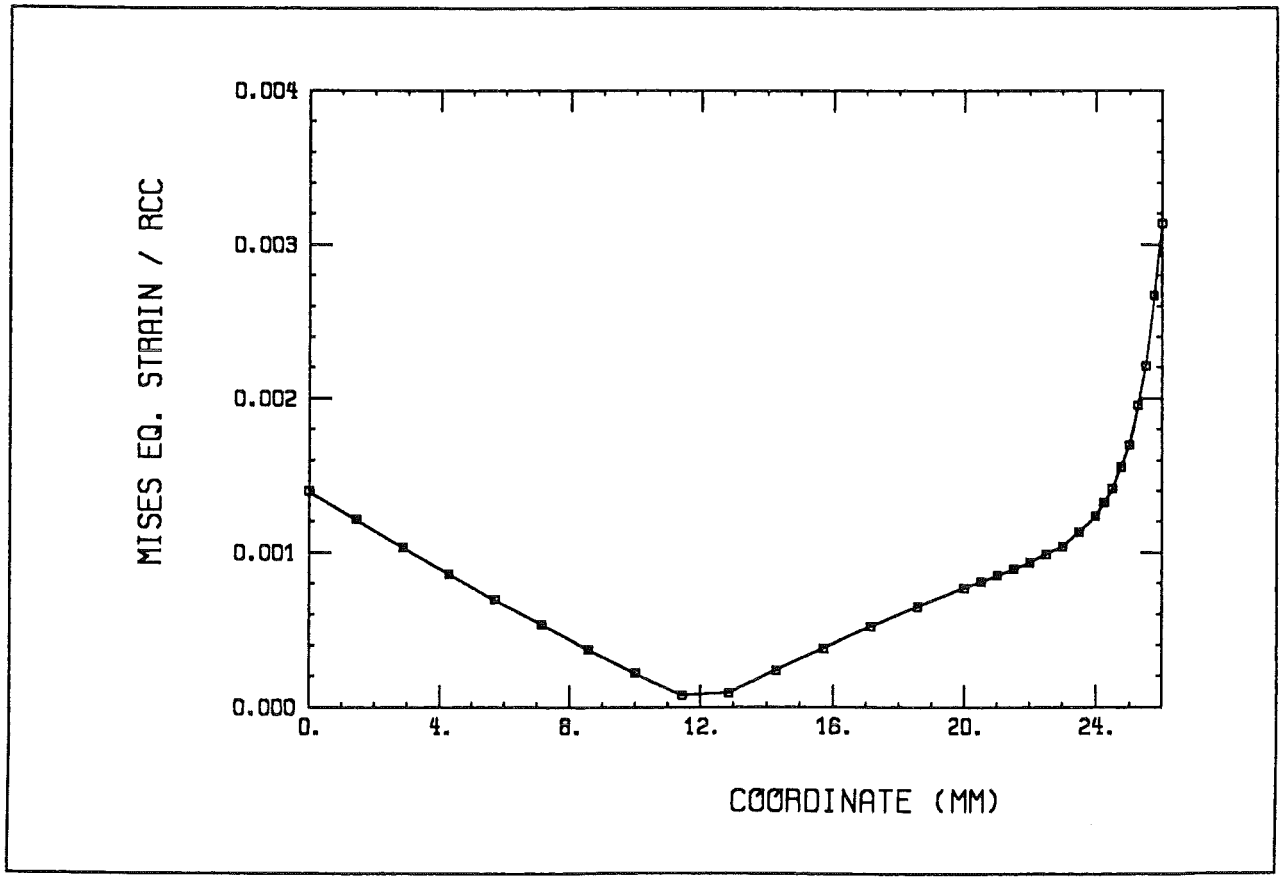

Figure 27. Results of elastic analysis: Von Mises equivalent mechanical strain along line L3

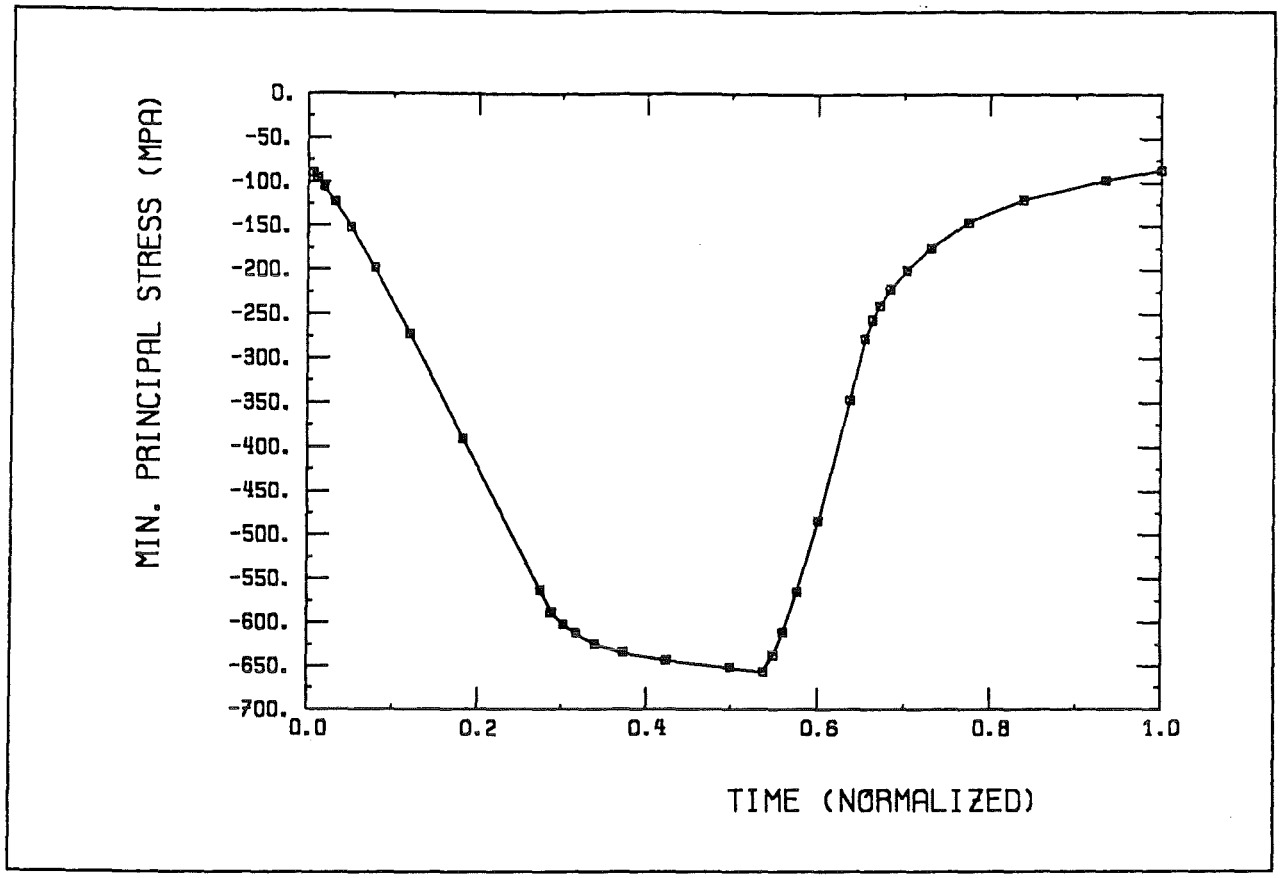

Figure 28. Results of elastic analysis: History plot of minimum principal stress at point F

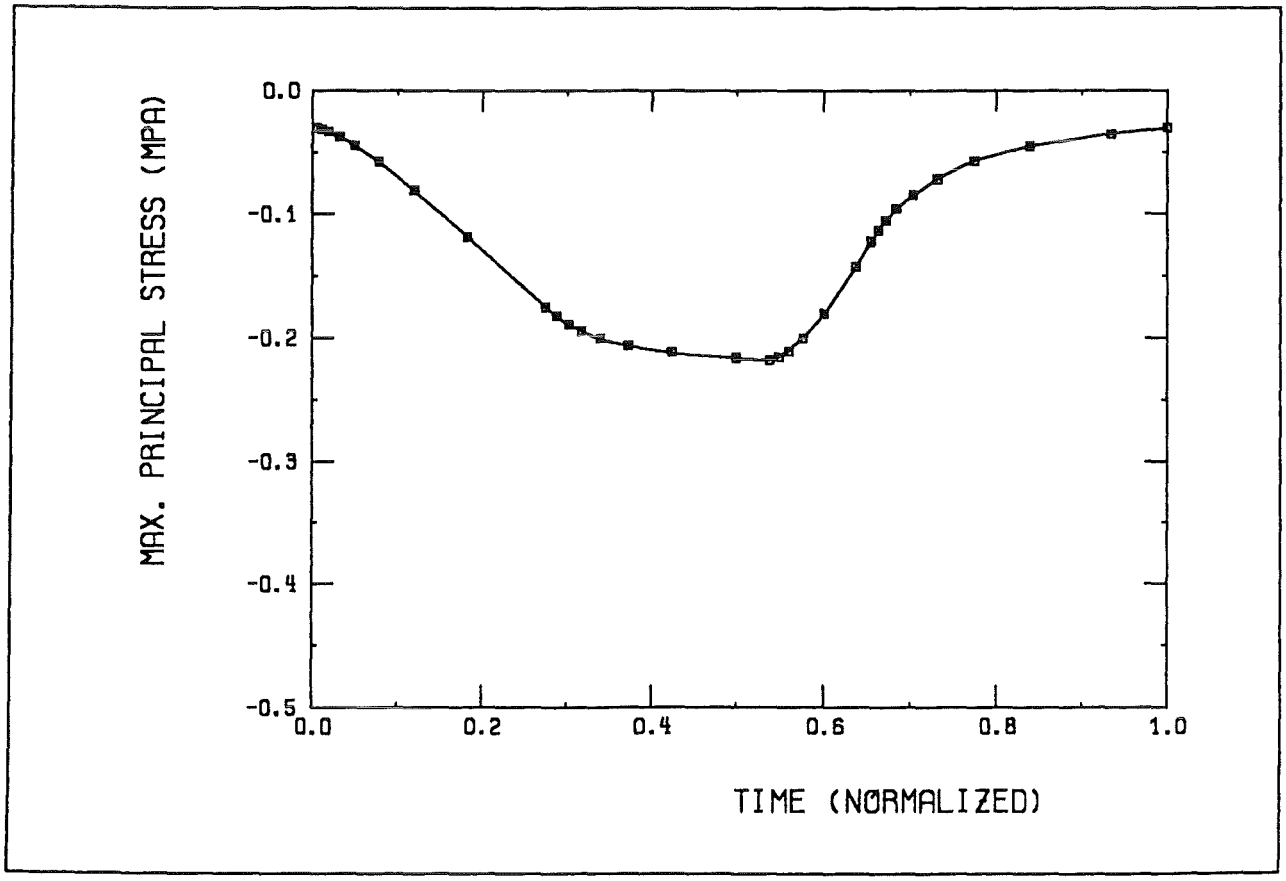

Figure 29. Results of elastic analysis: History plot of maximum principal stress at point F

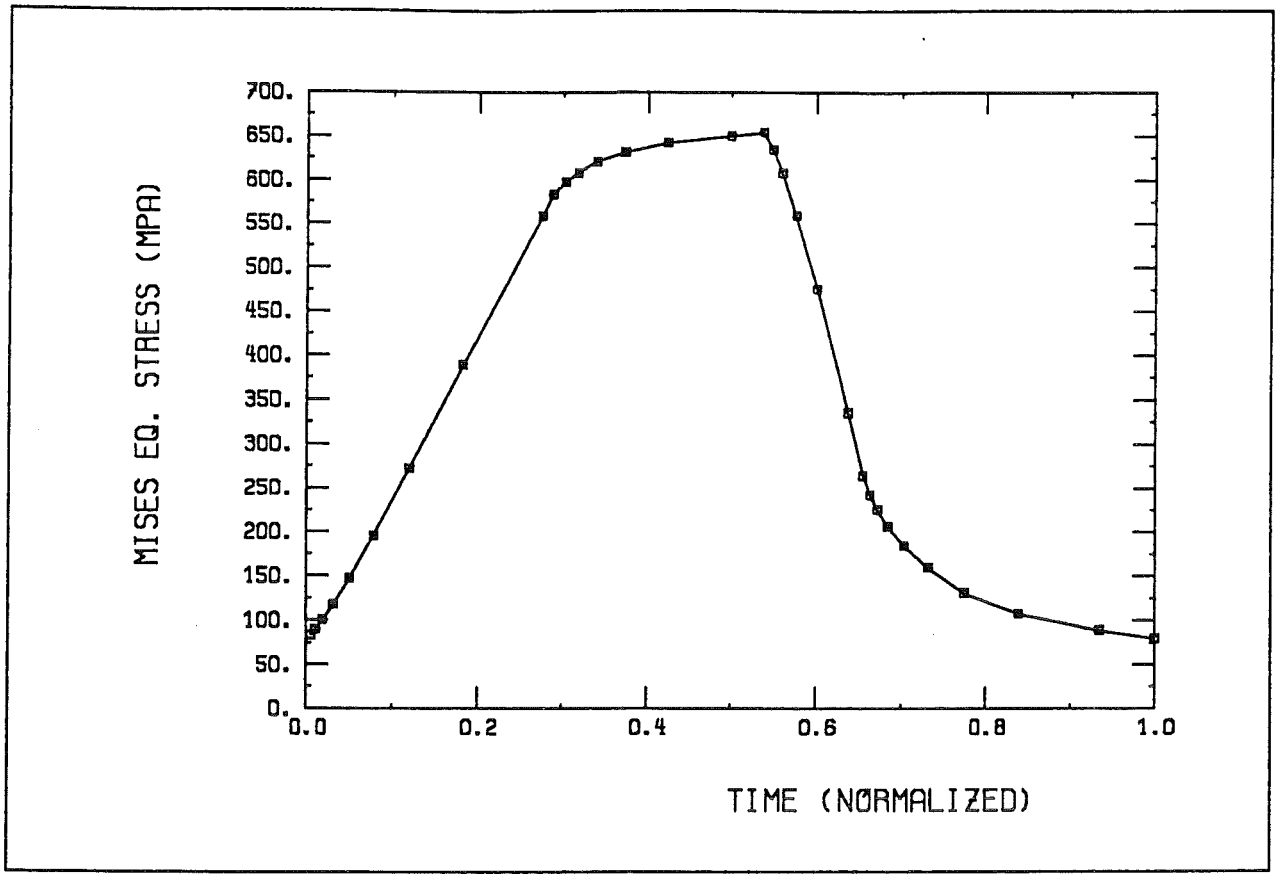

Figure 30. **Results of elastic analysis:** History plot of von Mises equivalent stress at point F

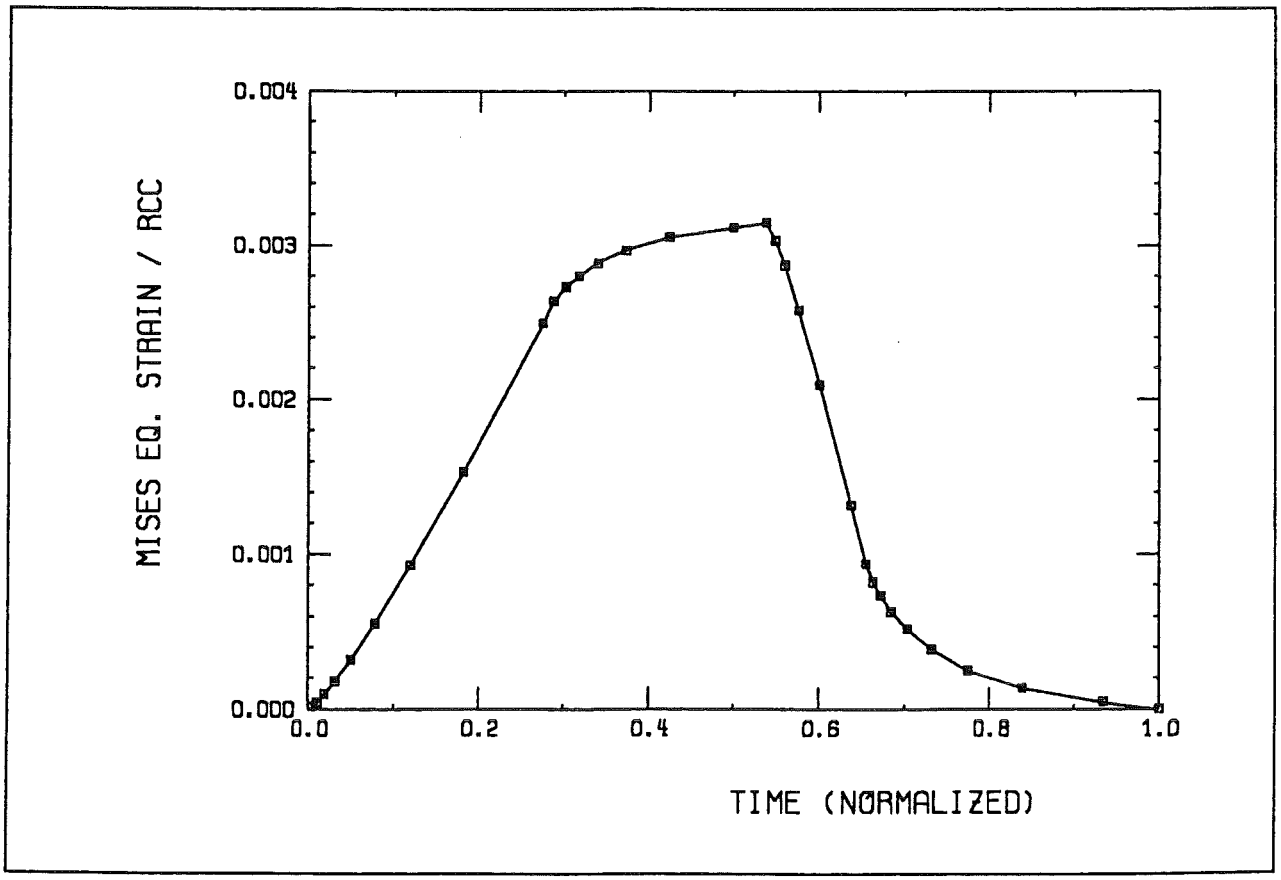

Figure 31. **Results of elastic analysis:** History plot of von Mises equivalent strain at point F

4. Elasto-plastic analysis

Plastic calculations have been performed by

- considering four cycles following the temperature history increment by increment,

- using the simplified linearized ORNL plasticity model (O66) as described in section 2, i.e.:

- applying the plasticity yield concept with the yield surface being defined by von Mises' criteria,

- decomposing the strain into an elastic part and a plastic part

$$\varepsilon_{mechanical} = \varepsilon_{elastic} + \varepsilon_{plastic} = \frac{\sigma}{E} + \varepsilon_{plastic}$$

$$\varepsilon_{total} = \varepsilon_{mechanical} + \varepsilon_{thermal}$$

- assuming isotropic hardening and

- kinematic hardening (variable yield surface), respectively.

- Two alternative plasticity models (M) and (C) have been taken into account:

  (M) uses the **monotonic** tension curves at 9 temperatures (20°C - 500°C) in a linearized form.

  (C) uses the **cyclic** tension curves at 3 temperatures (20°C, 450°C, 500°C) in a linearized form.

The model (M) has to be considered as a constitutive law resulting in conservative values in the sense that plastic strains will be overestimated, whereas stresses are undervalued.

Here are reported results calculated by means of model (O66). In Appendix 1, the influence of the material model on the predicted life will be outlined in order to quantify possible sources of error.

Anyway, the ORNL material model will give conservative lower bounds on the strain range, and, consequently also in terms of number of cycles to failure:
Within a bilinear representation of the nonlinaer kinematic hardening as required by the ORNL recommendations, the stress at maximum strain is underestimated. Under thermo-mechanical mechanical loading conditions, this is compensated by an increase in the local straining of the component.

Main results of elasto-plastic analysis

In table 6 an overview on the maximum and minimum stress levels at point F and point C is given.

Results [*MPa*]	Point (F)	Point (C)
von Mises stresses, at end of burn	192.1 MPa	248.6 MPa
von Mises stresses, at end of cycle	177.8 MPa	195.4 MPa
Mininum principal stress	-194.0 MPa	-216.7 MPa
Maximum principal stress	182.2 MPa	279.0 MPa
Mechanical strain range	.424 %	.436 %
Plastic strain range	.239 %	.236 %

Table 6: Overview on results of elasto-plastic calculations

Discussion of results:

At end of burn there are

tensile stresses (all tensorial components) near the coolant,
compressive stresses (all tensorial components) at the heated front part, where mainly the maximum (compressive) stresses are situated,
compressive stresses at the rear side.

At end of the thermal cycle there are

compressive stresses near the cooling tubes,
tensile stresses at the front and back of the wall.

- Stresses are higher near coolant tubes than at the heated surface. This is mainly due to the temperature dependance of the material data, e.g. the yield strength is strongly temperature dependent.
- The strain range is mainly influenced by the temperature difference $\varepsilon \simeq \alpha (T - \overline{T})$.
- The strain range of, both, the mechanical equivalent strain and the plastic equivalent strain, are of the same order of magnitude at the points F and C. At point F, significantly higher temperatures are reached within the load cycle. Therefore, the point F has to be considered as the most severe location in terms of cycle to failure, and point F is equivalent to point F.

List of results and figures

The results are listed in the tables of Appendix 5.

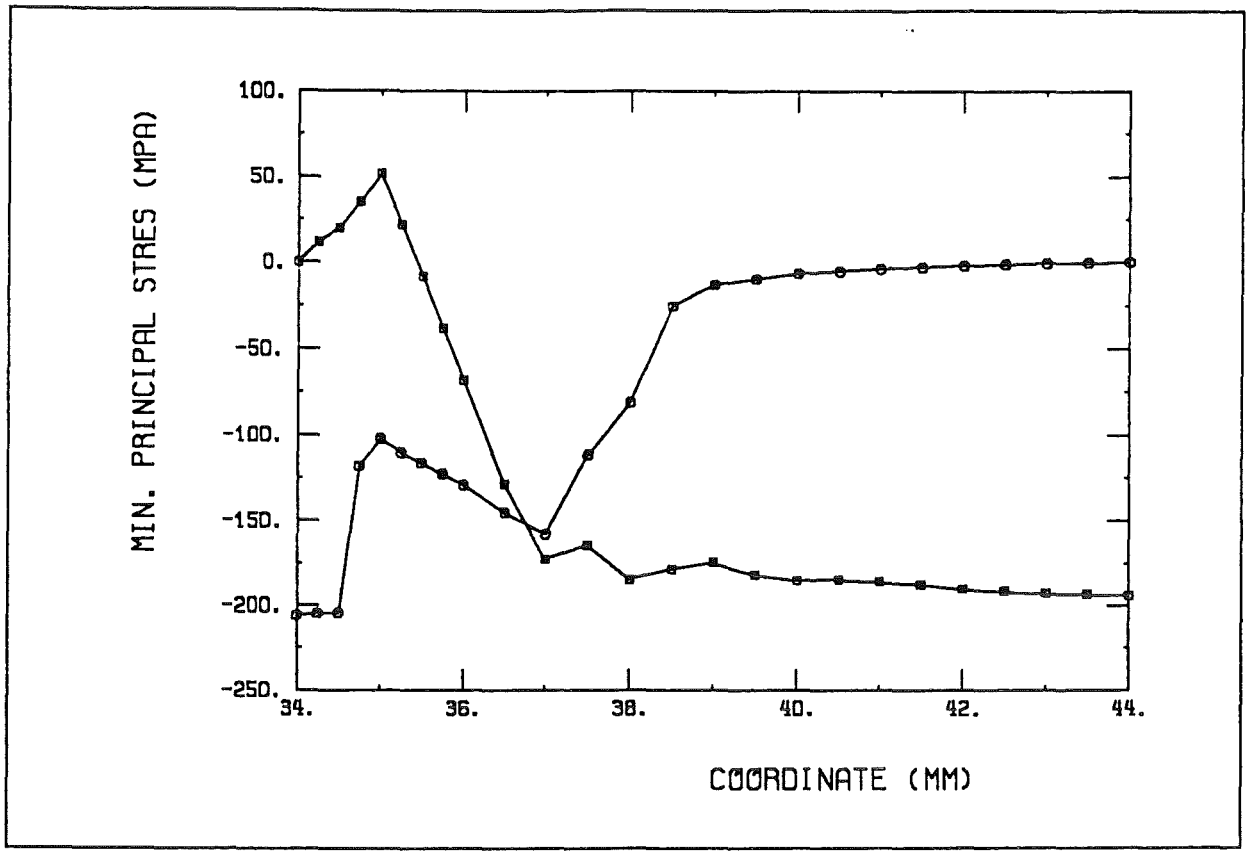

Figure 32. **Results of elasto-plastic analysis:** Minimum principal stress along line L1
(□ end of heating, O end of cycle)

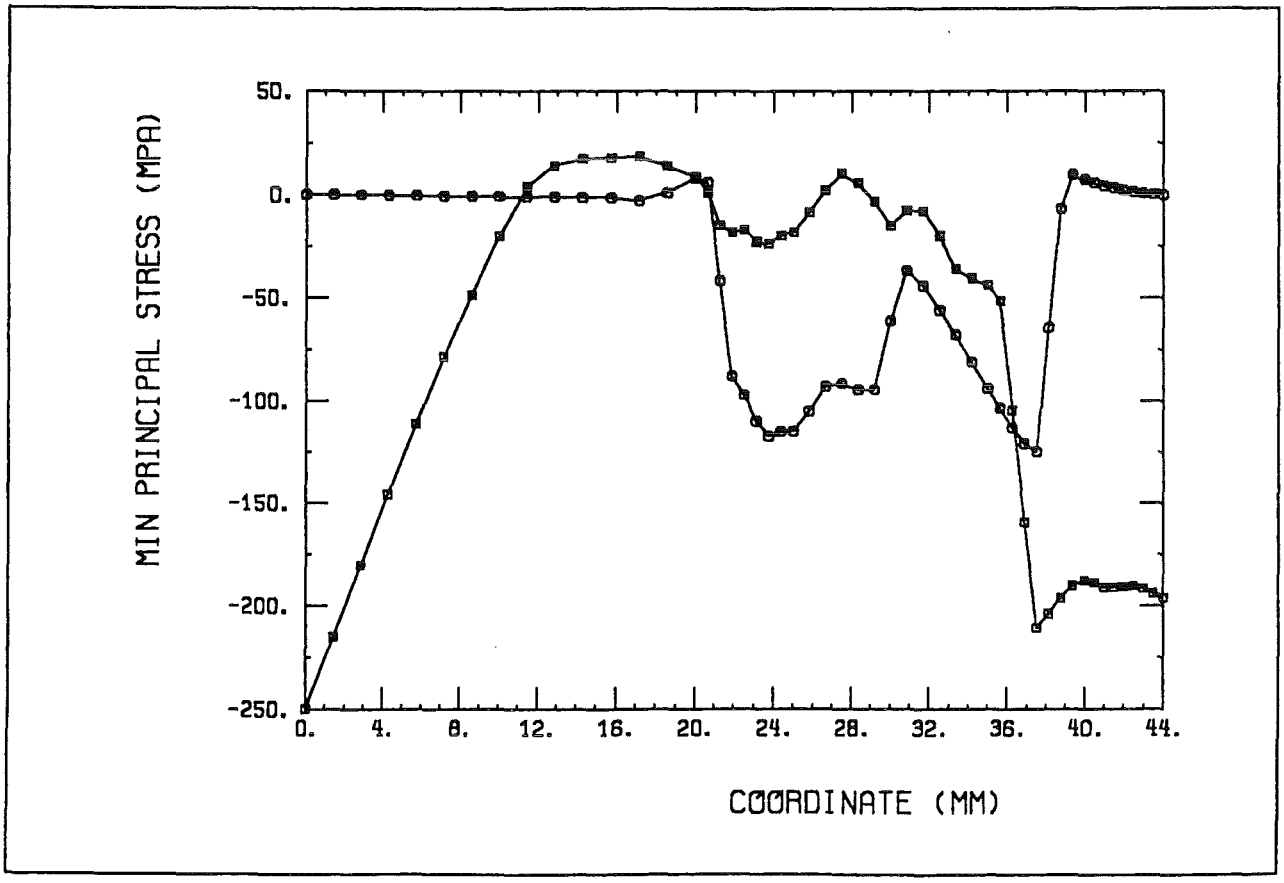

Figure 33. **Results of elasto-plastic analysis:** Minimum principal stress along line L2
(□ end of heating, O end of cycle)

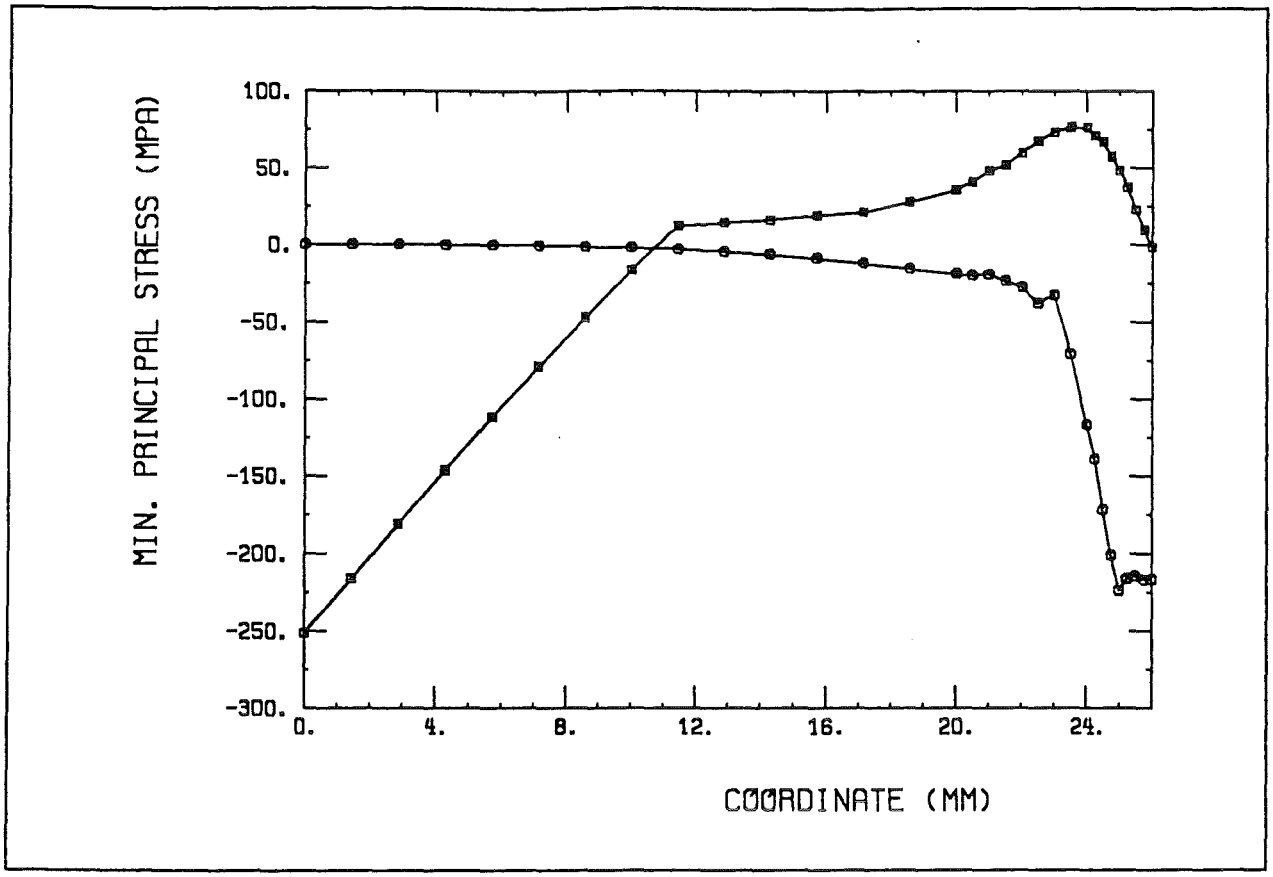

Figure 34. **Results of elasto-plastic analysis:** Minimum principal stress along line L3
(□ end of heating, O end of cycle)

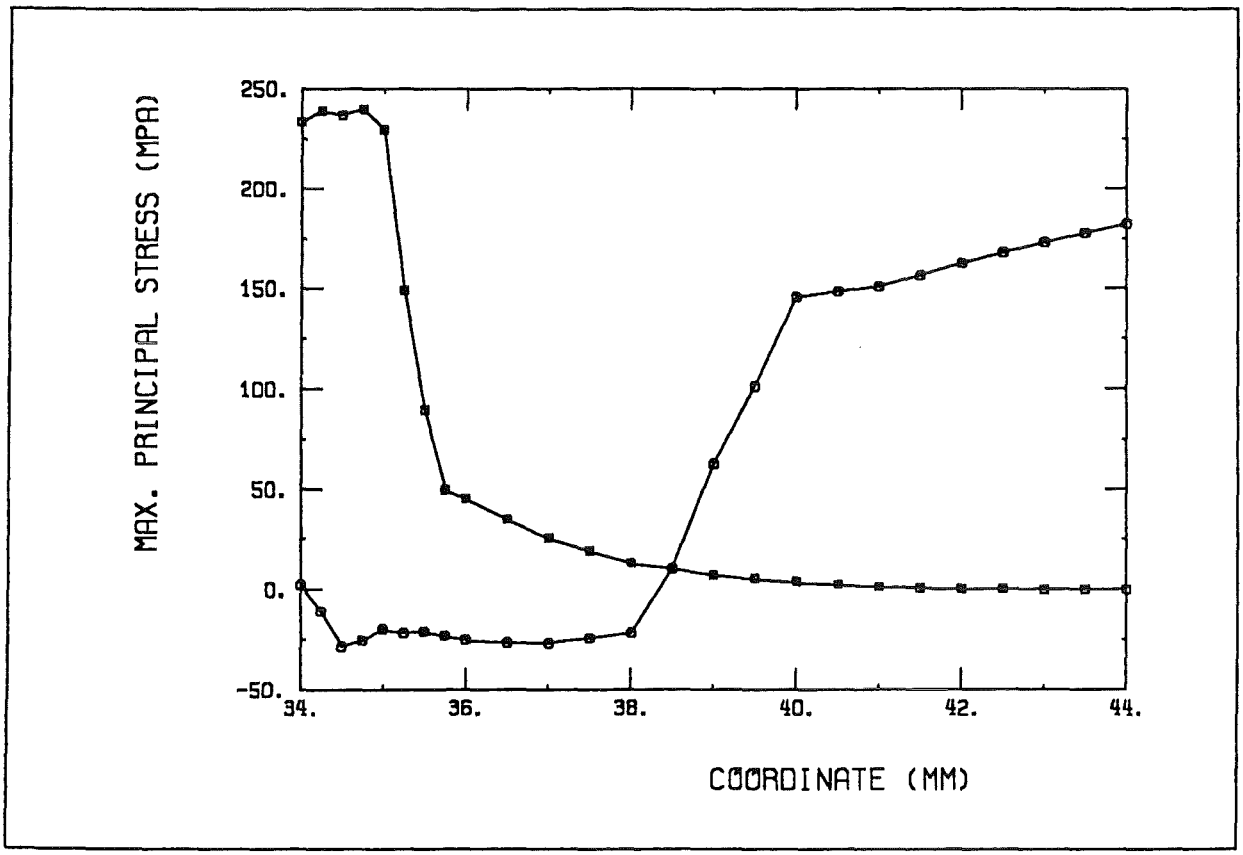

Figure 35. **Results of elasto-plastic analysis:** Maximum principal stress along line L1
(□ end of heating, O end of cycle)

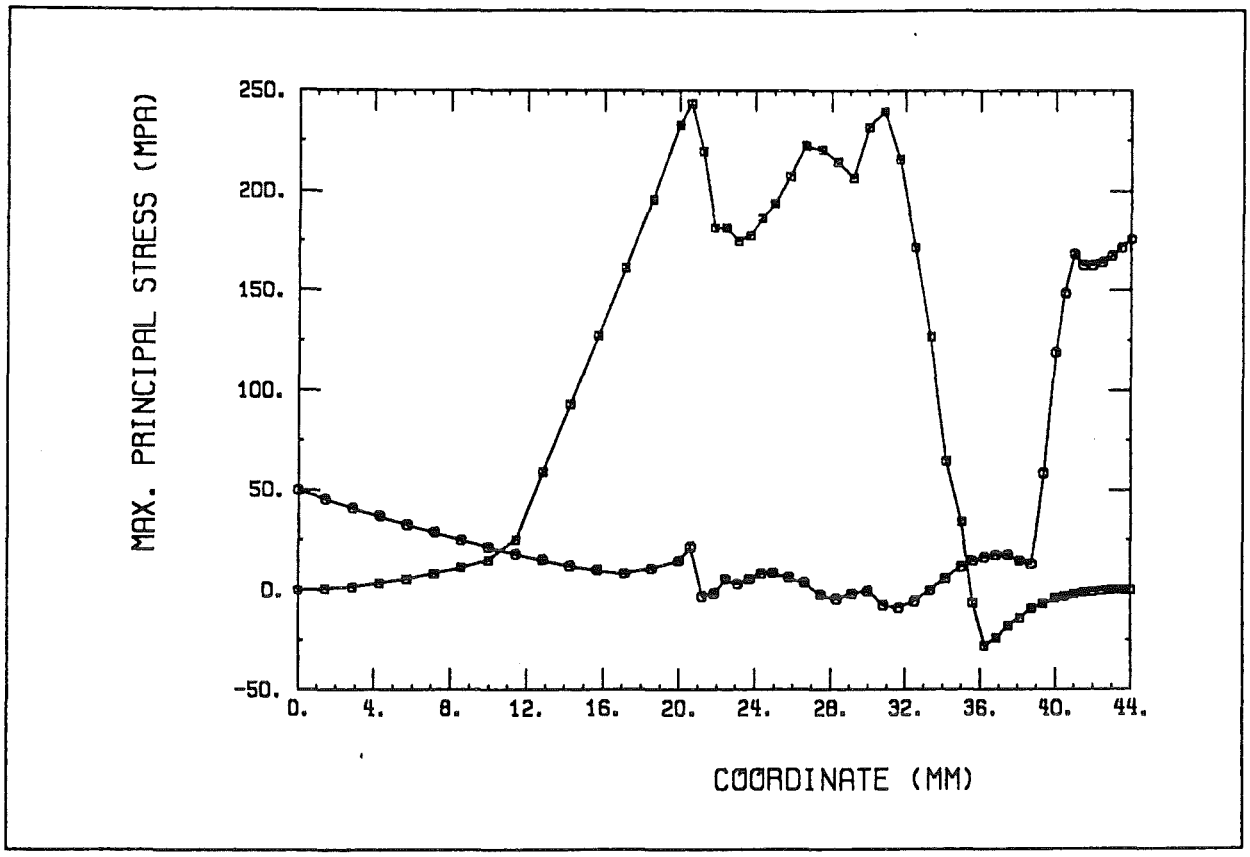

Figure 36. **Results of elasto-plastic analysis:** Maximum principal stress along line L2
(□ end of heating, O end of cycle)

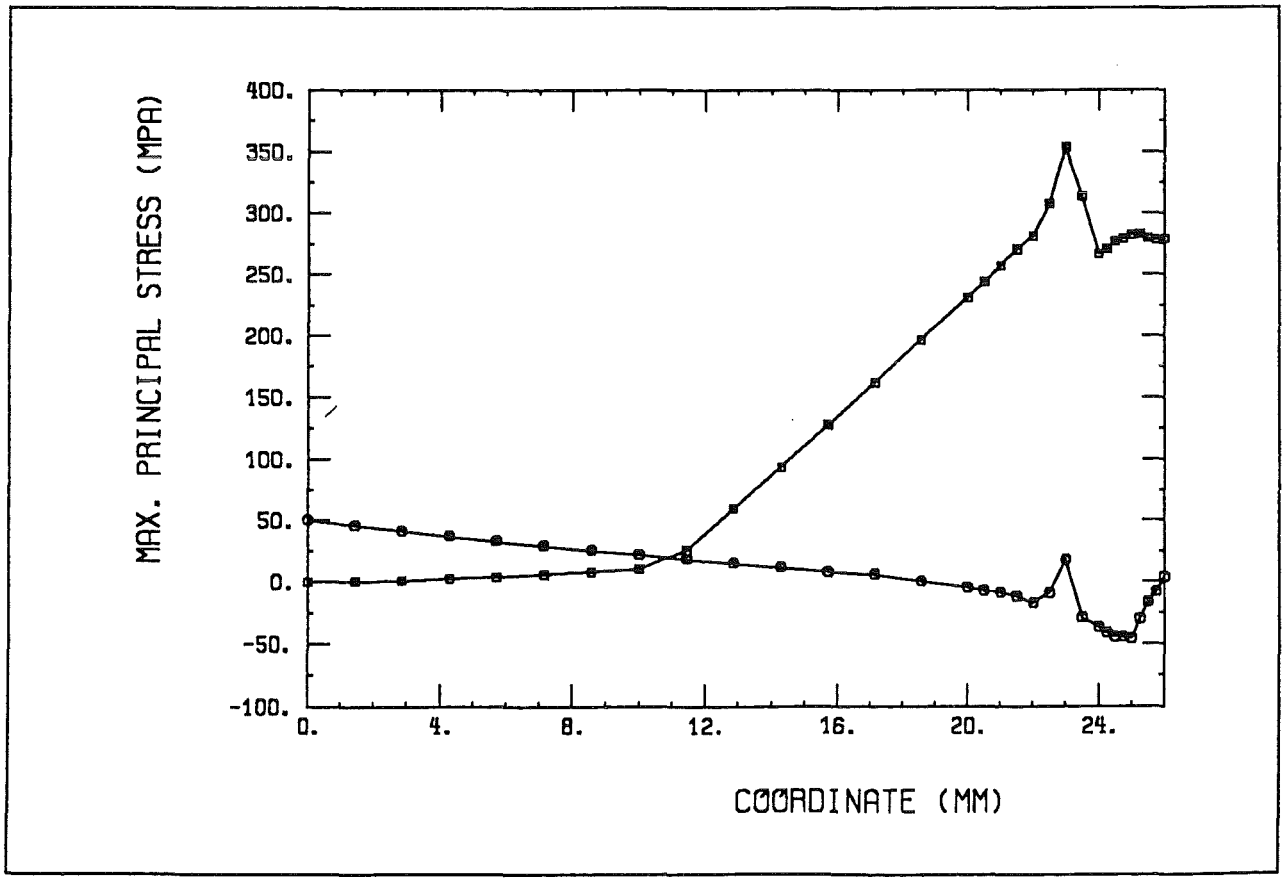

Figure 37. **Results of elasto-plastic analysis:** Maximum principal stress along line L3
(□ end of heating, O end of cycle)

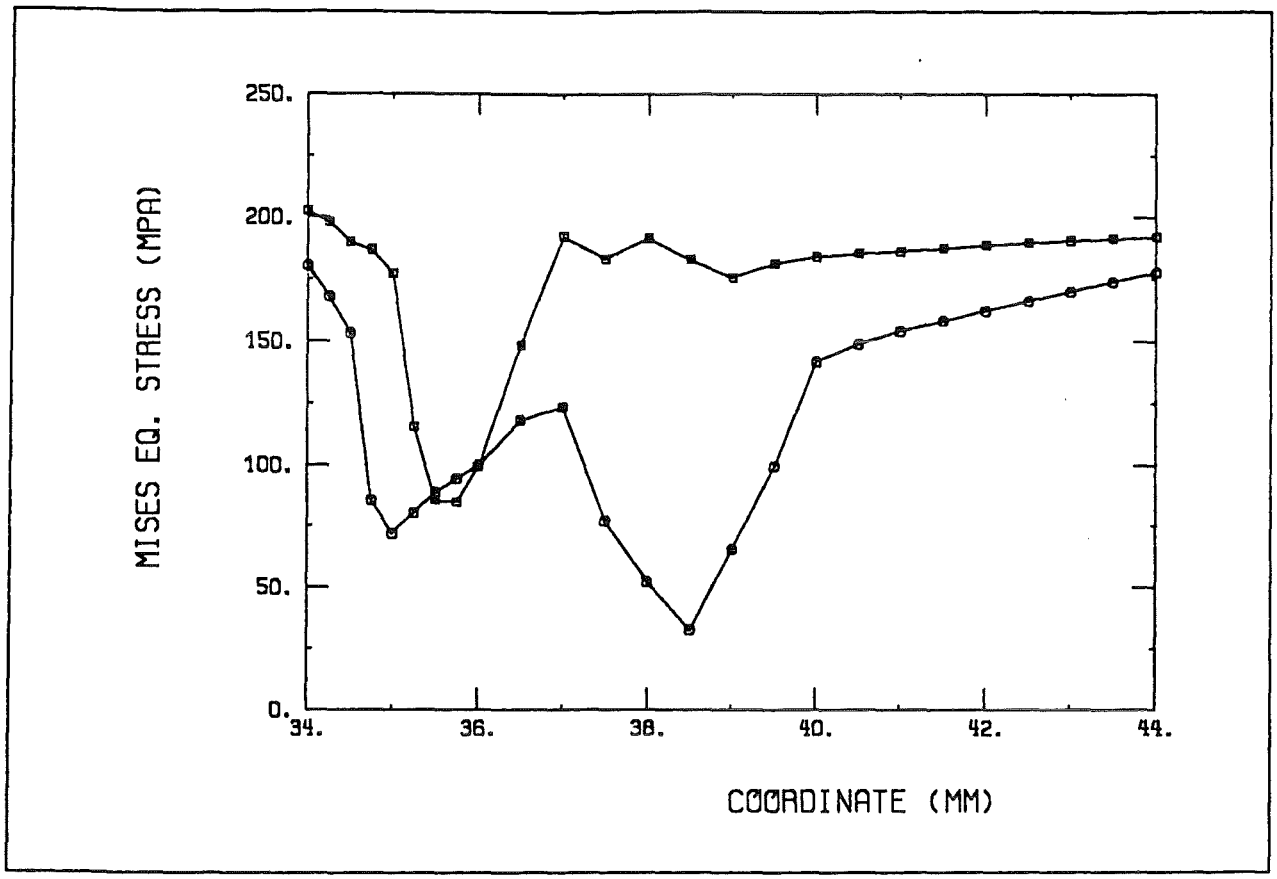

Figure 38. **Results of elasto-plastic analysis:** Von Mises equivalent stress along line L1
(□ end of heating, O end of cycle)

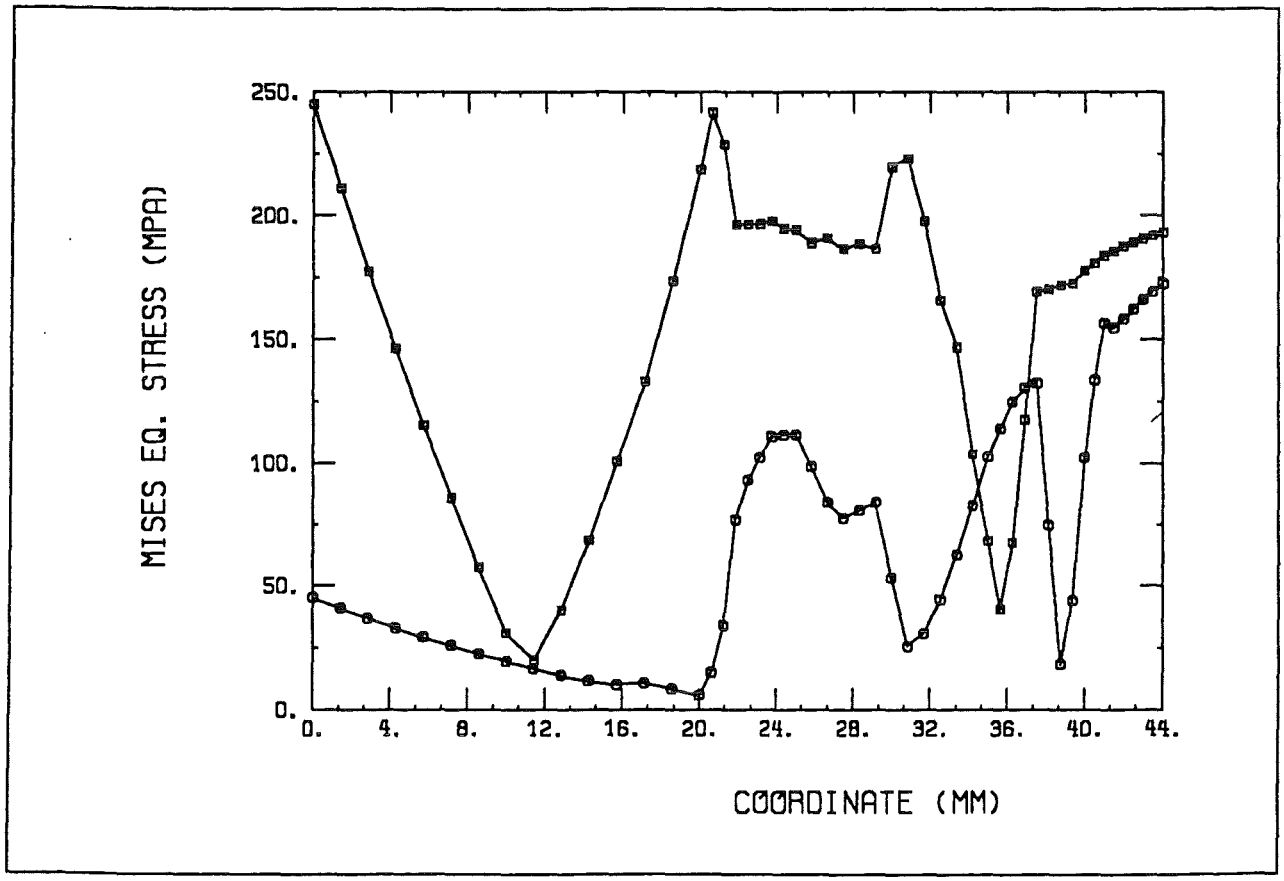

Figure 39. **Results of elasto-plastic analysis:** Von Mises equivalent stress along line L2
(□ end of heating, O end of cycle)

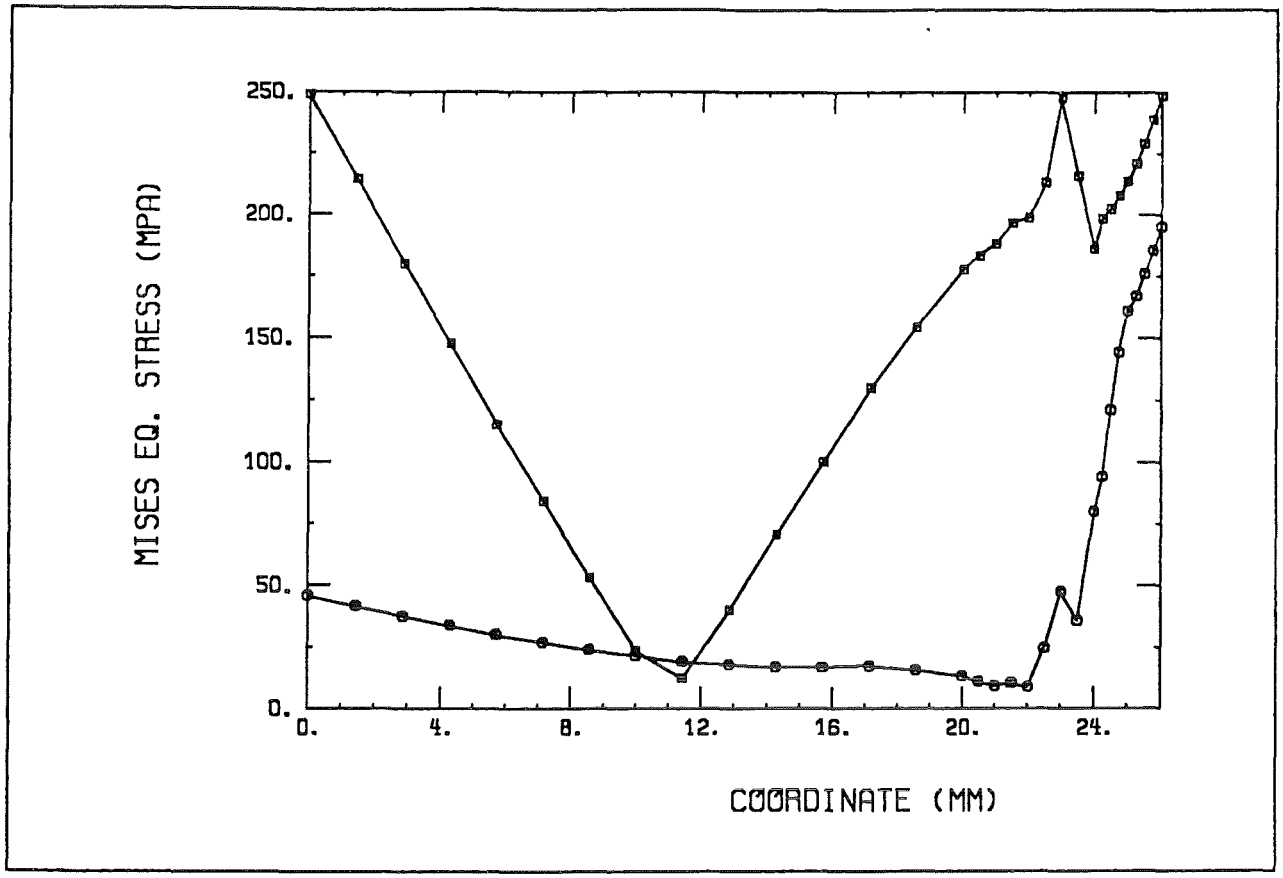

Figure 40. Results of elasto-plastic analysis: Von Mises equivalent stress along line L3 (□ end of heating, O end of cycle)

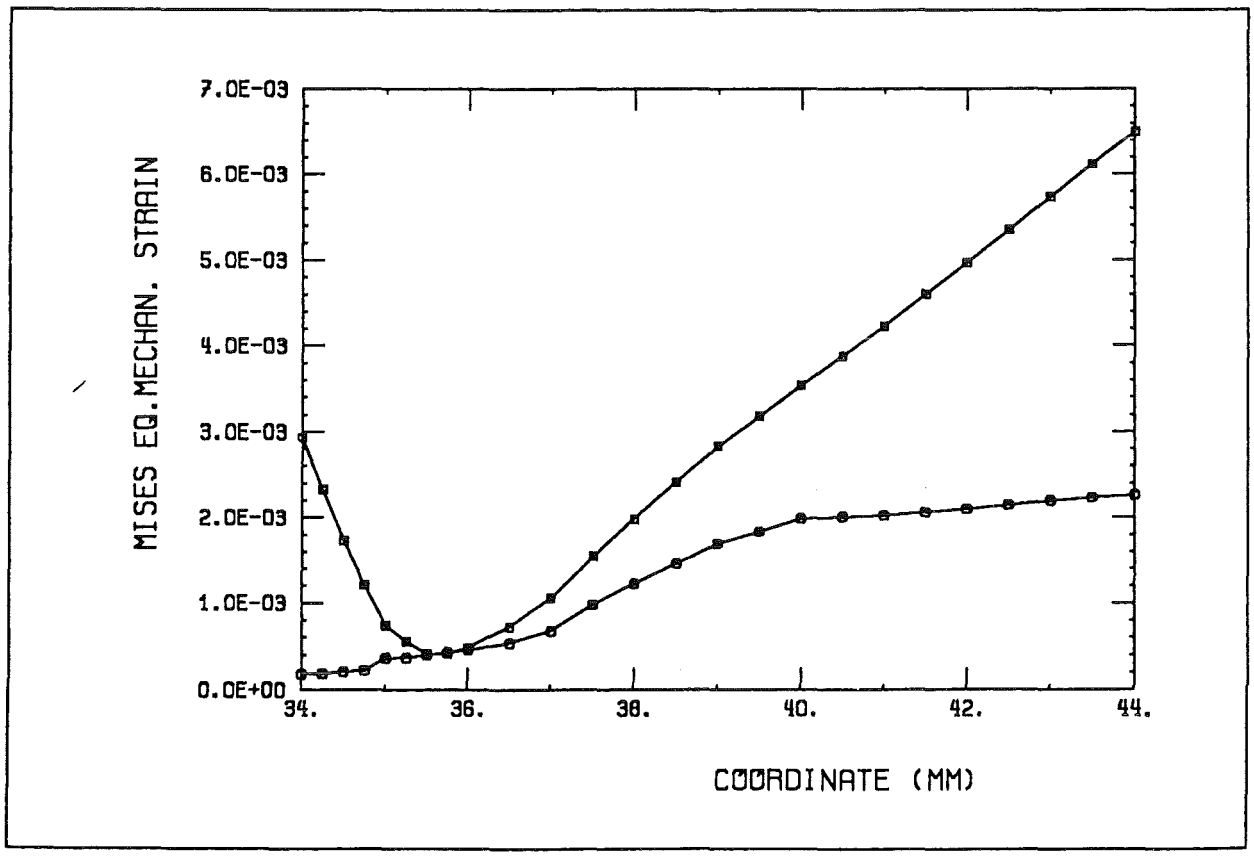

Figure 41. Results of elasto-plastic analysis: Von Mises equivalent mechanical strain along line L1 (□ end of heating, O end of cycle)

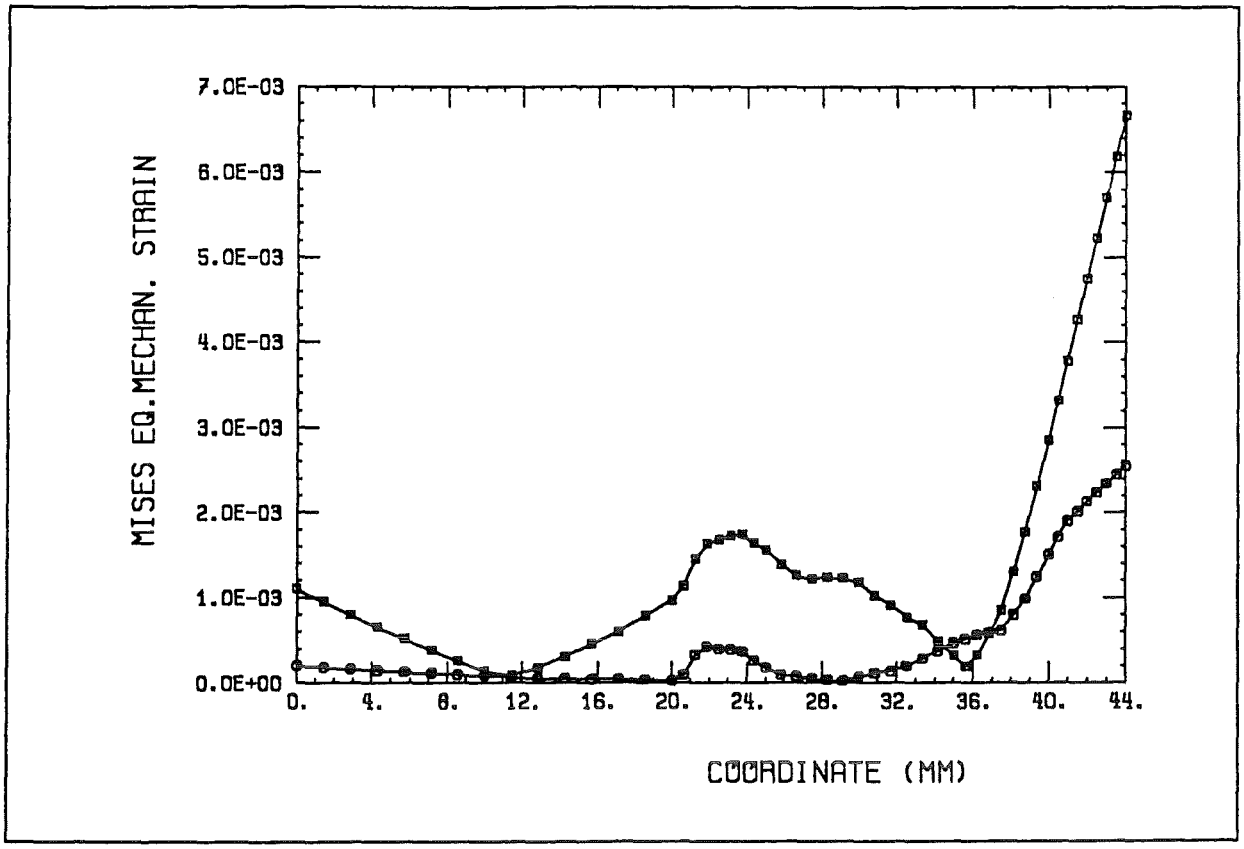

Figure 42. Results of elasto-plastic analysis: Von Mises equivalent mechanical strain along line L2 (□ end of heating, O end of cycle)

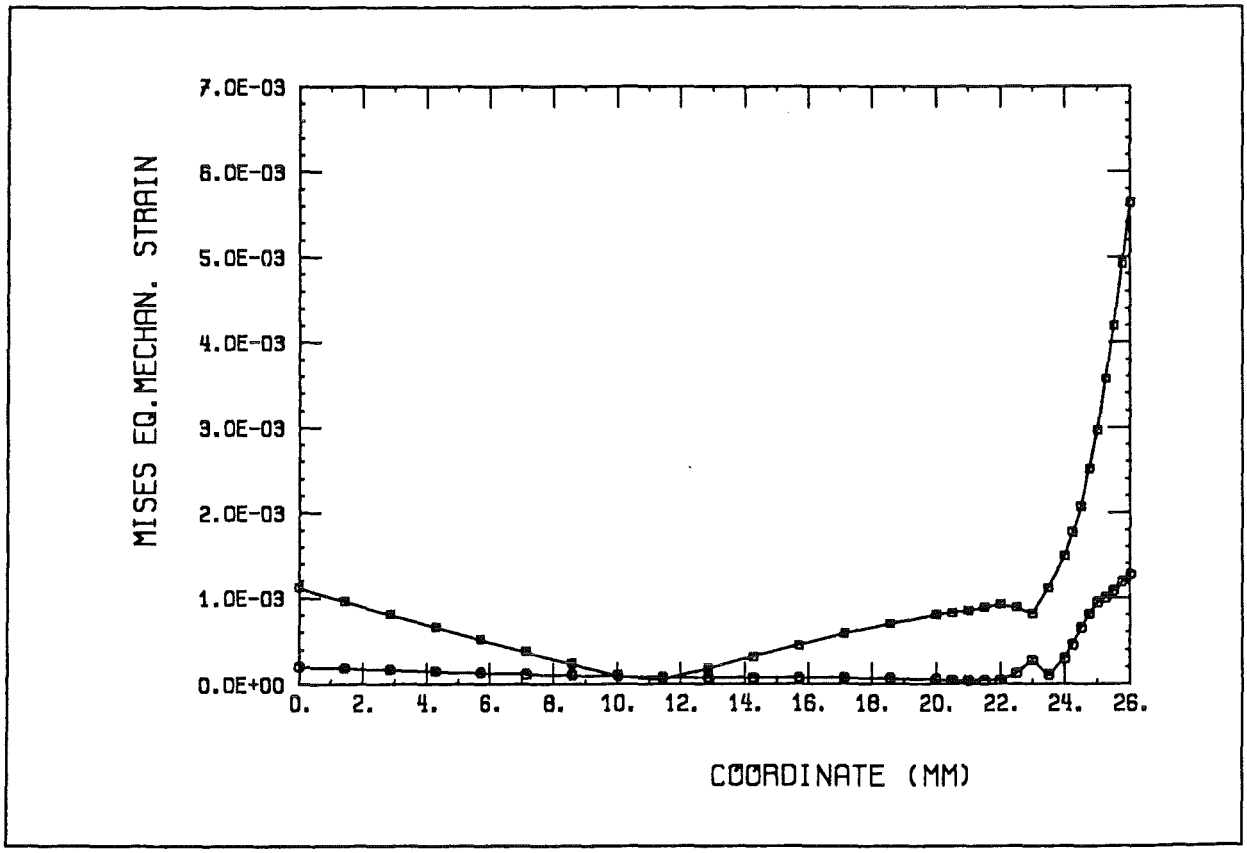

Figure 43. Results of elasto-plastic analysis: Von Mises equivalent mechanical strain along line L3 (□ end of heating, O end of cycle)

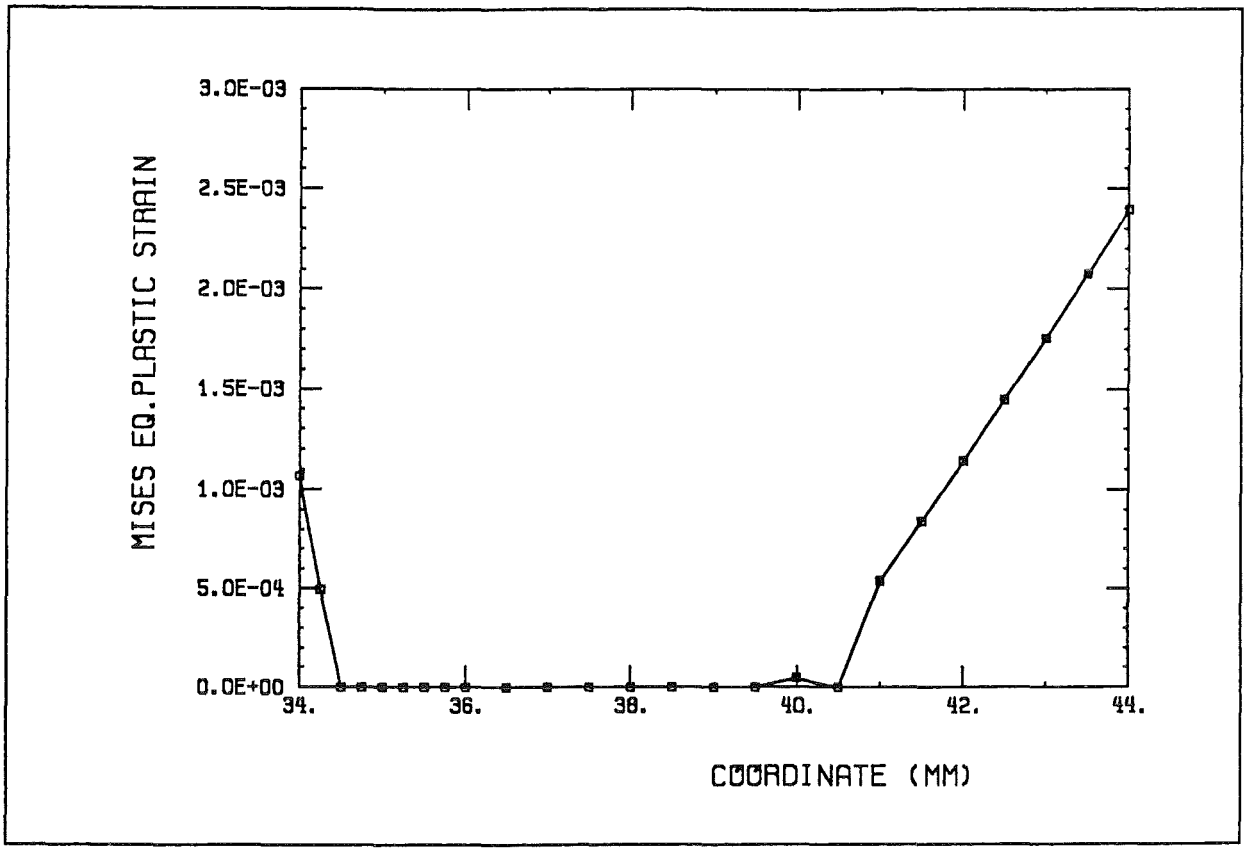

Figure 44. Results of elasto-plastic analysis: Von Mises equivalent plastic strain along line L1

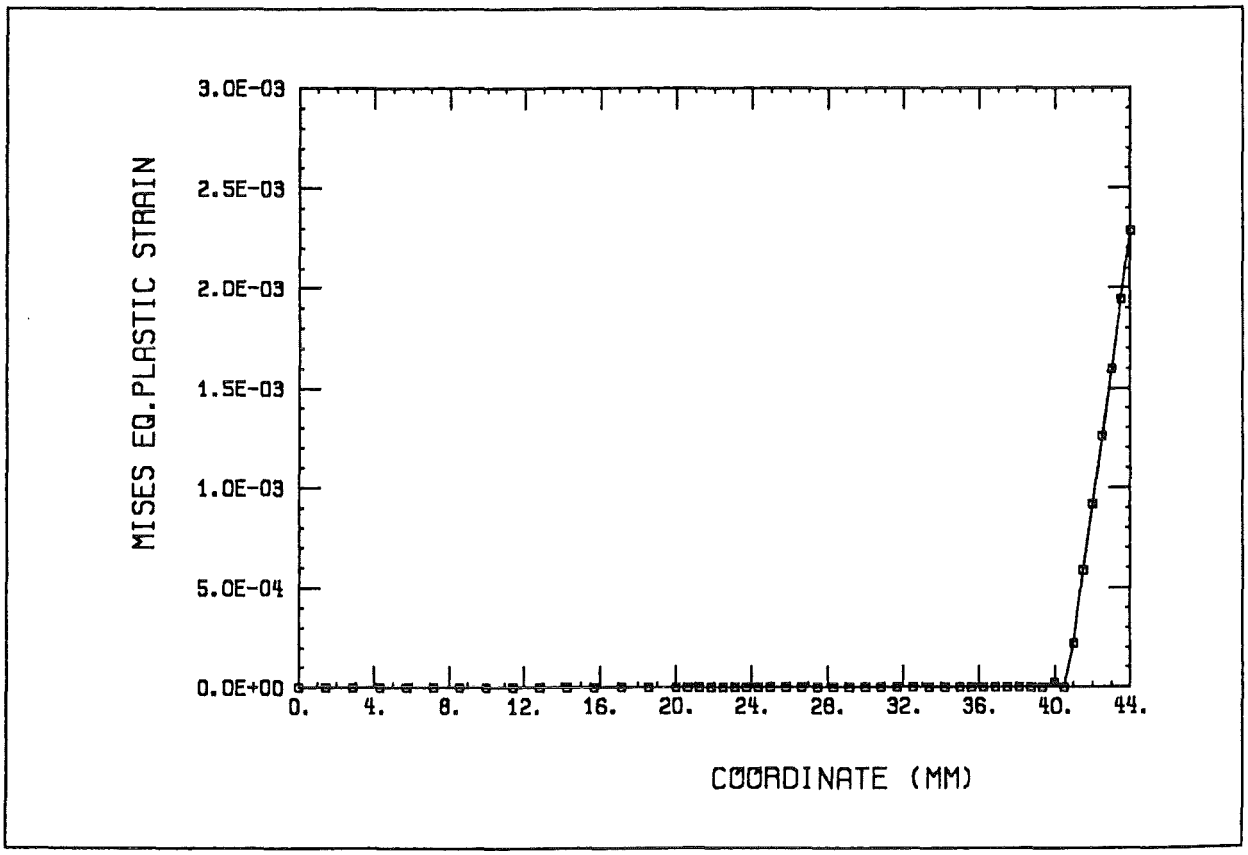

Figure 45. Results of elasto-plastic analysis: Von Mises equivalent plastic strain along line L2

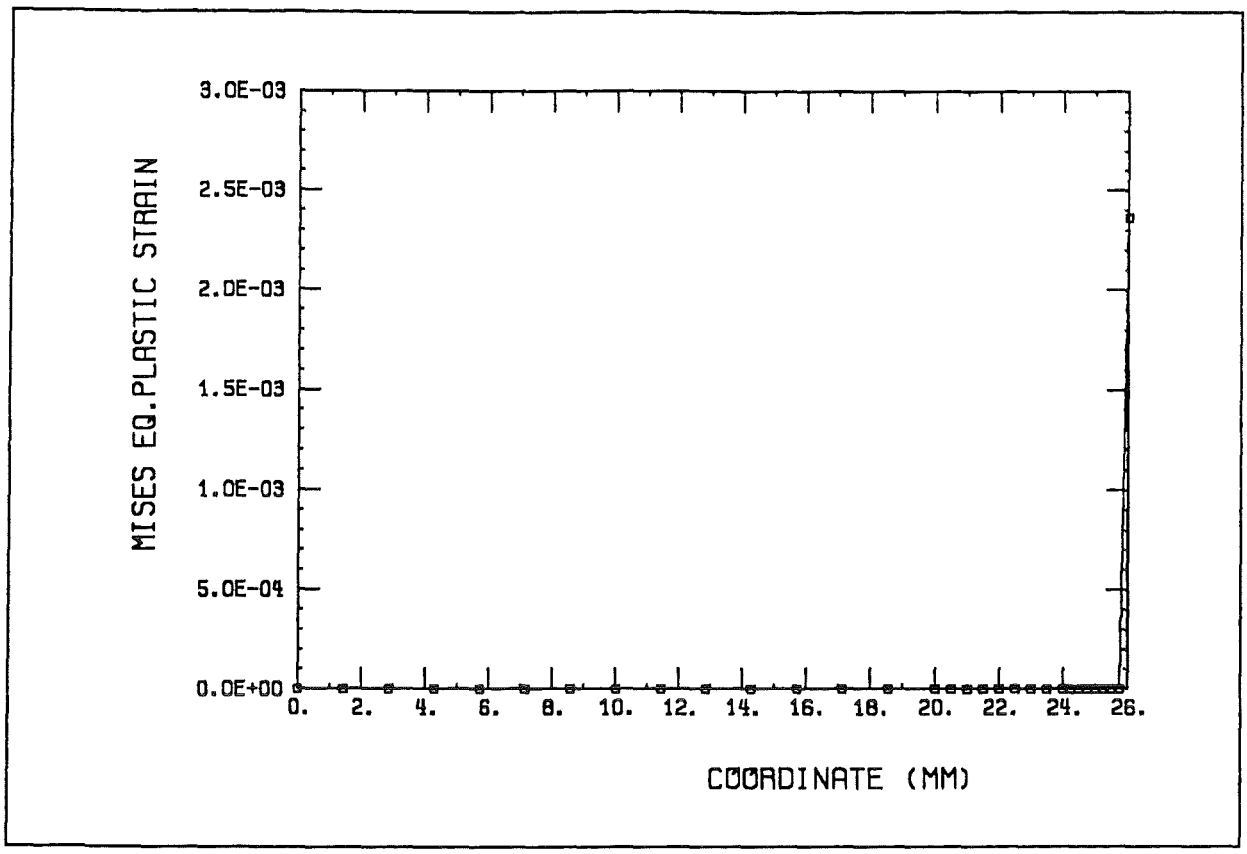

Figure 46. Results of elasto-plastic analysis: Von Mises equivalent plastic strain along line L3

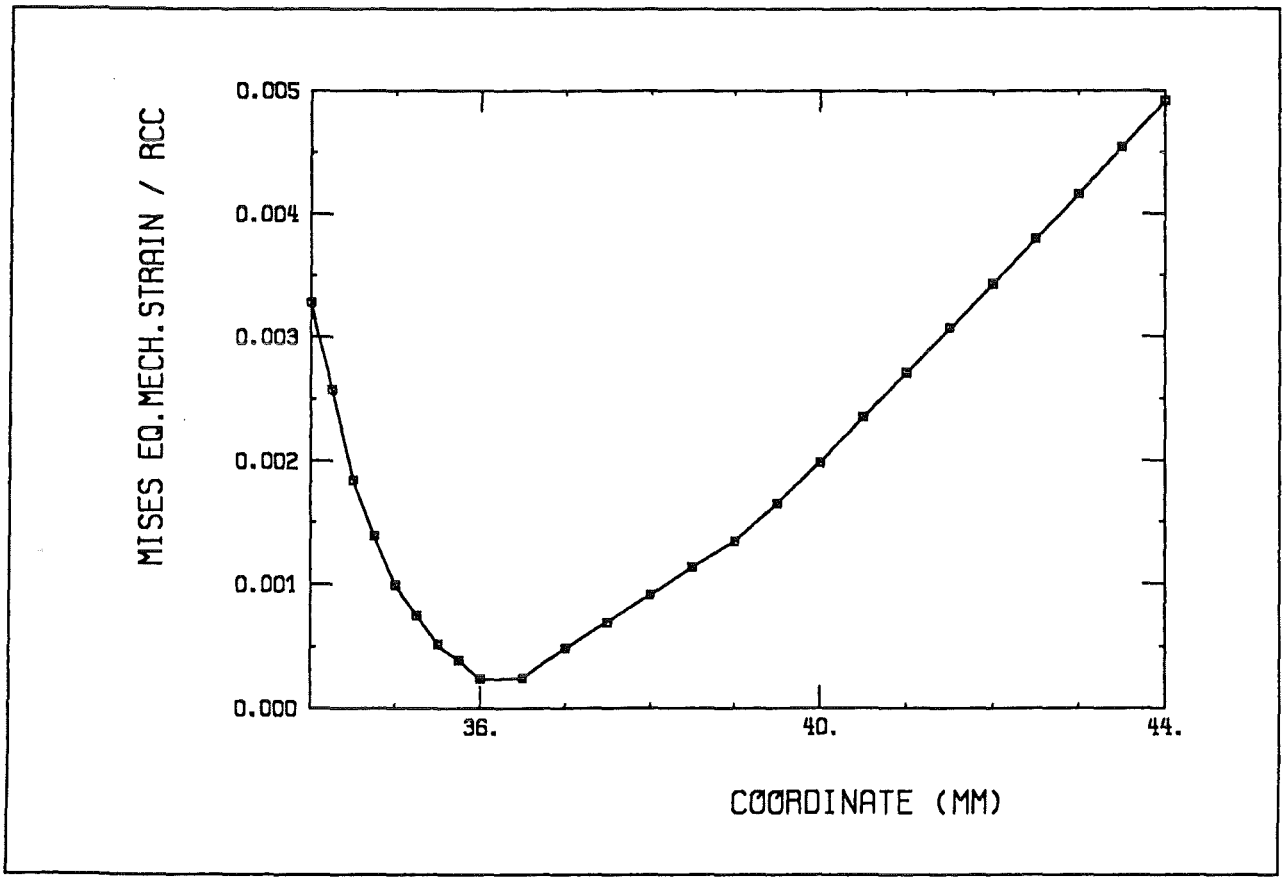

Figure 47. Results of elasto-plastic analysis: Von Mises equivalent mechanical strain range along line L1

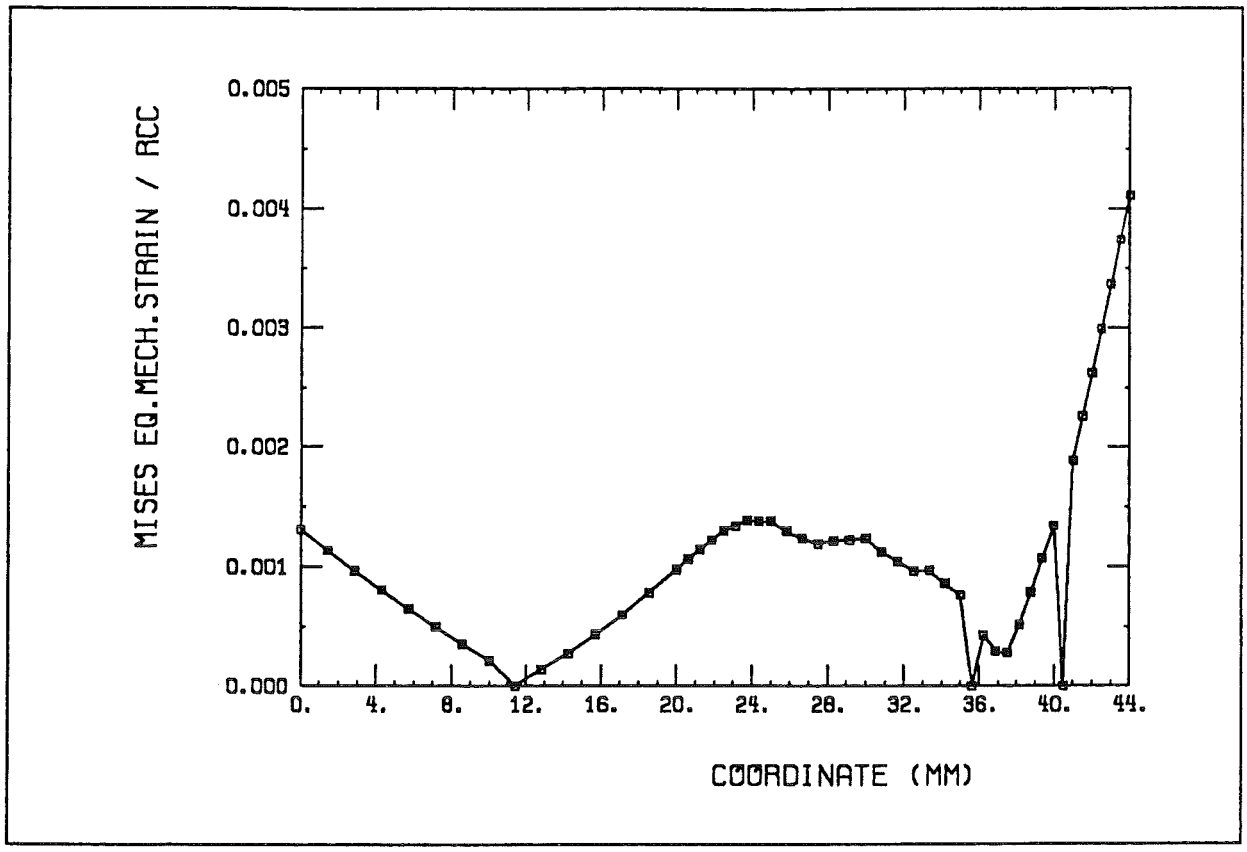

Figure 48. **Results of elasto-plastic analysis:** Von Mises equivalent mechanical strain range along line L2

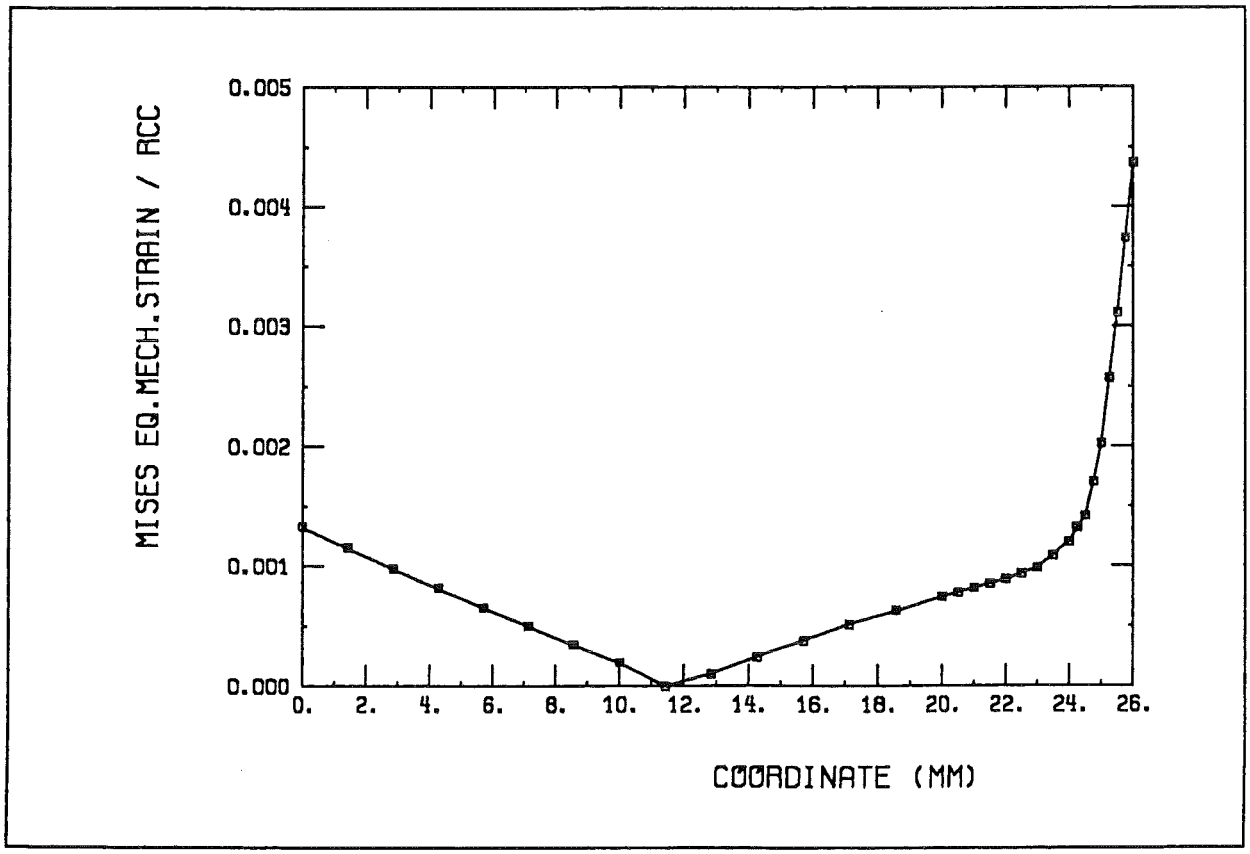

Figure 49. **Results of elasto-plastic analysis:** Von Mises equivalent mechanical strain range along line L3

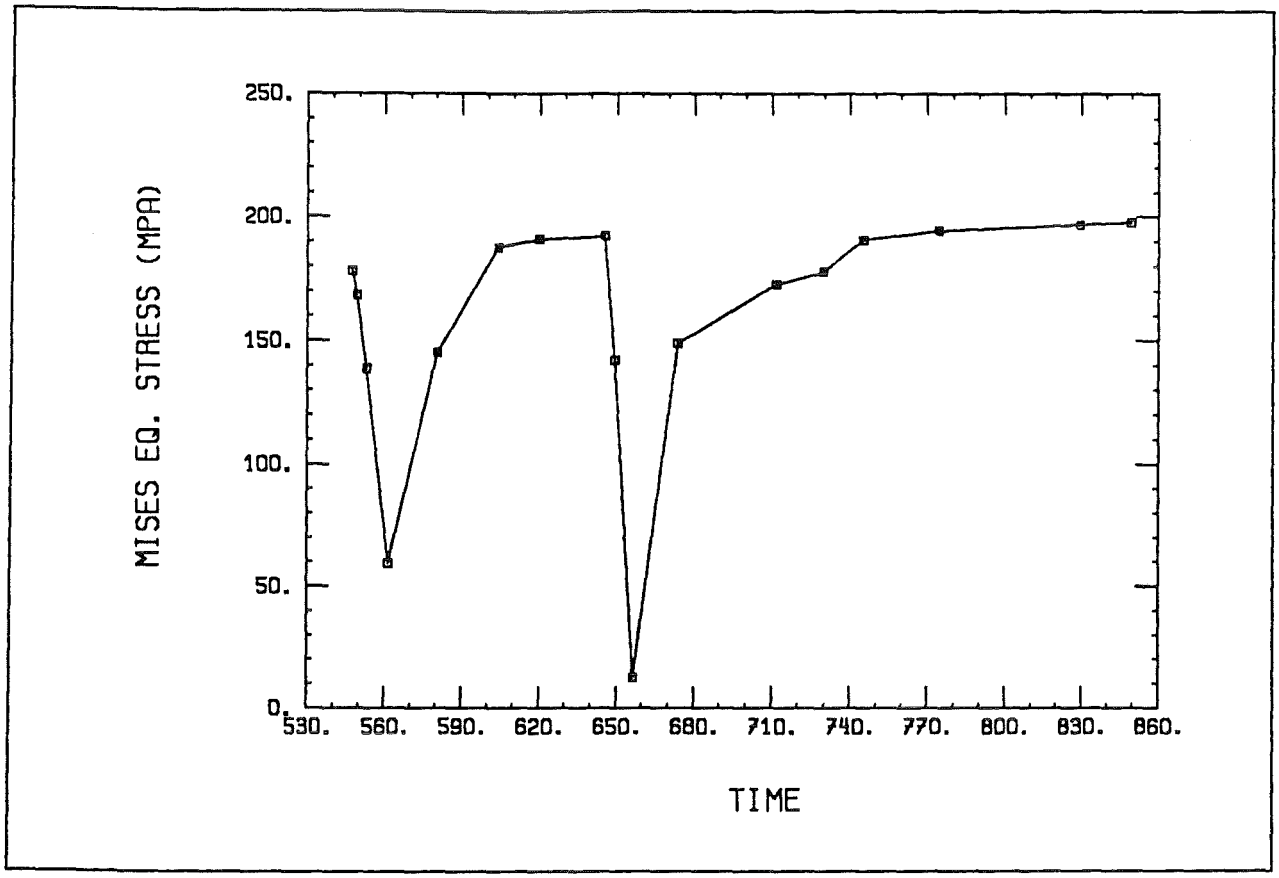

Figure 50. Results of elasto-plastic analysis: History plot of von Mises equivalent stress at point F

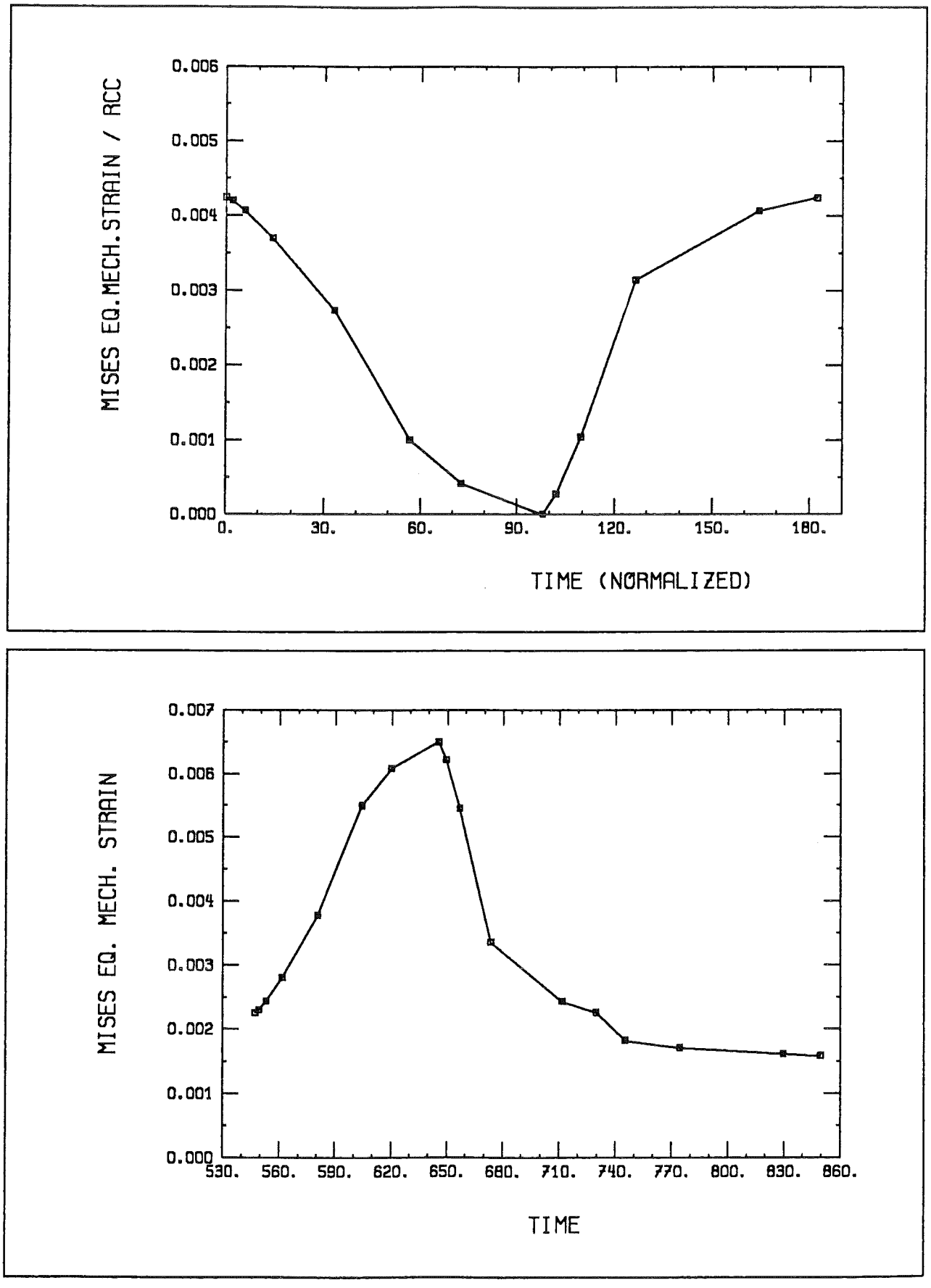

Figure 51. Results of elasto-plastic analysis: History plot of von Mises equivalent mechanical strain at point F

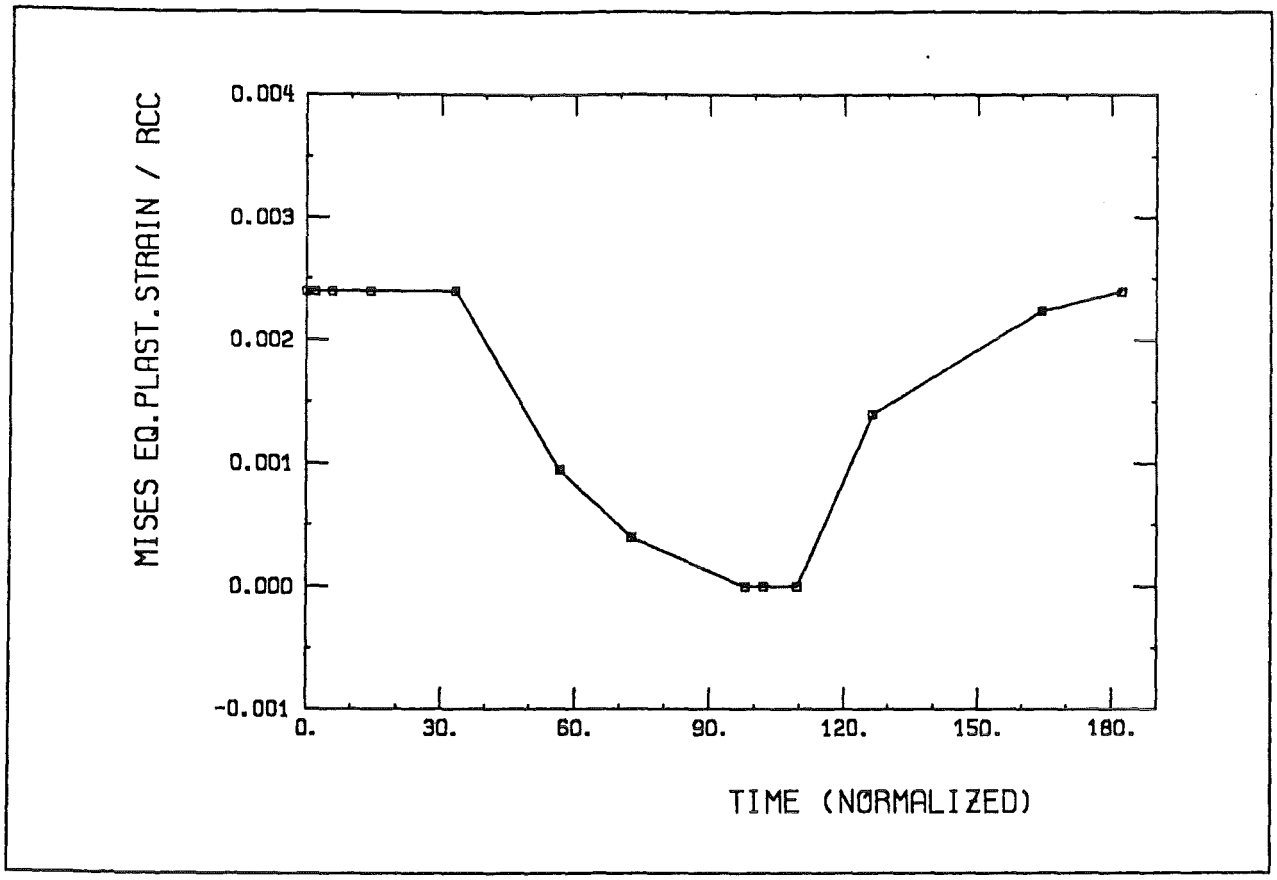

Figure 52. Results of elasto-plastic analysis: History plot of von Mises equivalent plastic strain at point F

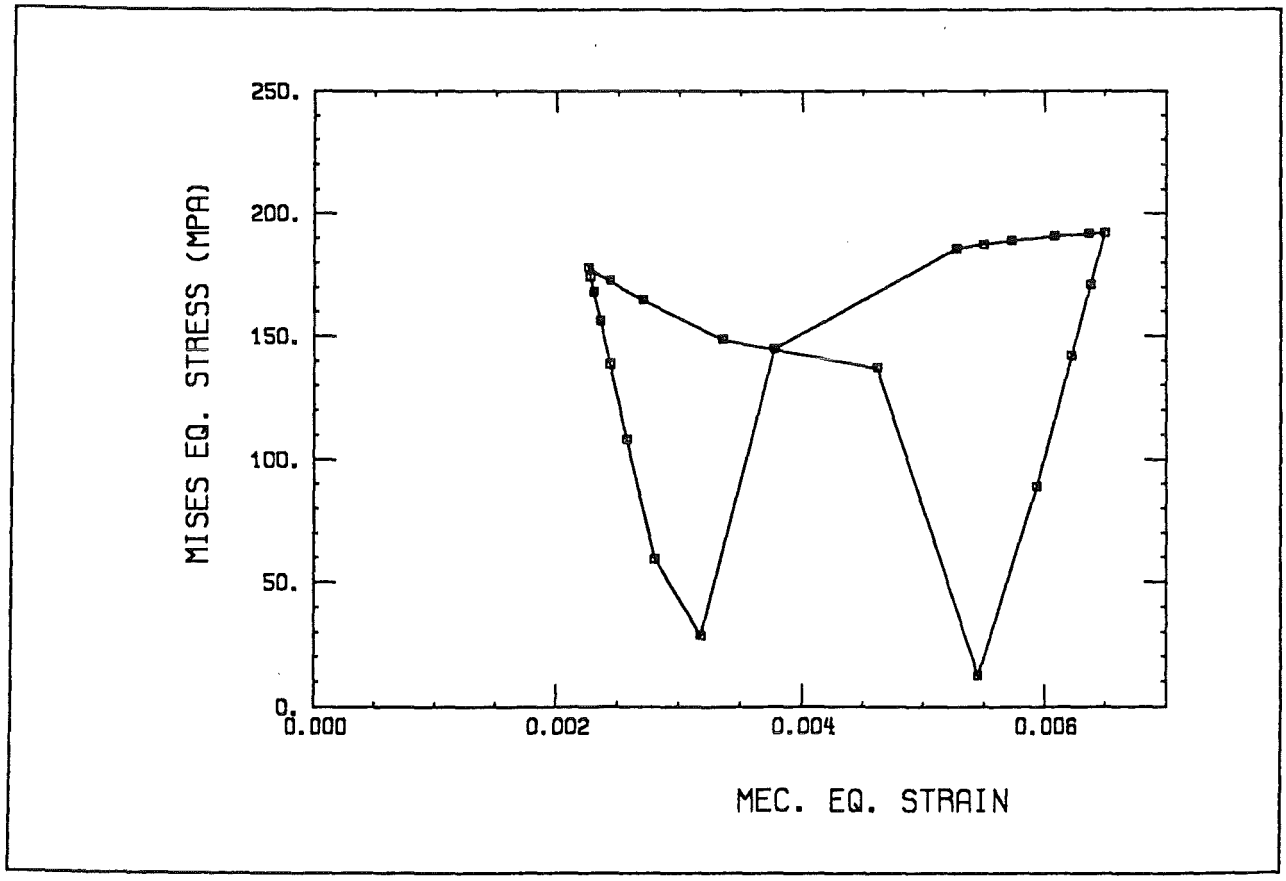

Figure 53. Results of elasto-plastic analysis: Hysteresis loop of equivalent Mises stress versus equivalent mechanical Mises strain

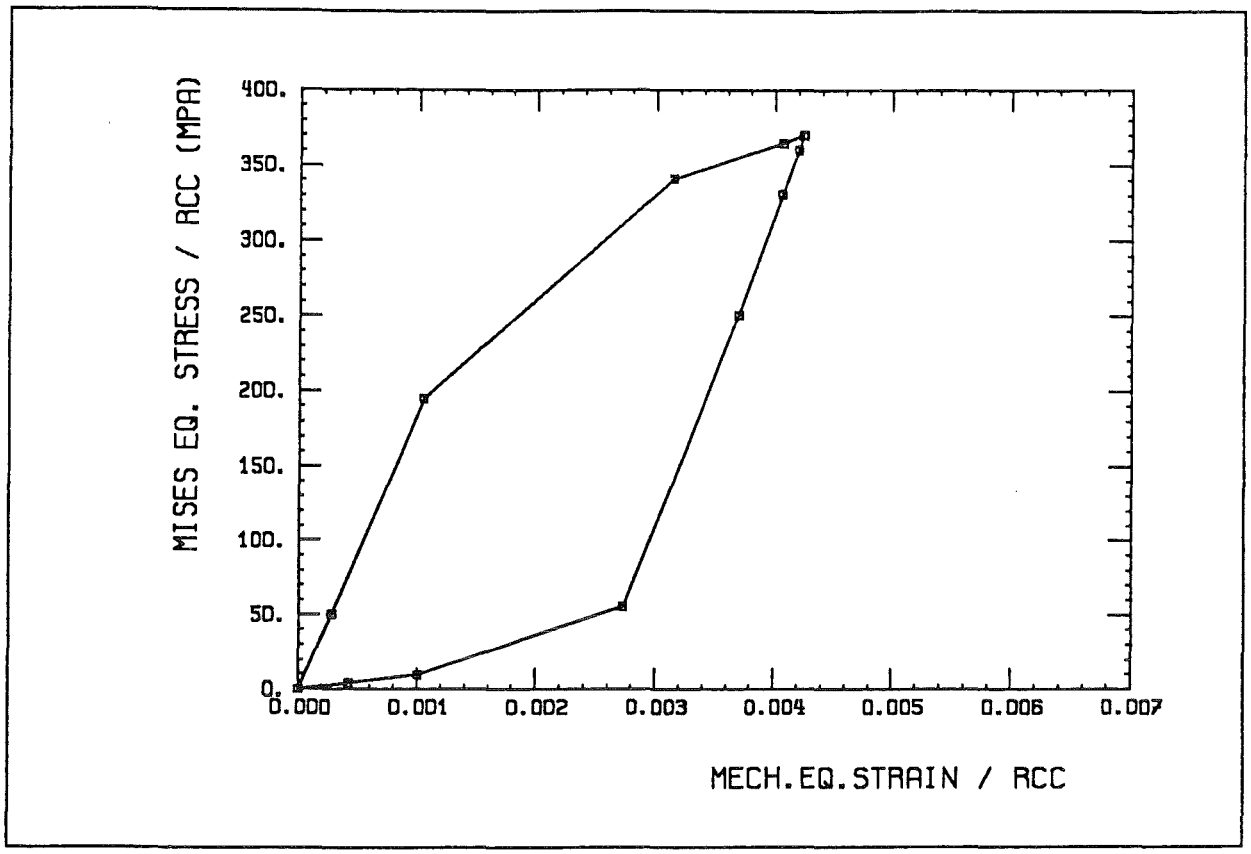

Figure 54. Results of elasto-plastic analysis: Hysteresis loop of equivalent Mises stress versus equivalent mechanical Mises strain (normalized according to RCC-code)

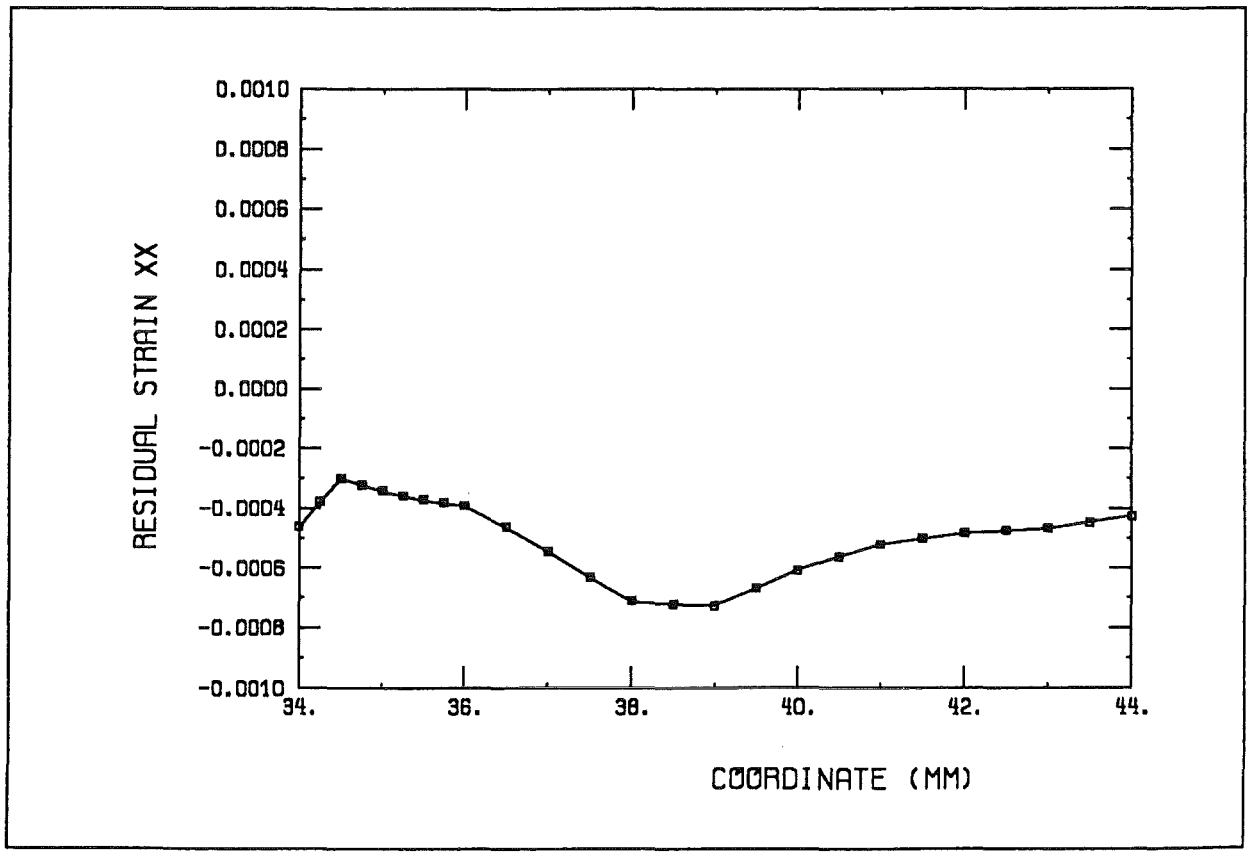

Figure 55. Results of elasto-plastic analysis: Residual strain xx along line L1

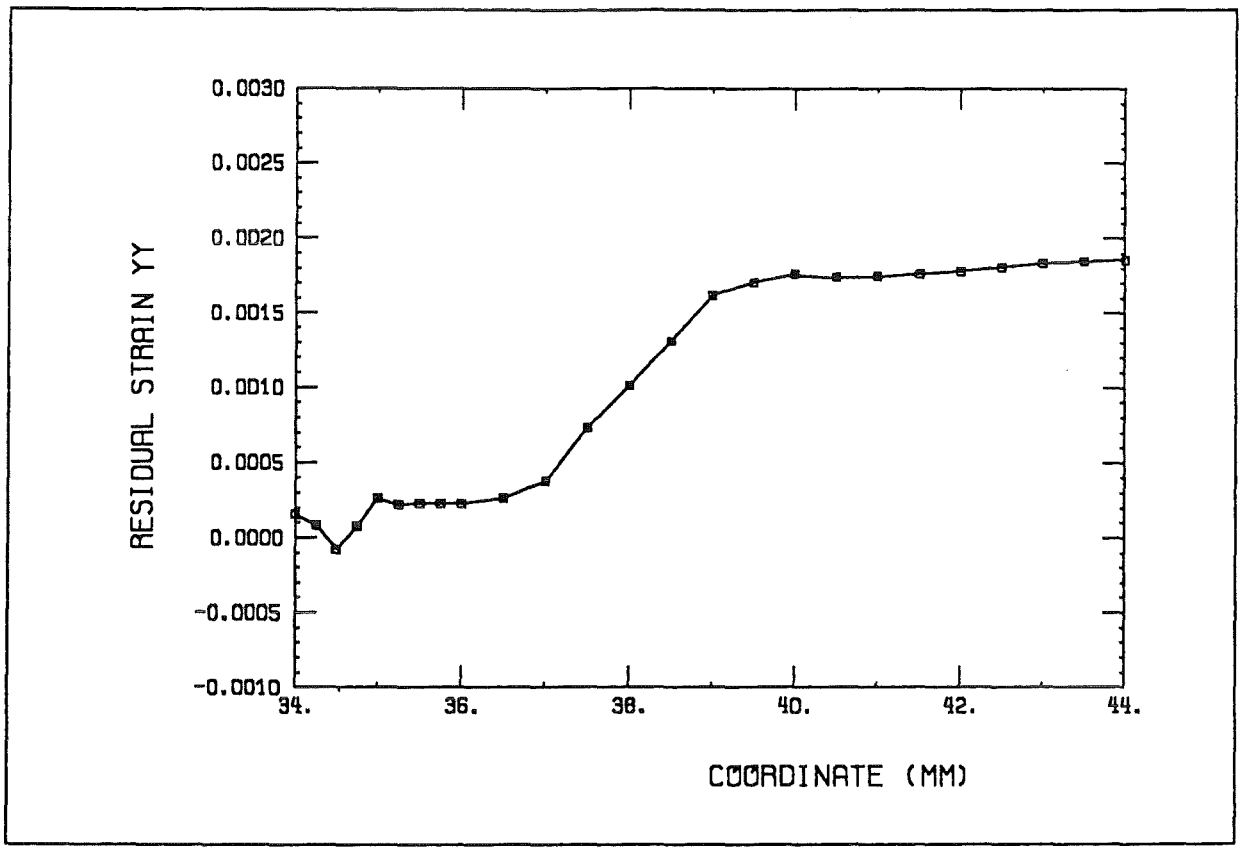

Figure 56. Results of elasto-plastic analysis: Residual strain yy along line L1

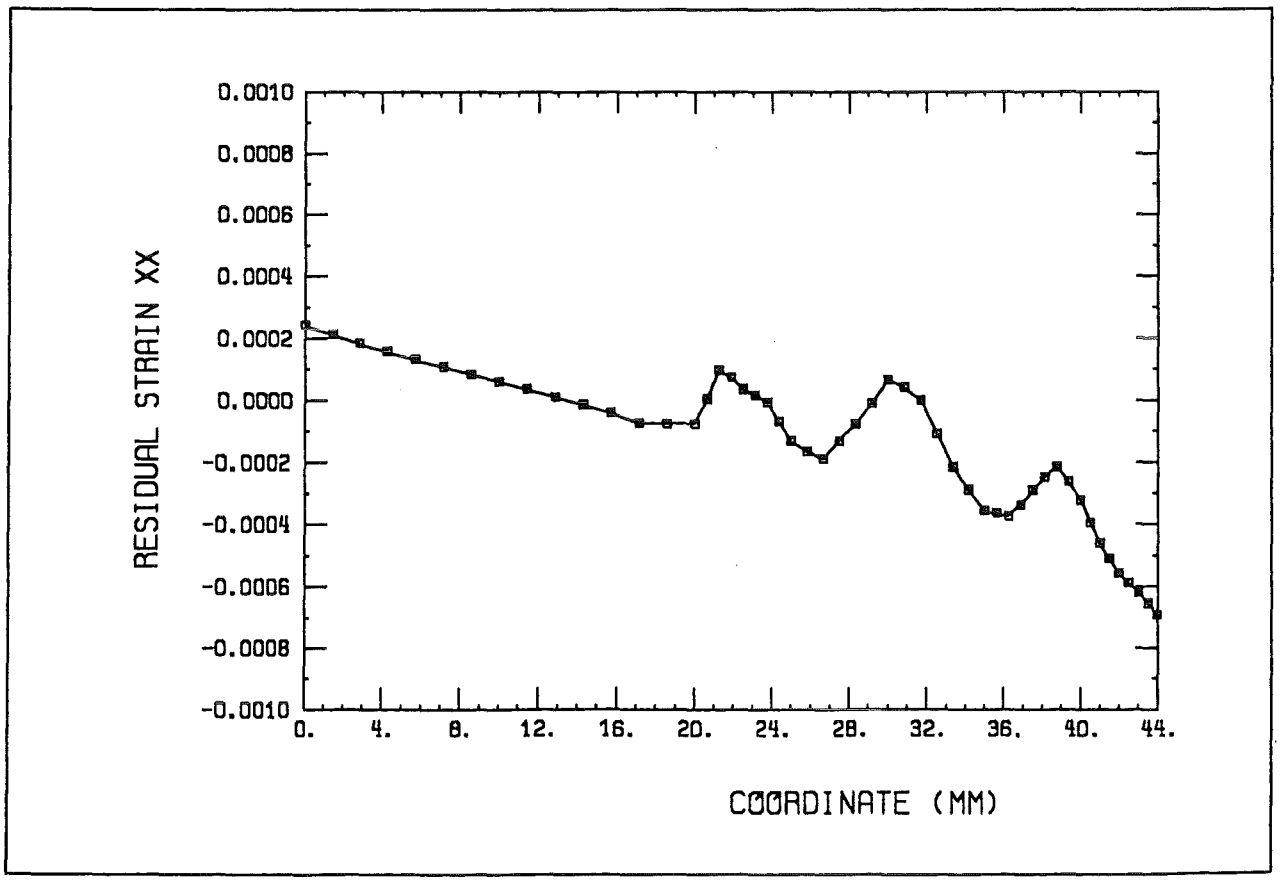

Figure 57. Results of elasto-plastic analysis: Residual strain xx along line L2

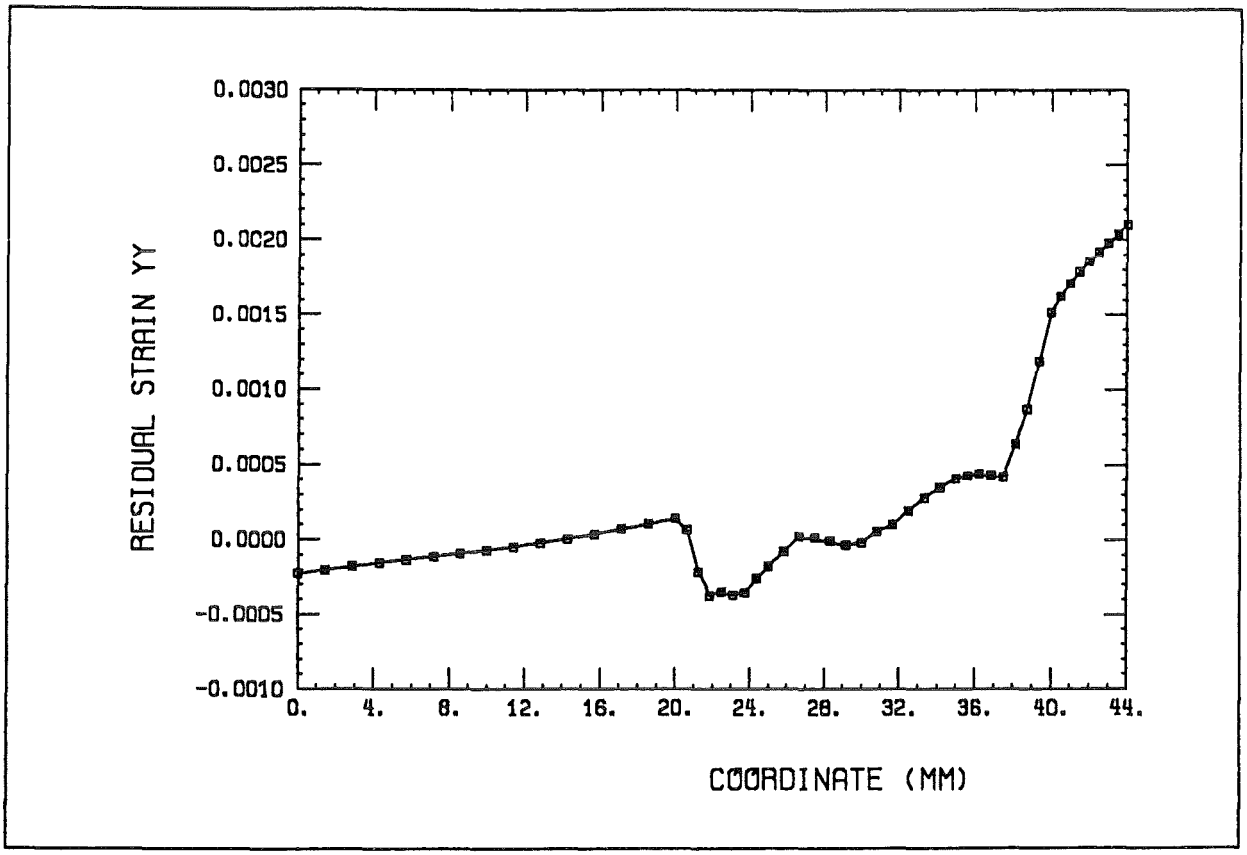

Figure 58. Results of elasto-plastic analysis: Residual strain yy along line L2

5. Lifetime prediction

5.1 *Design curves*

Within the ASME code Ref. [4]fatigue curves for AISI 316 LSPH are given by table T-1430-1A,1B and by figure F-1430-1A,1B for the use in elastic analysis. Alternatively, fatigue curves are also summarized in the RCC-code Annex A3-1S for different temperatures. For a temperature of 425 °C data can be fitted by a Manson-Coffin-law

$N_f = A\ \varepsilon^n$

from both codes. The best fits are summarized in table 7:

425 °C	ASME curve	RCC curve
A	293.3	167.81
n	-3.6186	-3.8685

Table 7: Parameter of Manson-Coffin-law for fatigue curves

The fatigue design curves taken from the ASME code and RCC code are shown in Figs. 59 and 60, respectively.

5.2 *Lifetime prediction from elastic analyses by means of RCC code.*

The RCC framework utilyzes the von Mises equivalent stress range $\Delta\sigma$ of one load cycle. From this an equivalent strain range $\Delta\varepsilon_1$

$$\Delta\varepsilon_1 = \frac{2}{3}\,\frac{1+\nu}{E}\,\Delta\sigma_{tot}$$

can be assessed. Under plastic conditions the 'real' strain $\Delta\varepsilon$ range is calculated taking into account plastic strain augmentations K_ε (due to nonlinearity) and K_ν (due to multiaxiality)

$$\Delta\varepsilon = (K_\varepsilon + K_\nu - 1)\,\Delta\varepsilon_1 .$$

The evaluation at point F leads to
$\Delta\varepsilon_1$ = .3095 %
$\Delta\varepsilon$ = .4971 %
resulting in N_f = 2500 cycles in case the RCC design curve is used or in N_f = 3700 cycles by utilyzing, alternatively, the ASME design curve.

5.3 *Lifetime prediction from plastic analyses*

From the reference model (O66) an equivalent strain range of $\Delta\varepsilon$ = .4240 % is calculated directly at point F. Therefore, from the RCC design curve a number of cycles to failure N_f = 4640 is assessed.

The design by code is conservative (roughly by a factor of 2) compared to design by analysis. This will be investigated in more detail in Appendix 2.

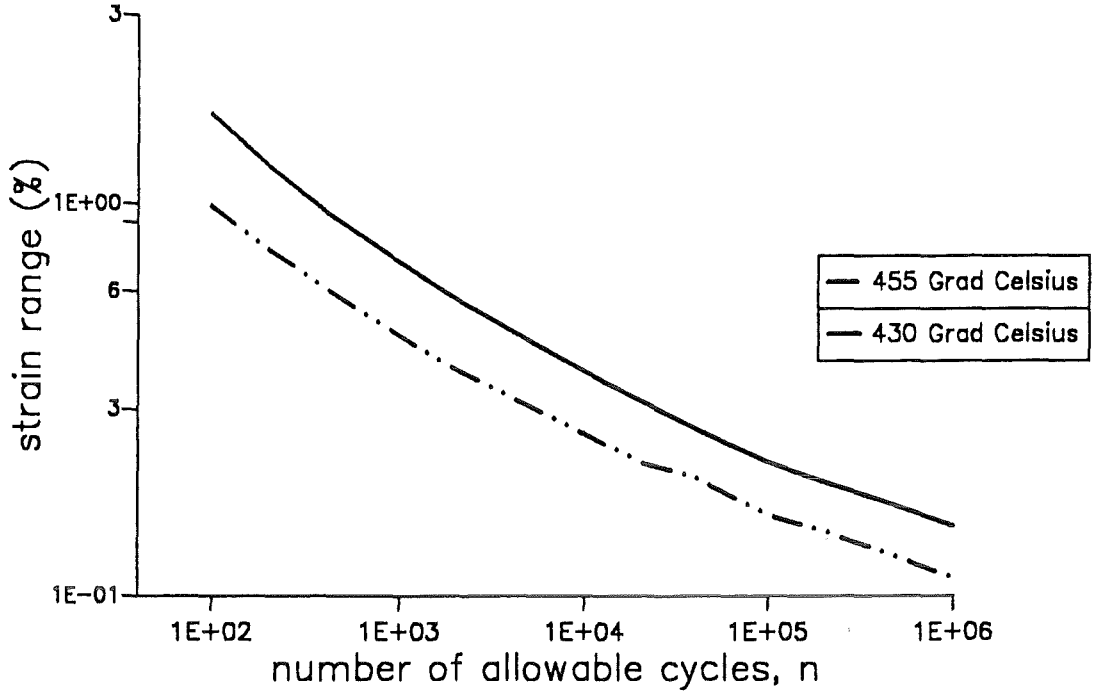

Figure 59. Fatigue design curve: ASME code F1430,1A,1B

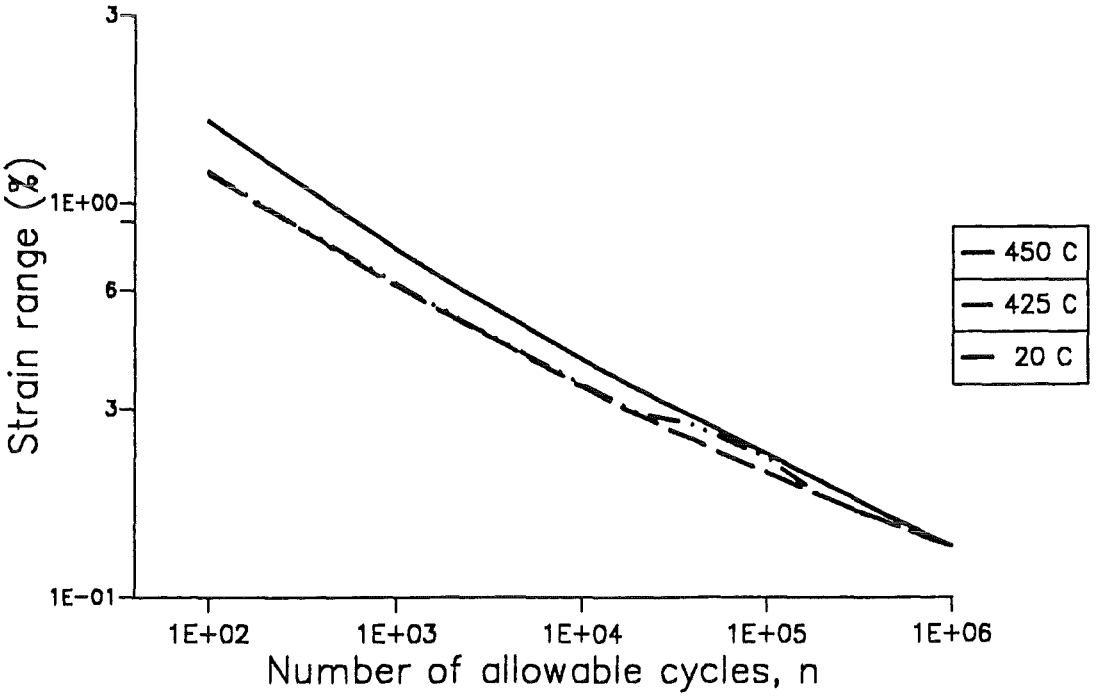

Figure 60. Fatigue design curve: RCC code curves

Literature

[1] P.Matera, P.Ruatto, Behaviour of First Wall Components under Thermal Fatigue, First Interim Report, JRC Technical Note I.90.20

[2] ABAQUS USER'S HANDBOOK, Hibbitt, Karlsson, Sörensen INC.

[3] RCC-MR, Règles de conception et de construction des matériels mécaniques des îlots nucléaires, Technical Annex A3.1S, A.F.C.E.N.. Paris, 1985.

[4] ASME, Boiler and Pressure Vessel Code, Section III, Div. 1, United Energy Center, The American Society of Mechanical Engineers, New York, 1979.

Appendix 1

Lifetime prediction - study on different material models

A source of error in lifetime assessment is the choice of the material model. The influence on the predicted number of cycles to failure is investigated by adopting various material models.

The first class of models are of ORNL type. The requirements on the ORNL model are given in section 1. If the model is adjusted to a maximum strain of ε_{max} = v (in units of 1/1000) of the virgin material and a strain range of $\Delta\ \varepsilon_{max}$ = h (units 1/1000) of the cyclic hardening curve, the model is denoted by O'vh'.
The second class is given by the models (C) and (M), which are described in more detail in section 2. The suffix "I" and "K" stand for an isotropic or a kinematic hardening rules, respectively.

The results of different material models are summarized in table 8:

Material model	strain range (%)	Number of cycles
O36	.4417	3960
O66	.4240	4640
O48	.4069	5440
O88	.4034	5620
C	.3412	10750
M-I	.3744	7500
M-K	.4230	4650

Table 8: Lifetime assessment of different material models

In any case, the evaluation is taken at point F. All models that are determined according to the ORNL requirements give approximatively the same result in terms of number of cycles to failure, even if the values of the actual underlying stress states are rather different. More generally, this statement holds for all types of models except for (C).

Appendix 2

Investigations on the conservatism of the design by code

The aim of this section is to compare design by code and design by analysis for different loading conditions. As is observed in the previous section, there is some conservatism in lifetime assessment by the code rules compared to designing by analysis. This needs some further investigation. In Appendix 1 the problem at hand has been studied by utilyzing different plasticity models. In Appendix 2 boths design methods are compared against each other at different load levels.

Steady state heat transfer analyses has been carried out for different values of the surface heat flux (i.e. for values of 35, 40, 45, 50 and 55 W/cm^2). The structure is periodically loaded between zero heat flux and maximum heat flux in such a way that the temperatures changes linearly in time.

Elastic analyses and elasto-plastic analyses utilyzing the material models C and O66 are carried out.

The results of elastic analyses and the results of elasto-plastic analyses at point F in terms of von Mises equivalent strain range are summarized in table 9. The calculated lifetimes are shown in table 10.

Surface heat flux (W/cm^2)	Strain range: elastic analysis $\Delta\varepsilon_1$ and $\Delta\varepsilon$ (%)	Strain range: inelastic analysis (Model C) (%)	Strain range: inelastic analysis (Model O66) (%)
35	.2554 / .3627	.2688	.3061
40	.2894 / .4300	.3212	.3700
45	.3323 / .5134	.3772	.4365
50	.3660 / .5819	.4077	.5060
55	.4031 / .6490	.4631	.5771

Table 9: Strain range for different thermal loading conditions.

Max. surface heat flux (W/ cm^2)	N_f elastic analysis	N_f (Model C)	N_f (Model O66)
35	8490	27030	16310
40	4390	13575	7865
45	2210	7290	4180
50	1360	5400	2340
55	900	3280	1400

Table 10: Comparison of lifetime assessment by code and by design for different thermal loading conditions.

The results of these analyses indicate, that at least under thermo-mechanical loading conditions, lifetime assessment by codes seems to be very conservative.

Appendix 3

Temperature - analysis

	Results of third cycle	
Point	end of heating	end of cycle
A	18.9	20.7
B	19.2	21.1
C	12.9	11.5
D	16.2	12.4
F	385.3	53.4
G	386.3	53.8
H	431.0	70.9

Appendix 4

RESULTS OF ELASTIC ANALYSIS

RESULTS AT END OF HEATING PERIOD
==========

1) RESULTS ALONG LINE L1 :

Y-COORD (MM)	MISES STRESS (MPA)	P1-STRESS (MPA)	P3-STRESS (MPA)	EQUIV.STRAIN
34.00	0.64392E+03	0.12970E+01	0.74189E+03	0.30023E-02
34.25	0.52049E+03	0.31191E+02	0.63063E+03	0.24274E-02
34.50	0.39773E+03	0.62224E+02	0.52094E+03	0.18560E-02
35.00	0.24336E+03	0.86474E+02	0.36732E+03	0.11395E-02
35.50	0.14190E+03	0.91199E+02	0.25458E+03	0.66746E-03
36.00	0.69845E+02	0.86643E+02	0.16397E+03	0.33057E-03
37.00	0.62876E+02	-0.49147E+01	0.66945E+02	0.29925E-03
38.00	0.14828E+03	-0.10908E+03	0.47175E+02	0.71449E-03
39.00	0.23317E+03	-0.20837E+03	0.31491E+02	0.11364E-02
40.00	0.31787E+03	-0.30383E+03	0.19837E+02	0.15660E-02
41.00	0.40382E+03	-0.39718E+03	0.11361E+02	0.20173E-02
42.00	0.49073E+03	-0.48851E+03	0.53531E+01	0.24905E-02
43.00	0.57841E+03	-0.57779E+03	0.13616E+01	0.29822E-02
43.50	0.62339E+03	-0.62405E+03	0.55465E+00	0.32418E-02
44.00	0.66847E+03	-0.67189E+03	-0.22339E+00	0.35019E-02

2) RESULTS ALONG LINE L2

Y-COORD (MM)	MISES STRESS (MPA)	P1-STRESS (MPA)	P3-STRESS (MPA)	EQUIV.STRAIN
0.00	0.35175E+03	-0.36105E+03	-0.29408E+00	0.15633E-02
5.71	0.17756E+03	-0.17504E+03	0.73837E+01	0.78914E-03
10.00	0.62439E+02	-0.46261E+02	0.19919E+02	0.27751E-03
15.71	0.11331E+03	0.20586E+02	0.14293E+03	0.50362E-03
20.00	0.25966E+03	0.39511E+01	0.27410E+03	0.11541E-02
25.00	0.38122E+03	-0.30382E+02	0.38601E+03	0.16942E-02
30.00	0.34093E+03	-0.14668E+02	0.37080E+03	0.15281E-02
32.52	0.26834E+03	-0.11410E+02	0.29840E+03	0.12222E-02
35.00	0.22227E+03	-0.64169E+02	0.16836E+03	0.10369E-02
37.50	0.44184E+02	-0.70695E+02	-0.19676E+02	0.21161E-03
40.00	0.26991E+03	-0.30058E+03	-0.17282E+02	0.13278E-02
41.00	0.37156E+03	-0.39161E+03	-0.10399E+02	0.18532E-02
42.00	0.47036E+03	-0.48134E+03	-0.50584E+01	0.23839E-02
43.00	0.56438E+03	-0.56864E+03	-0.13215E+01	0.29063E-02
43.50	0.60806E+03	-0.61086E+03	-0.50628E+00	0.31584E-02
44.00	0.65164E+03	-0.65307E+03	0.25454E+00	0.34098E-02

3) RESULTS ALONG LINE L3

Y-COORD (MM)	MISES STRESS (MPA)	P1-STRESS (MPA)	P3-STRESS (MPA)	EQUIV.STRAIN
0.00	0.35715E+03	-0.36315E+03	-0.25552E+00	0.15873E-02
4.29	0.22139E+03	-0.22256E+03	0.35225E+01	0.98394E-03
7.14	0.13707E+03	-0.12986E+03	0.88051E+01	0.60918E-03
10.00	0.56709E+02	-0.43855E+02	0.15646E+02	0.25204E-03
15.71	0.10008E+03	0.34521E+02	0.14625E+03	0.44480E-03
18.57	0.17023E+03	0.52150E+02	0.24060E+03	0.75656E-03
20.00	0.20307E+03	0.64579E+02	0.28926E+03	0.90254E-03
22.00	0.24661E+03	0.93643E+02	0.36528E+03	0.10960E-02
24.00	0.32546E+03	0.12471E+03	0.46299E+03	0.14465E-02
25.00	0.44740E+03	0.11084E+03	0.58330E+03	0.19884E-02
25.50	0.58080E+03	0.73525E+02	0.71283E+03	0.25813E-02

25.75	0.70044E+03	0.32442E+02	0.81721E+03	0.31131E-02
26.00	0.82371E+03	-0.83427E+01	0.92399E+03	0.36609E-02

RESULTS OF ELASTIC ANALYSIS (END OF CYCLE)

1) RESULTS ALONG LINE L1

Y-COORD (MM)	MISES STRESS (MPA)	P1-STRESS (MPA)	P3-STRESS (MPA)	EQUIV.STRAIN
34.00	0.86836E+02	0.15544E+00	0.10041E+03	0.38690E-03
34.25	0.70319E+02	0.42013E+01	0.85268E+02	0.31332E-03
34.50	0.54030E+02	0.83952E+01	0.70352E+02	0.24076E-03
35.00	0.33758E+02	0.11670E+02	0.49601E+02	0.15049E-03
35.50	0.20464E+02	0.12339E+02	0.34326E+02	0.91273E-04
36.00	0.10936E+02	0.11749E+02	0.23254E+02	0.48813E-04
37.00	0.62257E+01	0.26507E+01	0.91082E+01	0.27805E-04
38.00	0.16767E+02	-0.12818E+02	0.64255E+01	0.74994E-04
39.00	0.27651E+02	-0.26690E+02	0.42920E+01	0.12383E-03
40.00	0.38478E+02	-0.39686E+02	0.27088E+01	0.17252E-03
41.00	0.49215E+02	-0.52100E+02	0.15588E+01	0.22092E-03
42.00	0.59827E+02	-0.64077E+02	0.74091E+00	0.26886E-03
43.00	0.70330E+02	-0.75752E+02	0.19107E+00	0.31639E-03
43.50	0.75646E+02	-0.81576E+02	0.77876E-01	0.34050E-03
44.00	0.80976E+02	-0.87412E+02	-0.30834E-01	0.36466E-03

2) RESULTS ALONG LINE L2

Y-COORD (MM)	MISES STRESS (MPA)	P1-STRESS (MPA)	P3-STRESS (MPA)	EQUIV.STRAIN
0.00	0.41056E+02	-0.42477E+02	-0.39546E-01	0.18247E-03
5.71	0.21866E+02	-0.22095E+02	0.97584E+00	0.97184E-04
10.00	0.85013E+01	-0.73614E+01	0.24298E+01	0.37783E-04
15.71	0.15969E+02	0.24709E+01	0.20492E+02	0.70975E-04
20.00	0.36781E+02	-0.24908E+00	0.38987E+02	0.16347E-03
25.00	0.55943E+02	-0.57694E+01	0.55896E+02	0.24864E-03
30.00	0.51268E+02	-0.21614E+01	0.54932E+02	0.22786E-03
32.52	0.42843E+02	-0.30408E+01	0.46373E+02	0.19044E-03
35.00	0.35276E+02	-0.10081E+02	0.27206E+02	0.15719E-03
37.50	0.57333E+01	-0.72289E+01	-0.80984E+00	0.25644E-04
40.00	0.31324E+02	-0.36921E+02	-0.27561E+01	0.14043E-03
41.00	0.44680E+02	-0.50094E+02	-0.16699E+01	0.20055E-03
42.00	0.57233E+02	-0.62633E+02	-0.81478E+00	0.25719E-03
43.00	0.68766E+02	-0.74292E+02	-0.21233E+00	0.30935E-03
43.50	0.73856E+02	-0.79509E+02	-0.81828E-01	0.33242E-03
44.00	0.78930E+02	-0.84712E+02	0.41326E-01	0.35543E-03

3) RESULTS ALONG LINE L3

Y-COORD (MM)	MISES STRESS (MPA)	P1-STRESS (MPA)	P3-STRESS (MPA)	EQUIV.STRAIN
0.00	0.41676E+02	-0.43757E+02	-0.34530E-01	0.18523E-03
4.29	0.26596E+02	-0.27708E+02	0.47481E+00	0.11820E-03
7.14	0.16949E+02	-0.17367E+02	0.11543E+01	0.75328E-04
10.00	0.78357E+01	-0.70518E+01	0.19959E+01	0.34825E-04
15.71	0.14918E+02	0.42508E+01	0.21407E+02	0.66304E-04
18.57	0.24713E+02	0.65048E+01	0.34521E+02	0.10984E-03
20.00	0.29467E+02	0.81573E+01	0.41439E+02	0.13096E-03
22.00	0.35872E+02	0.12231E+02	0.52536E+02	0.15943E-03
24.00	0.46688E+02	0.16897E+02	0.66983E+02	0.20750E-03
25.00	0.63093E+02	0.15241E+02	0.79915E+02	0.28041E-03
25.50	0.81304E+02	0.10176E+02	0.98102E+02	0.36135E-03
25.75	0.97775E+02	0.45215E+01	0.11277E+03	0.43455E-03

26.00	0.11481E+03	-0.10806E+01	0.12778E+03	0.51028E-03

Appendix 5

RESULTS OF ELASTO-PLASTIC ANALYSIS
==========

RESULTS AT THE END OF HEATING PERIOD

1) RESULTS ALONG LINE L1

Y-COORD (MM)	MISES STRESS (MPA)	P1-STRESS (MPA)	P3-STRESS (MPA)	MISES STRAIN MECH. RCC	MISES STRAIN PLAS. RCC
34.00	0.20256E+03	0.40126E-01	0.23348E+03	0.28479E-02	0.1065E-02
34.25	0.19809E+03	0.11563E+02	0.239048+03	0.22005E-02	0.4944E-03
34.50	0.18994E+03	0.19593E+02	0.23699E+03	0.15612E-02	0.0000E+00
35.00	0.17731E+03	0.51387E+02	0.22971E+03	0.88224E-03	0.0000E+00
35.50	0.85697E+02	-0.84413E+01	0.89319E+02	0.48129E-03	0.0000E+00
36.00	0.98964E+02	-0.68727E+02	0.45301E+02	0.00000E-03	0.0000E+00
37.00	0.19208E+03	-0.17281E+03	0.25591E+02	0.40332E-03	0.0000E+00
38.00	0.19136E+03	-0.18465E+03	0.12954E+02	0.77113E-03	0.0000E+00
39.00	0.17559E+03	-0.17454E+03	0.72031E+01	0.11491E-02	0.0000E+00
40.00	0.18418E+03	-0.18510E+03	0.38524E+01	0.15514E-02	0.4562E-04
41.00	0.18643E+03	-0.18575E+03	0.13291E+01	0.22049E-02	0.5384E-03
42.00	0.18882E+03	-0.19015E+03	0.30058E+00	0.28697E-02	0.1142E-02
43.00	0.19071E+03	-0.19284E+03	-0.24712E-01	0.35434E-02	0.1756E-02
43.50	0.19140E+03	-0.19337E+03	0.65311E-02	0.38911E-02	0.2075E-02
44.00	0.19213E+03	-0.19403E+03	-0.38301E-01	0.42390E-02	0.2394E-02

2) RESULTS ALONG L2

Y-COORD (MM)	MISES STRESS (MPA)	P1-STRESS (MPA)	P3-STRESS (MPA)	MISES STRAIN MECH. RCC	MISES STRAIN PLAS. RCC
0.00	0.24495E+03	-0.24987E+03	-0.21339E+00	0.13073E-02	0.0000E+00
5.71	0.11527E+03	-0.11133E+03	0.53491E+01	0.64923E-03	0.0000E+00
10.00	0.30958E+02	-0.20114E+02	0.14862E+02	0.21504E-03	0.0000E+00
15.71	0.10065E+03	0.17743E+02	0.12707E+03	0.43396E-03	0.0000E+00
20.00	0.21840E+03	0.88889E+01	0.23289E+03	0.97629E-02	0.0000E+00
25.00	0.19423E+03	-0.18168E+02	0.19375E+03	0.13796E-02	0.0000E+00
30.00	0.21953E+03	-0.15151E+02	0.23179E+03	0.12375E-02	0.0000E+00
32.52	0.16585E+03	-0.19998E+02	0.17149E+03	0.96602E-02	0.0000E+00
35.00	0.68099E+02	-0.44079E+02	0.34104E+02	0.76622E-02	0.0000E+00
40.00	0.17779E+03	-0.18778E+03	-0.42030E+01	0.13437E-02	0.2395E-04
41.00	0.18385E+03	-0.19112E+03	-0.21784E+01	0.18808E-02	0.2190E-03
42.00	0.18771E+03	-0.19103E+03	-0.70813E+00	0.26209E-02	0.9174E-03
43.00	0.19071E+03	-0.19158E+03	-0.93845E-01	0.33659E-02	0.1597E-02
43.50	0.19197E+03	-0.19389E+03	-0.42882E-01	0.37384E-02	0.1942E-02
44.00	0.19327E+03	-0.19624E+03	0.14305E-01	0.41106E-02	0.2293E-02

3) RESULTS ALONG L3

Y-COORD (MM)	MISES STRESS (MPA)	P1-STRESS (MPA)	P3-STRESS (MPA)	MISES STRAIN MECH. RCC	MISES STRAIN PLAS. RCC
0.00	0.24878E+03	-0.25120E+03	-0.17619E+00	0.13265E-02	0.0000E+00
4.29	0.14746E+03	-0.14646E+03	0.38986E+01	0.81528E-03	0.0000E+00
7.14	0.84092E+02	-0.79008E+02	0.78878E+01	0.49812E-03	0.0000E+00
10.00	0.23614E+02	-0.16512E+02	0.10021E+02	0.19627E-03	0.0000E+00
15.71	0.99982E+02	0.18714E+02	0.12798E+03	0.37624E-03	0.0000E+00
18.57	0.15445E+03	0.27704E+02	0.19652E+03	0.62743E-03	0.0000E+00
20.00	0.17791E+03	0.35552E+02	0.23119E+03	0.74277E-03	0.0000E+00
22.00	0.19885E+03	0.59663E+02	0.28110E+03	0.89017E-02	0.0000E+00
24.00	0.18620E+03	0.76018E+02	0.26688E+03	0.11997E-02	0.0000E+00
25.00	0.21374E+03	0.48195E+02	0.28251E+03	0.20236E-02	0.0000E+00
25.50	0.22904E+03	0.22496E+02	0.27954E+03	0.31132E-02	0.0000E+00
25.75	0.23882E+03	0.95522E+02	0.27855E+03	0.37345E-02	0.0000E+00
26.00	0.24859E+03	-0.89874E+01	0.27901E+03	0.43641E-02	0.2362E-02

RESULTS AT THE END OF CYCLE

1) RESULTS ALONG LINE L1

Y-COORD (MM)	MISES STRESS (MPA)	P1-STRESS (MPA)	P3-STRESS (MPA)
34.00	0.18045E+03	-0.20601E+03	0.22943E+01
34.25	0.16816E+03	-0.20468E+03	-0.10738E+02
34.50	0.15311E+03	-0.20450E+03	-0.28534E+02
35.00	0.71749E+02	-0.10229E+03	-0.19773E+02
35.50	0.88523E+02	-0.11658E+03	-0.21225E+02
36.00	0.99706E+02	-0.12930E+03	-0.25172E+02
37.00	0.12332E+03	-0.15801E+03	-0.26992E+02
38.00	0.52063E+02	-0.81211E+02	-0.21890E+02
39.00	0.65410E+02	-0.12998E+02	0.62436E+02
40.00	0.14174E+03	-0.63700E+01	0.14550E+03
41.00	0.15423E+03	-0.38420E+01	0.15080E+03
42.00	0.16224E+03	-0.18750E+01	0.16237E+03
43.00	0.17006E+03	-0.48066E+00	0.17303E+03
43.50	0.17396E+03	-0.18051E+00	0.17761E+03
44.00	0.17781E+03	0.53396E-01	0.18215E+03

2) RESULTS ALONG LINE L2

Y-COORD (MM)	MISES STRESS (MPA)	P1-STRESS (MPA)	P3-STRESS (MPA)
0.00	0.45306E+02	0.13372E-01	0.49859E+02
5.71	0.29375E+02	-0.34958E+00	0.32572E+02
10.00	0.19667E+02	-0.85061E+00	0.21480E+02
15.71	0.10261E+02	-0.14218E+01	0.99464E+01
20.00	0.58073E+01	0.79631E+01	0.14622E+02
25.00	0.11149E+03	-0.11468E+03	0.85617E+01
30.00	0.53111E+02	-0.61170E+02	-0.33930E+00
32.52	0.44471E+02	-0.56002E+02	-0.56230E+01
35.00	0.10268E+03	-0.94055E+02	0.11722E+02
37.50	0.13235E+03	-0.12494E+03	0.11899E+03
40.00	0.10227E+03	0.70610E+01	0.16845E+03
41.00	0.15655E+03	0.41722E+01	0.16749E+03
42.00	0.15828E+03	0.20708E+01	0.16275E+03
43.00	0.16603E+03	0.50718E+00	0.16749E+03
43.50	0.16940E+03	0.18717E+00	0.17159E+03
44.00	0.17275E+03	-0.94836E-01	0.17571E+03

3) RESULTS ALONG LINE L3

Y-COORD (MM)	MISES STRESS (MPA)	P1-STRESS (MPA)	P3-STRESS (MPA)
0.00	0.45897E+02	0.17848E-01	0.50585E+02
4.29	0.33947E+02	-0.25513E+00	0.33421E+02
7.14	0.27153E+02	-0.83913E+00	0.25743E+02
10.00	0.21661E+02	-0.20546E+01	0.22184E+02
15.71	0.16861E+02	-0.88769E+01	0.84022E+01
18.57	0.15833E+02	-0.15379E+02	0.54248E+00
20.00	0.13464E+02	-0.18667E+02	-0.44641E+01
22.00	0.88376E+01	-0.27333E+02	-0.17147E+02
24.00	0.80153E+02	-0.11660E+03	-0.36423E+02
25.00	0.16103E+03	-0.22360E+03	-0.45624E+02
25.50	0.17616E+03	-0.21430E+03	-0.16771E+02
25.75	0.18559E+03	-0.21680E+03	-0.78732E+01
26.00	0.19541E+03	-0.21674E+03	0.39684E+01